Drop formation from particulate suspensions

A Thesis
Presented to
The Academic Faculty

by

Roy J. Furbank

In Partial Fulfillment
of the Requirements for the Degree of
Doctor of Philosophy in Chemical Engineering

School of Chemical and Biomolecular Engineering
Georgia Institute of Technology
May 2004

Drop formation
from particulate suspensions

Approved by:

F. Joseph Schork, Committee Chair

Jeffrey F. Morris, Advisor

Victor Breedveld

Larry J. Forney

Peter J. Mucha

Marc K. Smith

Date Approved: 3 May 2004

For my loving wife, Mary

ACKNOWLEDGEMENTS

First and foremost I would like to thank my research advisor, Dr. Jeffrey Morris. Dr. Morris has provided me with a rich and rewarding graduate school experience on many levels, and I am truly thankful for his guidance throughout these last five years. His intellectual curiosity and enthusiasm for scientific research have provided an excellent model for me to learn from and to follow. Lastly, I would like to thank Dr. Morris for his almost daily involvement in my work and his continued accessibility to me despite our geographical separation over the last two years.

I would also like to thank Dr. F. Joseph Schork for his involvement in my research and for giving me an academic home when I was in need. I am also indebted to the rest of my thesis committee (Dr. Victor Breedveld, Dr. Larry Forney, Dr. Peter Mucha, and Dr. Marc Smith) for their critical reading of my work. I would also like thank Dr. Wallace "Chuck" Carr and his research group (Dr. Heungsup Park and Hyunyoung Ok) for their interest in my research and for our various collaborations.

My peers in the Chemical Engineering department have also been a great resource for me. I would specifically like to thank Brian Timberlake and the rest of our dwindling research group (Ryan Miller and Fangbin Zhou). Brian and I have worked closely over the last five years and have had many (often lively) discussions which have helped me in my research as well as made this experience more rewarding in general. I would also like to thank Dave Desrocher for his friendship and support. Dave has been a true friend and has helped me navigate many difficult personal and professional challenges for which I am truly grateful. I am also thankful for the friendship of Matthew Spuller and Shilpa Damle who helped make my experience at Georgia Tech more enjoyable.

I would also like to thank my family for their support over the years. My mother, Christine Deter, has given me so much over the years and has been a source of continued inspiration for me; this work would not be possible without her. My stepfather, Dwight Deter, my grandparents, Roy and Betty Furst, as well as the rest of my family, have given me encouragement and support throughout. I would also like to extend heartfelt thanks to the newest members of my family, Dr. John and Carole Seffrin, whose friendship and support have helped me greatly in this effort and many others as well.

Last, but definitely not least, I would like to thank my wife, Mary, who has stood by me throughout this long endeavor and shared many of the hardships. Her love and friendship have greatly enriched my life and helped me to overcome many obstacles.

TABLE OF CONTENTS

LIST OF TABLES

LIST OF FIGURES

SUMMARY

This research presents an experimental study of the formation of drops of suspensions consisting of a viscous liquid and spherical, neutrally buoyant, noncolloidal particles. In this work pendant drop formation and low Reynolds number jetting of suspensions are investigated, as is the transition between the two. Throughout this study the particles utilized are on the order of 100 μm and the orifice from which the drops are formed is on the order of 1 mm.

In the pendant drop formation regime the pinch-off structures of the particle-laden systems are much different than those for the suspending liquid. New structures, termed "spindles" here, form at either end of the thread connecting the forming drop to the remaining mixture at the capillary tip. These new structures are thick cone-like regions consisting of particles which have been forced out of the thread during the necking process and are unable to rearrange adequately to become fully incorporated into either the mixture remaining at the capillary tip or into the forming drop. These spindles become more pronounced with increasing particle concentration.

During necking, particles in the thread resist its further thinning and, depending on the number of particles present, this resistance can have either a destabilizing or a stabilizing effect on the thread relative to the case of the pure liquid. The presence of a small number of particles in the thread introduces regions within the thread which cannot thin beyond the size of an individual particle and leads to earlier rupture. A large number of particles in the thread tends to have a stabilizing effect both before and after pinch-off. In this case there are sufficient particles present in the thread that their individual motions are restricted and the necking of the thread is slowed. These

two conflicting particulate effects provide an explanation for the observed changes in satellite drop generation and jetting transition with increasing particle concentration. The stabilizing effect of high particle concentration suppresses satellite drops and induces earlier jetting while the destabilizing effect is responsible for reducing the coherent jet lengths.

The ability of a two-stage model to describe the necking of suspensions for pendant drop formation has also been proposed. The first stage, termed initial necking, applies for times relatively far away from pinch-off and occurs in a manner similar to that of pure liquids, but with added resistance to thinning due to the particulate phase. During initial necking, the effect of the particles on the thread thinning can be accounted for by increasing the effective viscosity of the mixture. In this stage the size effects of the particles are negligible as long as the orifice to particle diameter ratio is large enough (≥ 12.8 in this study) since the thinning rate was not observed to depend on particle size.

The second stage is the final necking stage and occurs at times close to pinch-off, when the thread has thinned to only a small number of particle diameters. During this stage the particles resist the stretching of the thread and lead to shorter pinch-off lengths than those for the pure suspending liquid. In this stage the motions of individual particles and the complex interactions between the particles and the free surface of the thread lead to the formation of the new spindle structures observed at pinch-off. The individual particles also resist the thinning of the thread during this stage and must be rearranged within the thread so that a region devoid of particles forms where the thread ultimately ruptures. As particle concentration is increased, the transition from thinning over a region with particles to one free of particles causes a sharp increase in the thinning rate at times near pinch-off.

The ability to describe the thinning of concentrated suspensions using the effective viscosity of the mixture represents a considerable simplification of the process. From

the experiments, it is observed that the rate of thinning of the mixture scales as the effective viscosity to the $-1/3$ power for all of the suspensions examined, which indicates a similar scaling with the capillary number. This result will likely be of value to future researchers interested in modelling such flows and, while the scaling result may be unique to the specific experiments conducted here, the general conclusion that effective bulk properties can adequately describe the drop formation of concentrated suspensions during the early stages of necking should be widely applicable.

CHAPTER 1

INTRODUCTION

Drop formation is an area of research which has a rich and diverse history, yet continues to generate much interest today. A large majority of past and present effort in this area has involved systems where drops of a single, homogeneous liquid are formed into an immiscible fluid. In this work we seek to extend this base of knowledge by experimentally probing drop formation processes for liquids containing solid particles.

1.1 Background and literature review

Pure fluid drop formation has been extensively studied for over 100 years. A review by Eggers (1997) [14] on the subject contained over 250 references with the earliest dated from the year 1686.

In contrast to the situation for pure fluids, the formation of drops from particle-laden liquids has received little attention despite its importance in a variety of applications which include spray drying, slurry fuel combustion, and certain applications of ink-jet printing. Of particular interest to this work is the growing desire to extend the range of traditional ink-jet printing technology to applications requiring the use of solids-laden inks, with examples in ceramics manufacture [4, 47, 52] and textile printing [48]. While some progress has been made in developing particle-laden inks for use in traditional ink-jet printers [4, 47, 52] and designing printers that will jet more complex materials [36], little effort has been made to understand in detail the role the particles play in the overall process. Our goal in this work is to provide insight into this problem at a more fundamental level by examining drop formation from suspensions of solid spherical particles in a viscous liquid. We examine the

dripping mode, the transition to the jetting mode, and the jetting mode and focus on identifying and understanding the effects introduced by the particulate phase and quantifying how the processes differ from those for the corresponding pure liquids.

Drops are typically formed as fluid exits an orifice (usually a nozzle or capillary). Depending on the flow rate of the fluid, drops are formed either pendantly (the so-called dripping mode), by jetting, or by atomization [11]. Figure 1 illustrates how the length of the thread at breaking changes with increasing flow rate for the three different modes. If the flow rate is low enough drops will form uniformly at the tip of the capillary or nozzle, as when water drips from a faucet. After the flow rate exceeds a certain critical value jetting occurs and drops are formed at the tip of a column of fluid due to the capillary instability first studied by Rayleigh [38]. At even higher flow rates the liquid undergoes atomization where drops are again formed at the orifice but the drops are no longer of uniform size as in the dripping mode. In this work we will limit the scope to investigating only the dripping and jetting modes as well as the transition between the two.

1.1.1 Dripping

The dripping mode is characterized by low flow rates where pendant drops are formed at the tip of the orifice. A common example of this is a dripping faucet. Pure fluid behavior in this mode has been extensively studied both experimentally [23, 24, 37, 44, 51, 55] and numerically [6, 15, 13, 43, 54, 53]. While the formation of drops has been studied for many years, focused examination on the bifurcation, or pinch-off, process is relatively recent. Peregrine *et al.* [37] presented a detailed qualitative description of this process for water into air using high-speed photography. The authors highlighted an asymmetry of the developing structure which had not been previously noted. As the drop fell, a slender liquid column (also commonly referred to as a thread or filament) formed which connected the liquid at the orifice tip with

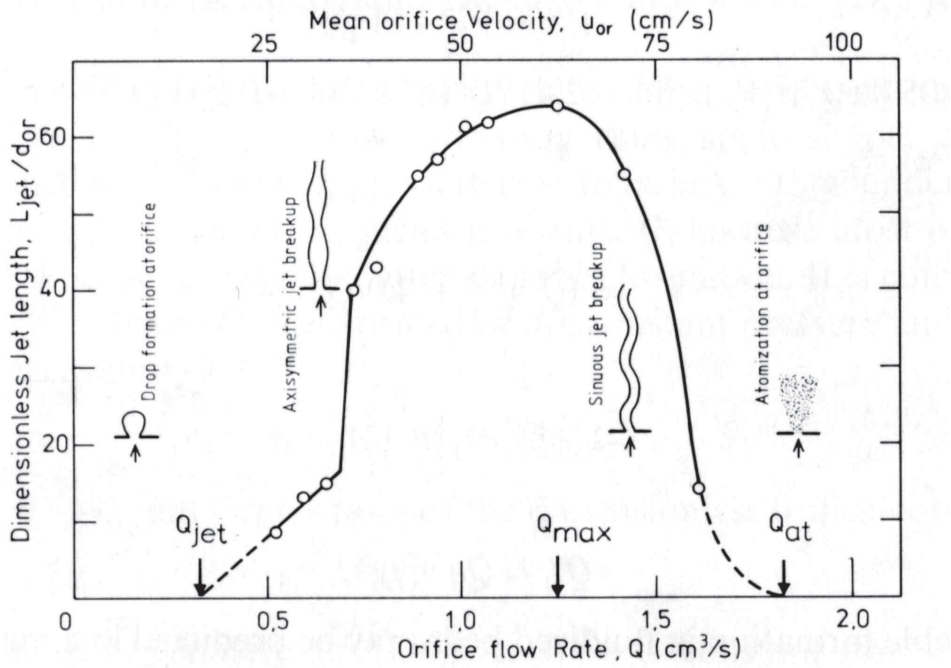

Figure 1: Results of Meister & Scheele [29] as reprinted by Clift *et al.* [11] illustrating the different regimes of drop formation as a function of flow rate.

that of the forming drop, with eventual rupture near the surface of the forming drop rather than at the middle of the thread. Following pinch-off, the thread was observed to retract due to the now unbalanced surface tension and also to undergo a secondary rupture near the orifice to yield a satellite drop.

Shi *et al.* [44] extended this work to more viscous liquids and examined the effect of viscosity on the shape of the forming drop near pinch-off. Increasing viscosity was found to lead to a lengthening of the thread at pinch-off as well as a smoothing in the transition from the thread to the surface of the drop. These authors also implemented the one-dimensional equations derived by Eggers & Dupont [15], and their numerical solutions qualitatively reproduce the pinch-off structures observed experimentally.

A group of recent studies by Basaran and coworkers has probed the pure fluid problem. Zhang & Basaran [55] studied the formation of pendant drops of viscous liquid into air, by performing a wide range of experiments in which they were able

to carefully follow the evolution of the forming drop with time. Among other results, the authors determined that increasing flow rate, orifice size, or viscosity led to longer thread lengths at pinch-off. Subsequently, Zhang numerically investigated both pendant drop formation into air [54] and into a second immiscible liquid [53]. Basaran and coworkers published a series of studies in which the region very near pinch-off was examined in detail before and after thread rupture both computationally and experimentally [3, 7, 34, 50], showing the interface of the forming drop can overturn prior to rupture.

The presence of this thread-like structure near pinch-off observed for pure fluids in the dripping mode is likely to play a critical role in particle-laden systems. We have been unable to find published work aside from a French thesis for dripping-mode drop formation from suspensions [1]. This thesis examined suspensions up to 23% solids primarily by image analysis, with a focus on the frequency of drop formation and coherent jet length in the dripping and jetting modes, respectively. We know of no work concerned with the structures formed near pinch-off for these systems. The work described here shows that the introduction of a new length scale to the problem, namely the particle diameter, fundamentally changes the evolution of the liquid thread near the pinch event: regardless of their size, the particles become significant relative to the narrowing thread at some point before pinch-off. This problem thus presents a challenge to bulk flow simulation by continuum methods [31, 45].

1.1.2 Transition to jetting

As the flow rate is elevated sufficiently, the flow at the orifice undergoes a transition from dripping to jetting. The transition from dripping to jetting has been experimentally examined by Scheele & Meister [29, 28, 41, 42], who measured jetting velocities in liquid-liquid systems and developed a correlation for predicting the onset of jetting and the resulting drop size based on a force balance at the orifice tip. Richards *et*

al. [39] developed a numerical model based on a volume-of-fluid method and were able to accurately reproduce the data of Scheele & Meister both before and after the transition. Still more recently Clanet & Lasheras [10] considered the transition from dripping to jetting for water into air. They experimentally determined the jetting transition for different orifice sizes and presented analysis for estimating this transition in the inviscid limit.

1.1.3 Jetting

Following this transition jetting ensues. The initial study of jetting behavior for pure liquids dates to Rayleigh [38] and his linear stability analysis for the inviscid case. The breakup of a liquid column to drops by capillary forces is, as a consequence, now a classic problem in hydrodynamic stability [12]. More recent works are detailed in reviews by Bogy [5] and Eggers [14]. In contrast to the dripping mode, the jetting mode has been considered for such complex fluids as polymeric solutions [9, 19], magneto-rheological fluids [16], and a few simpler particle-laden systems [1, 35]. The works on both polymer solutions and magneto-rheological fluids reveal an inhibition of jet breakup, relative to the pure fluid, and the development of a "beads-on-string" structure where forming drops are connected by long slender liquid filaments. In contrast to these systems, the work of Ogg & Schetz [35] describes slurries composed of water and glass beads jetting into air and shows that the particles introduce nonaxisymmetric disturbances and lead to irregular breakup.

1.2 Problem description

The problem considered here is that of a neutrally buoyant suspension of particle volume fraction ϕ and particle diameter d_p ($d_p = 2a$) flowing through a capillary tube with outer diameter d at a constant flow rate Q (Figure 2); note that $\phi = \pi d_p^3 n/6$ where n is the particle number density (number of particles per unit volume). The suspending liquid has density ρ (as do the particles), viscosity μ, and surface tension

σ. The drop forms in the direction of gravity and fully wets the outer edge of the capillary orifice. For sufficiently small Q, drop formation occurs in the dripping mode and drops are formed directly at the tip of the capillary tube. Increasing Q eventually leads to a transition from the dripping mode to the jetting mode in which drops are formed away from the orifice at the end of a stable column of suspension. Figure 2 illustrates the asymmetric shape of the thread just prior to pinch-off characteristic of pure liquids, as well as the general geometry of the problem.

Figure 3 illustrates the situation for a suspension of $\phi = 0.05$ in the dripping mode and introduces the notation used in describing the drop formation process throughout this work. Initially, the drop grows essentially statically at the capillary orifice (Figure 3(a)), implying that during this stage the surface tension acting along the contact line balances the drop weight. Hence, if the flow were stopped the forming drop would remain attached to the tip of the capillary tube. Once the weight of the forming drop exceeds some critical value it begins to fall (Figure 3(b)) and the width of the liquid column between the orifice exit and the drop begins to rapidly narrow. This process of rapid radial thinning is referred to as necking and continues until a time very near that shown in Figure 3(c), the last image captured before the drop detached. This configuration is termed the pinch-off structure and the time corresponding to this picture is referred to throughout as the pinch-off time ($t = t_0$).[1] In subsequent analysis this time is used as the reference time for comparing the dynamics of different drop formation events. The time over which necking occurs, t_n, is short relative to τ, the time between drops; $t_n/\tau \doteq 0.06$ in Figure 3. Throughout the process $L(t)$ denotes the total length of suspension, measured from the orifice outlet, which is continuously attached to the capillary tip and the slightly subjective quantity L_N is the length of the slender thread-like region which develops as pinch-off is approached

[1]Pinch-off actually occurs at a time between this picture and the next so is only known within $\pm 1/2$ of the time between pictures (as determined by the frame rate of the camera for a given experiment) if we assume that pinch-off occurs at the midpoint of these two pictures.

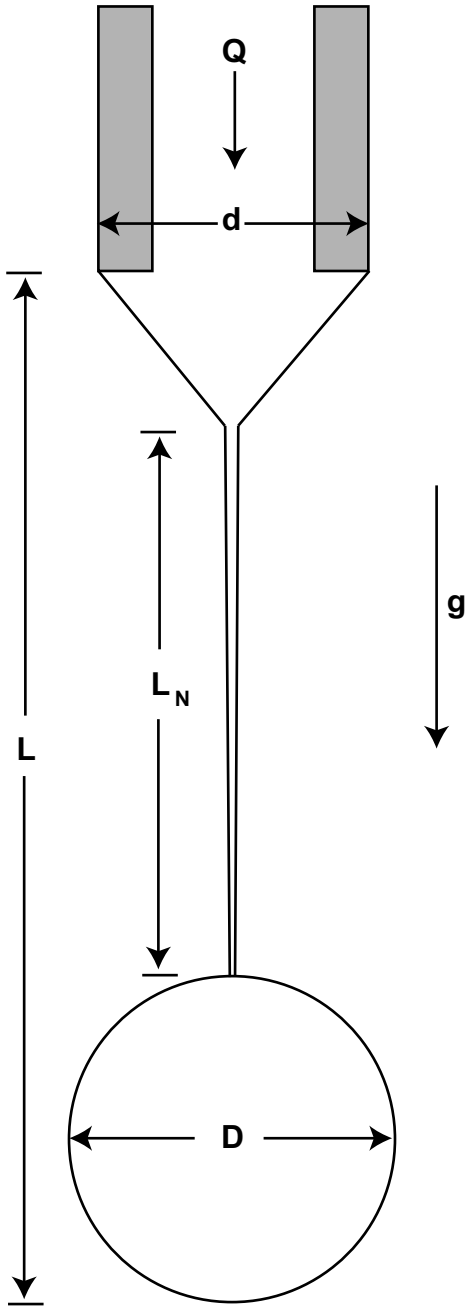

Figure 2: Drawing of a pendant drop illustrating the asymmetric structure formed just prior to pinch-off and the geometry of the problem in general.

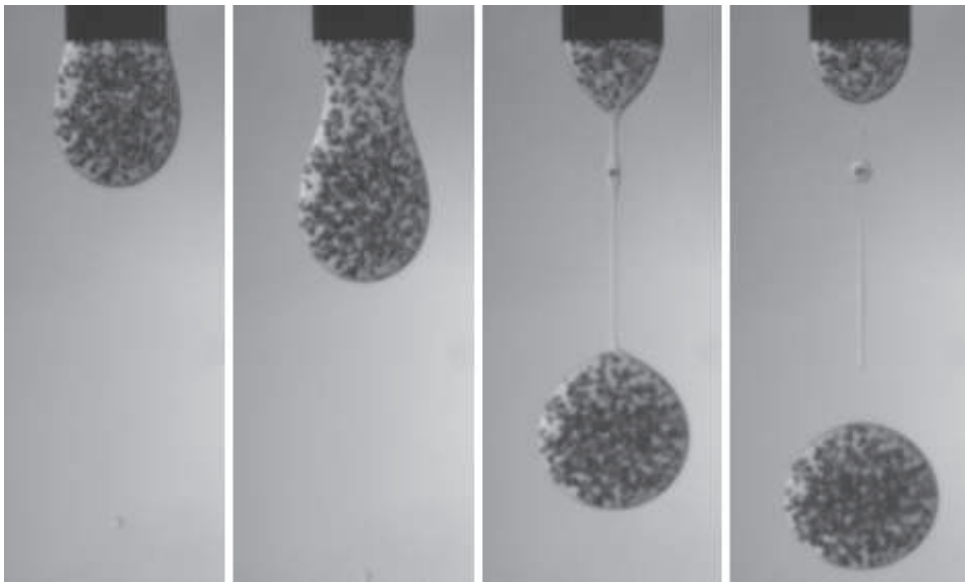

Figure 3: Formation of a pendant drop of suspension ($\phi = 0.05$) from an orifice of outer diameter $d = 0.32$ cm into ambient silicone oil with particle diameter $d_p = 212$ - 250 μm and flow rate $Q = 0.70$ cm^3/min ($Re = 0.01$). The images are not uniformly spaced in time.

(Figure 2). The width of the forming drop is denoted by $W(z,t)$ and is measured at each location along the drop structure for $0 \leq z \leq L(t)$, where z is the direction of gravity. A brief time after the instant captured in Figure 3(c) the thread ruptures and the primary drop (diameter D) is formed (Figure 3(d)), potentially accompanied by some number of smaller secondary, or satellite, drops.

The dimensionless parameters characterizing the problem include the Bond (Bo), capillary (Ca), and Reynolds (Re) numbers in the absence of particles:

$$Bo = \frac{\rho g d^2}{\sigma}, \quad Ca = \frac{U\mu}{\sigma}, \quad \text{and} \quad Re = \frac{\rho U d}{\mu}, \tag{1}$$

where $U = 4Q/\pi d^2$ is the mean velocity at the orifice outlet. The Weber number ($We = Ca\,Re$) is commonly used in describing the process in the jetting mode although is not independent of the three dimensionless quantities in (1). Each of these

dimensionless quantities represent a measure of the importance of different forces within the system with Bo the ratio of gravitational to surface tension forces; Ca the ratio of viscous to surface tension forces; and Re the ratio of inertial to viscous forces. The particles, in the case of monodisperse and neutrally-buoyant suspensions upon which we focus in this work, introduce two further dimensionless parameters: the particle volume fraction ϕ, and the ratio of the orifice diameter to particle diameter d/d_p. The particles are sufficiently large that Brownian motion is negligible (the Péclet number is infinite). Colloidal forces are also of no relevance, as the particles are over 100 microns in nearly all of the experiments.

1.3 Drop size determination in the dripping mode

In this section we will examine the problem of determining the size of the resulting drop in the purely pendant drop formation case and the theory associated with it. If we consider a pendant drop at the tip of a capillary tube just before it detaches and perform a force balance in the vertical direction we find that the normal component of the surface tension force acting along the three phase contact line is balanced by the weight of the drop:

$$F_\sigma \cos\theta = F_g \tag{2}$$

where F_σ is the force of surface tension acting at an angle θ to the normal and F_g is the weight of the pendant drop. In this discussion we assume that the drop is filled very slowly and the rate of flow into the drop is negligible. If the drop fully wets the outer diameter of the capillary, d, and θ goes to zero just before the drop detaches we can simplify (2) and rearrange to get an expression for the volume of the drop:

$$V^i_{\text{drop}} = \frac{\sigma \pi d}{\rho g}. \tag{3}$$

Equation (3) is commonly referred to as Tate's law [46] and is the simplest expression for determining the volume of a pendant drop. The drop volume determined

using this method is typically referred to as the volume of an "ideal" drop and is indicated here by the superscript i. In practice this method systematically overestimates the size of the resulting drop since a portion of the liquid comprising the drop before it detaches actually remains attached to the capillary tip.

This problem was addressed by Harkins & Brown [22] who determined a correction factor to Equation 3 experimentally by comparing measurements of actual drop volumes with those predicted by Tate's law for a wide range of liquids and capillary sizes. The Harkins-Brown correction factor, f_{HB}, can be used to determine the drop volume according to

$$V_{\text{drop}} = V^i_{\text{drop}}\, f_{HB} = \frac{\sigma \pi d}{\rho g} f_{HB} \tag{4}$$

where f_{HB} is a function of the capillary outer radius, r_0, and the so-called capillary length, L_σ, which is dependent on the liquid properties,

$$f_{HB} = \frac{f(r_0/L_\sigma)}{2\pi} \tag{5}$$

where

$$L_\sigma = \sqrt{\frac{2\sigma}{\rho g}}. \tag{6}$$

For small r_0/L_σ the value of f_{HB} approaches unity since surface tension dominates and the shape of the forming drop is highly spherical.

In addition to providing a ready technique for determining the size of drops formed in the dripping mode based on the liquid properties and the outer diameter of the capillary, this approach by Harkins & Brown forms the basis of the drop-weight technique for measuring surface tension. Since this method determines the drop size based only on a balance of surface tension and gravity, we would expect no change in the drop size due to the addition of a particulate phase. This assertion will be examined experimentally in Chapter 3 when we measure the drop size of various suspensions.

1.4 Thesis organization

The remainder of this thesis is organized into four chapters. Chapter 2 describes the experimental apparatus and the various suspensions used in performing the experiments. A detailed description of the protocol for analyzing the experimental data is also presented. The next three chapters present the experimental results: the first two dealing with the formation of pendant drops and the third with both the transition to jetting and the behavior once jetting has ensued. The first of the two pendant drop chapters, Chapter 3, presents the effect of the particulate phase on the pinch-off structure and investigates the influence of particle concentration on drop size and satellite drop formation. Chapter 4 continues the examination of pendant drop formation and focuses on the dynamics of the thread-like structure during necking. In Chapter 5, the last of the results chapters, the transition from dripping to jetting and the jetting behavior of suspensions are studied. Lastly, Chapter 6 presents a summary of the conclusions of this research and a discussion of the recommendations for future investigations in this area.

CHAPTER 2

EXPERIMENTAL

In this chapter we describe the details of the experimental set-up and protocol for the experiments which have been conducted in the course of this research. The experimental apparatus will be described, as will the composition of the suspensions used and their preparation. Lastly in this chapter, we will present a detailed examination of the techniques used in analyzing the experimental results and provide a sample set of results to highlight the procedure.

2.1 Apparatus

Experiments were performed using the apparatus depicted in Figures 4 and 5. Suspension was driven from the reservoir of a drop delivery vessel through a short (3–5 cm) stainless steel capillary tube using a Harvard Apparatus PHD 2000 syringe pump (accuracy of imposed flow rate $\pm 1\%$), employing silicone oil (polydimethylsiloxane) as a driving fluid in order that particle migration effects not lead to maldistribution in the syringe or tubing upstream of the reservoir. The silicone oil is less dense than and immiscible with the suspending liquid, providing a particle-free driving fluid; a stable interface between the suspension and silicone oil within the reservoir was always observed. The ends of the capillary tubes were electrolytically cut and polished (Valco Instruments), with outer diameters 0.16, 0.32, 0.64 cm and inner diameters 0.10, 0.22, 0.53 cm. The ratio of capillary length, l, to inner diameter varies in the range of $l/d_i = 5.7 - 50$, and both experiments [21] and suspension flow models [31, 33] suggest that particle migration toward the tube axis should be a minor influence except perhaps at the highest ϕ and largest l/d_i studied.

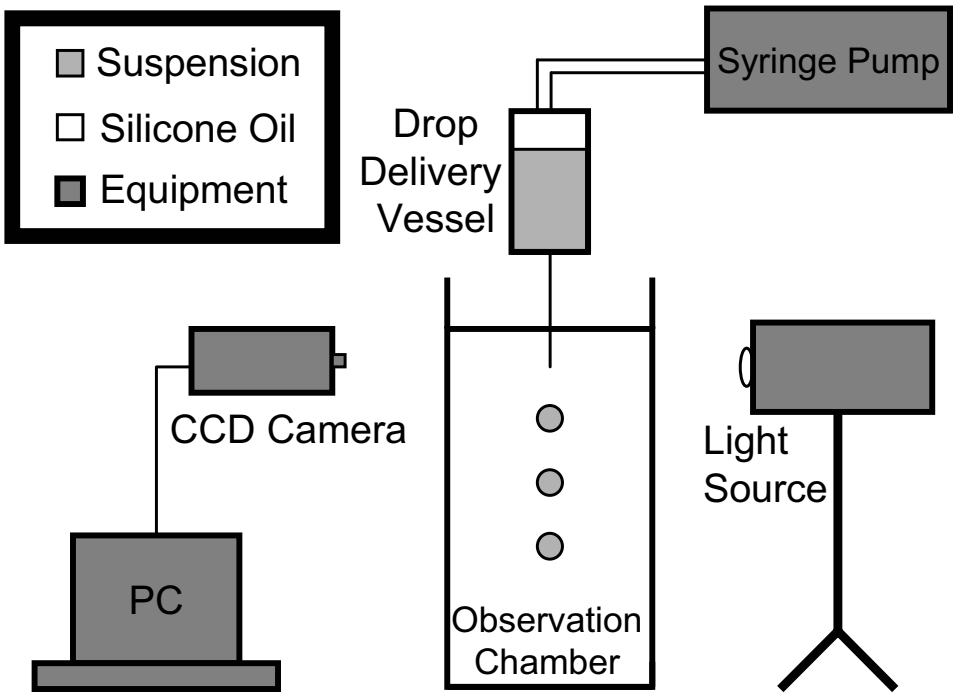

Figure 4: Schematic of the experimental apparatus.

Figure 5: Photograph of the experimental apparatus.

The evolution of the forming drops at the capillary tip was captured photographically using one of two CCD cameras: a Cooke SensiCam camera with a frame rate of 30 frames per second (fps), and a Kodak MotionCorder Analyzer, Model 1000 with variable frame rates up to 10,000 fps (the highest rate used was 500 fps in the work described here). Back-lighting was provided by a 300 W bulb diffused through translucent Lexan of 0.64 cm thickness.

The observation chamber was an open-top glass box filled with silicone oil (ρ = 0.95 g/cm^3, μ = 19 cP) or left empty. In the latter case the chamber served only to isolate the forming drop from air currents in the laboratory. The drop delivery vessel consisted of a 7 cm diameter Lexan cylinder (the reservoir) with a removable aluminum bottom into which the capillary was pressed. This cylinder was later replaced with aluminum, as shown in Figure 5, for improved durability and resistance to leakage. When assembled, the two end caps of the cylinder were parallel and the capillary tube was normal to both. To ensure that the capillary tube was parallel to gravity, a Newport tilt platform was used and a level was placed in the center of the upper end piece of the cylinder to precisely position the entire drop delivery vessel. The tilt platform was mounted to an aluminum frame (Figure 5) and the drop delivery vessel was clamped to the platform. Both delivery vessel and observation chamber were fixed to a vibration-damped table (Newport) and the pump was located on a separate table.

2.2 Suspensions

Suspensions were prepared such that the particles were neutrally buoyant. The liquid viscosity was chosen large enough to examine the pinch-off region in detail without requiring extremely high camera frame rates (rates greater than 250 fps reduce the resolution), but not so large that the stretching and subsequent pinch-off occurred over too great a distance. A three-component mixture of zinc chloride ($ZnCl_2$), water,

and UCON (a highly viscous liquid) was found to satisfy these requirements and was used throughout the experiments.

Spherical poly(methyl methacrylate) (PMMA) particles were suspended in a mixture of 23%(wt.) $ZnCl_2$ in water solution and UCON 90,000 (polyalkylene glycol; Dow Chemical). The composition of the final mixture was 30%(wt.) UCON with properties $\rho = 1.184 \pm 0.001$ g/cm^3, $\mu = 400 \pm 20$ cP, and $\sigma = 49 \pm 3$ dyne/cm by drop weight and 47 ± 2 dyne/cm by du Nuoy ring.

Particles were used in various size ranges in the experiments. All of the particles came from a large stockpile ($\sim$ 125 kg drum from ICI Acrylics) containing sizes ≤ 350 μm in diameter. To obtain particles for use in the experiments, particles from the drum were sieved by hand using brass frame steel cloth sieves (W.S. Tyler) to narrow size distributions, as determined by the available mesh sizes of the sieves. The two primary particle size ranges used in performing the experiments were 106-125 μm and 212-250 μm. In these distributions the upper bound is more rigid in the sense that the particles had to pass through a sieve of this size in order to be included in the distribution. The lower bound is fixed by the size of the smaller sieve and particles which do not pass through the mesh are retained in the distribution. This bound is less severe since sieving was performed until it was deemed that "all" the particles of smaller size had passed through and this is, in practice, impossible to accomplish in realistic times for the sieving technique employed. However, the number of particles smaller than the lower bound included in the final particle distribution is estimated to be extremely small.

Preparing the suspensions such that the particles were neutrally buoyant was one critical aspect of the experimental procedure. Although the actual drop formation events occur on a time scale much shorter than any particle settling, even for a poorly density-matched suspension, neutral buoyancy is needed in order to ensure that the particle concentration of the suspension remains constant throughout the course of an

experiment (typically 2-3 hours). The suspension within the drop delivery reservoir must retain a constant composition over this time frame with negligible settling (or rising) of the particles.

To accomplish this goal a number of suspending liquid mixtures of slightly different densities were prepared and particles added to them. The suspensions were then observed over time and the density of the particles determined based on whether the particles rose or settled in a given density liquid mixture. The density of the particles was only known roughly ($1.180\ \mathrm{g/cm^3} \leq \rho \leq 1.190\ \mathrm{g/cm^3}$) and this technique was utilized to determine it more precisely. Mixtures of density $\rho_1 = 1.182\ \mathrm{g/cm^3}$, $\rho_2 = 1.184\ \mathrm{g/cm^3}$, and $\rho_3 = 1.186\ \mathrm{g/cm^3}$ were prepared and the particles were observed to settle to the bottom of the container for ρ_1 and to rise for ρ_3. The particles in the mixture with density ρ_2 actually "split", with some particles rising and some settling. These particle motions were very gradual and were only evident after many hours ($\sim$ 1 day for all of the mixtures). From these observations it was concluded that the density of the particles was very nearly equal to $\rho_2 = 1.184\ \mathrm{g/cm^3}$ and that using a suspending liquid of this density would satisfy the requirement of constant composition throughout the time required to conduct the experiments.

2.3 Experimental parameters

The experimental parameters examined are presented in Table 1. We conducted experiments where drops of suspension of various particle fraction were formed into both ambient silicone oil and air using three different size orifices and three different particle size distributions. The range of flow rates encompassed both dripping and jetting behavior with $Re < 1$ throughout and $Re \ll 1$ before the onset of jetting. Drops formed into silicone oil provide primarily qualitative information and allow visualization of the suspended particles, while quantitative results were obtained for drop formation into air.

Table 1: Parameters for which experiments were performed.

Ambient fluid	d(cm)	$d_p(\mu$m)	d/d_p	ϕ	Re	Ca	Bo
silicone	0.16	212-250	6.4	0-0.25	0.007-0.14	0.04-0.8	0.1
silicone	0.32	212-250	12.8	0-0.25	0.003-0.07	0.009-0.2	0.4
silicone	0.64	212-250	25.6	0-0.25	0.002-0.04	0.002-0.05	1.5
air	0.16	106-125	12.8	0-0.30	0.02-0.4	0.03-0.7	0.6
air	0.16	212-250	6.4	0-0.30	0.02-0.4	0.03-0.7	0.6
air	0.32	106-125	25.6	0-0.40	0.01-0.4	0.009-0.4	2.4
air	0.32	212-250	12.8	0-0.40	0.01-0.4	0.009-0.4	2.4
air	0.32	< 106	30.2	0-0.10	0.01-0.4	0.009-0.4	2.4

2.4 Data analysis

A critical part of this work is the ability to analyze the photographs resulting from the experiments. Each experiment yields a series of pictures (typically 1,092 as determined by the maximum storage capacity of the camera's hard drive) which depict the formation of either a single drop or multiple drops, depending on the flow rate of the pump and the frame rate of the camera. Since each experiment lasts only a few seconds (downloading the resulting pictures from the camera to a PC is the most time consuming step and takes approximately 5 minutes for each series of pictures), a large number of pictures can be generated in the course of a single day of experiments. Typically 20-30 experiments are conducted in examining a single concentration which can yield upwards of 30,000 pictures.[1] In this section the techniques employed to deal with this large amount of raw data and generate meaningful measurements of the drop formation process will be described in detail.

In performing the experiments an important consideration was the ability to capture the entire drop formation process within the field of view of the camera. This allows measurement of the thread length (L) and width (W) up to pinch-off. Once

[1] We estimate that during the course of this research we have amassed a collection of ~ 1.2 million pictures of drops in various stages of being formed, saved in a library of over 220 CD-ROM's.

Figure 6: Single picture of a forming drop after necking has begun for a suspension of $\phi = 0.10$, with $d = 0.32$ cm, $d_p = 106 - 125$ μm. The time away from pinch-off is $t_0 - t = 0.04$ s

the liquid viscosity is chosen, the camera field of view—and hence the resolution—is fixed by this requirement. In each photograph the tip of the capillary tube was also captured and its diameter (d) was used as the length scale for making subsequent measurements of the forming drop. An example of a typical picture of a forming drop after necking has begun ($t_0 - t = 0.04$ s) is shown in Figure 6. This photograph will be used to illustrate the procedure followed in analyzing the experimental data.

For a given set of pictures a few measurements must first be made "by hand" before an automated process can be implemented. These include identifying the location of the capillary tip within the field of view as well as the location on either side of the capillary outside of which there is no useful information. This information is used in cropping the pictures to reduce the computational time required when analyzing large numbers of pictures (the photograph in Figure 6 has already been cropped) and fixing the origin from which L is measured. The location of the capillary tip is required as a reference location in order to make accurate measurements of L, which is measured from the capillary tip to the edge of the forming drop. Various automated techniques were attempted to determine this location but it was found that this made the algorithms unnecessarily complex and was less reliable than determining it manually. For a given experimental set the camera is not moved and these manually determined values can be used repeatedly for all subsequent picture sequences in the data set.

Figure 7: Black and white image of the forming drop shown in Figure 6 generated after thresholding and edge-detection.

The principal step in analyzing the photographic sequences is converting the grayscale images to black and white images which can be represented as matrices and manipulated to make the necessary measurements. This step is accomplished using thresholding and edge-detection algorithms in MATLAB's image analysis toolbox. The result of this step for the sample picture of the forming drop (Figure 6) is shown in Figure 7. This image is actually a matrix composed of ones (white pixels) and zeros (black pixels) from which the subsequent measurements are made.

From each black and white image two primary measurements are made.[2] The first is the thread length, L, which is measured in two ways: the first is the length of liquid connected to the tip of the capillary and the second is the length from the capillary tip to the furthest black pixel from it (*i.e.* the leading edge of the drop). These two measurements are required in order to accurately determine L very near pinch-off, since at this point the thread has become very slender and can fall below the detection level of the edge-detection algorithm. Near pinch-off the first method fails and underestimates L because the algorithm has prematurely broken the thread. In this region the second technique is used to measure L up until the pinch-off picture since this technique always measures the length from the capillary tip to the leading edge of the drop (regardless of whether or not it has pinched-off or not). Once the thread has ruptured, L is again determined using the first method. Measurements

[2]Measurements are actually made from the negative of the image shown in Figure 7 because of how various MATLAB routines deal with the pixel groups.

Table 2: Measurements of thread length, L, in pixels for the two techniques employed. L_1 measures the length of the liquid connected to the tip of the capillary while L_2 measures the length of the object furthest from the capillary. L in the fourth column is the corrected thread length using the appropriate technique (indicated by bold type).

$t_0 - t$(s)	L_1	L_2	L	L/d
0.004	**323**	323	**323**	4.61
0.002	144	**338**	**338**	4.97
0	82	**353**	**353**	5.04
-0.002	**66**	369	**66**	0.94
-0.004	**54**	386	**54**	0.77

for the series of pictures near pinch-off in Figure 8 using both techniques are shown in Table 2. In Table 2 the values in bold type are the correct L measurements and indicate how the switching between the two techniques is accomplished.

In all of the experiments the picture just before thread rupture is referred to as the pinch-off picture and is used as the time reference ($t = t_0$) for comparison between experiments. This picture is identified visually and is supplied as an input to the L measurement algorithm in order to determine when to switch between the two techniques. Identifying the pinch-off picture using an automated technique proved to be unfeasible since the thread width near rupture was too thin for the edge-detection algorithm to detect. Attempts to adjust the thresholding algorithm in order to correctly detect the thread were unsuccessful since the difference between the thread and the background becomes very small near pinch-off. In addition, determining t_0 correctly is critical since further analysis between different drops requires comparisons based on events referenced to this time. The drop is also moving quite rapidly near pinch-off and a small error in determining the pinch-off time can lead to large errors in subsequent analysis.

Once L has been measured (in pixels) and corrected to ensure that the proper measurement technique was used, the length values are made non-dimensional by

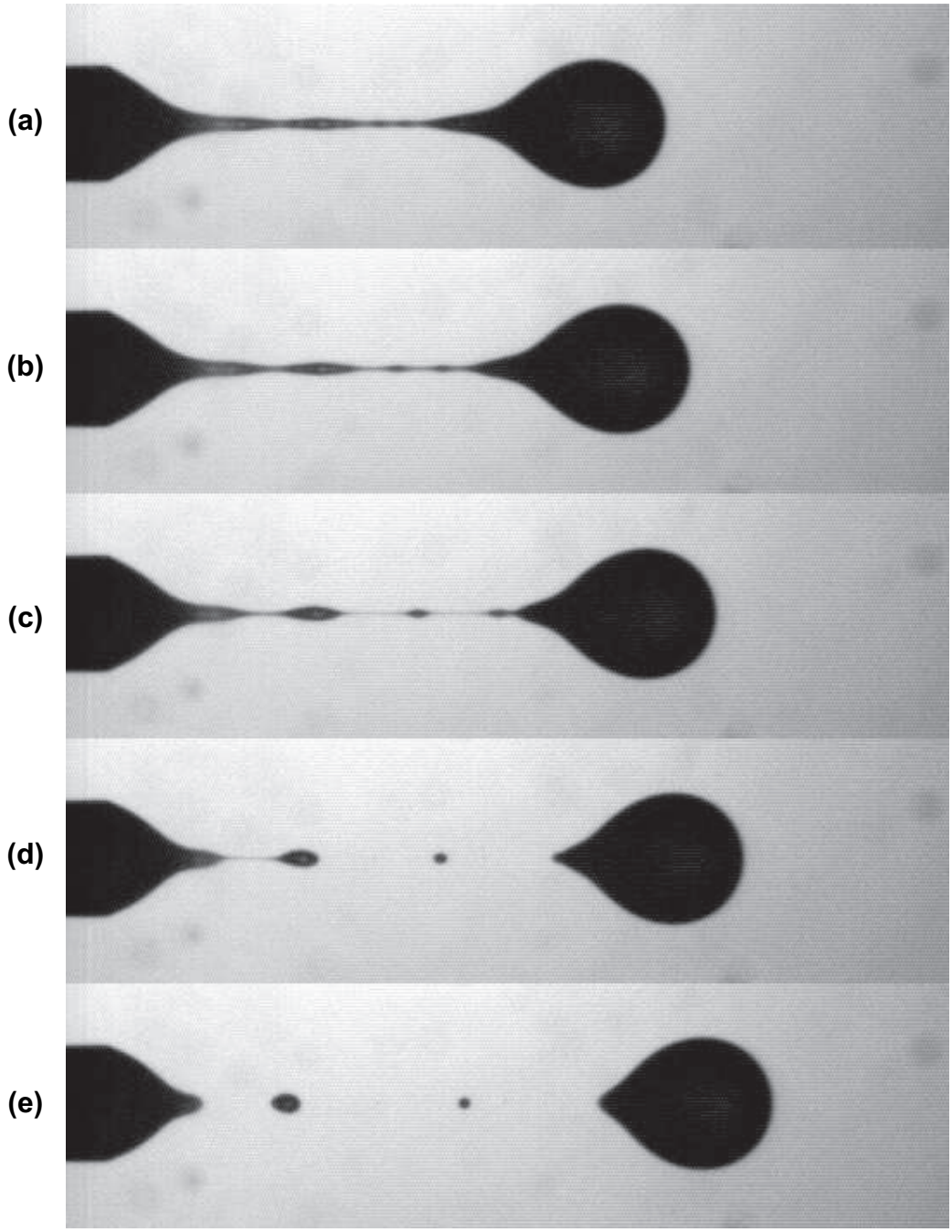

Figure 8: Series of photographs near pinch-off for $\phi = 0.10$, $d = 0.32$ cm, $d_p = 106 - 125$ μm. These are the same photographs for which the L measurements are presented in Table 2. The times before pinch-off are (a) $t_0 - t = 0.004$, (b) 0.002, (c) 0, (d) -0.002, and (e) -0.004.

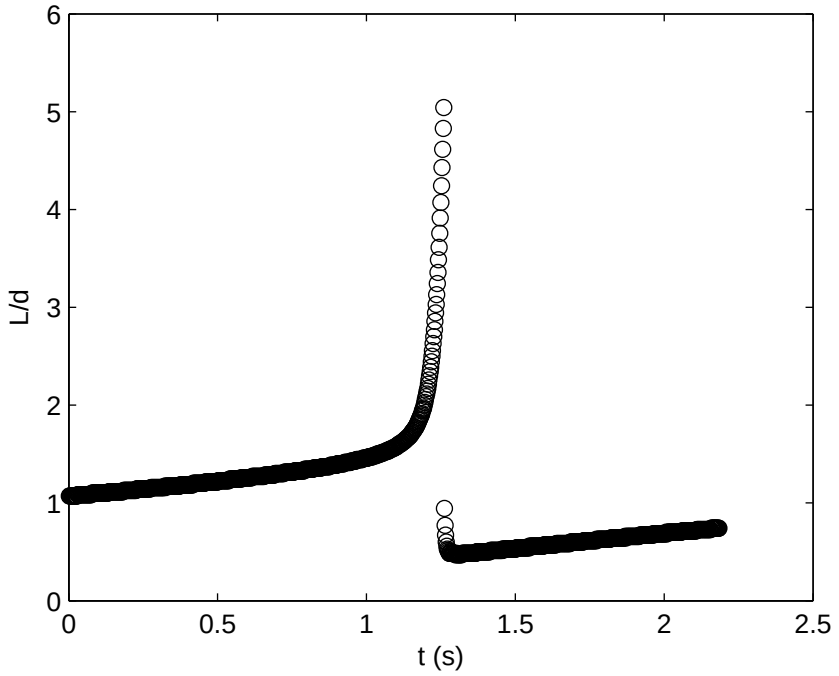

Figure 9: Plot of the dimensionless thread length, L/d versus time for $\phi = 0.10$, $d = 0.32$ cm, $d_p = 106 - 125$ μm.

scaling with the capillary diameter, d. The resulting L/d data can then be plotted against time in order to capture the full time sequence of the growth of the thread for a given experiment (Figure 9).

The second primary measurement made from the black and white image is the width, W, of the forming drop as a function of position in the z-direction (parallel to gravity) from the capillary tip to the leading edge of the drop (L). This measurement is made by finding the minimum and maximum pixel location at a given point and subtracting them (*i.e.* the cross-sectional width of the forming drop at a given z). The width measurements for the sample image in Figures 6 and 7 is plotted in Figure 10. These measurements are useful in analyzing the thinning of the thread in time and will be discussed in detail in Chapter 4.

From the width measurements it is possible to determine the size of the drop after pinch-off. Although the detached drop will eventually obtain a spherical shape this

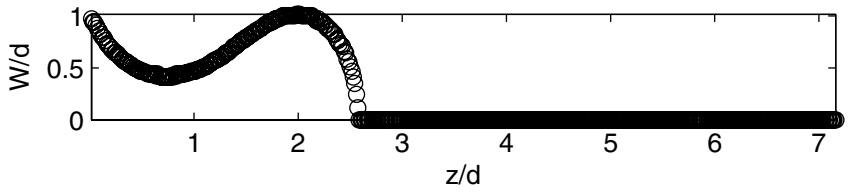

Figure 10: Result of the width measurement of the forming drop at each pixel location in the field of view.

Table 3: Results of drop size measurement technique for the four drop images shown in Figure 11.

$t_0 - t$(s)	V_{drop}(pixel^3)	D(pixel)	D/d
-0.002	2.7686e5	80.864	1.155
-0.004	2.7766e5	80.942	1.156
-0.006	2.7933e5	81.103	1.159
-0.008	2.8074e5	81.239	1.160

often does not occur until after it has fallen out of the field of view of the camera (Figure 11). For the case of concentrated suspensions the drop is often highly non-spherical. The technique employed is to determine the volume of the drop by rotating the measured width data about the z-axis:

$$V_{\text{drop}} = \pi \int_a^b [R(z)]^2 dz \tag{7}$$

where V_{drop} is the volume of the drop measured in pixels, $R(z) = W(z)/2$ the location of the drop edge as a function of position in the direction of gravity, and a and b are the lower and upper bounds corresponding to z such that $R(z) = 0$ (*i.e.* either "end" of the drop). This technique has been performed on the drop shown in the sequence in Figure 11 and the results presented in Table 3.

In order to assess the accuracy of this technique for measuring the various characteristics of the forming drop structure, photographs were taken of two objects of

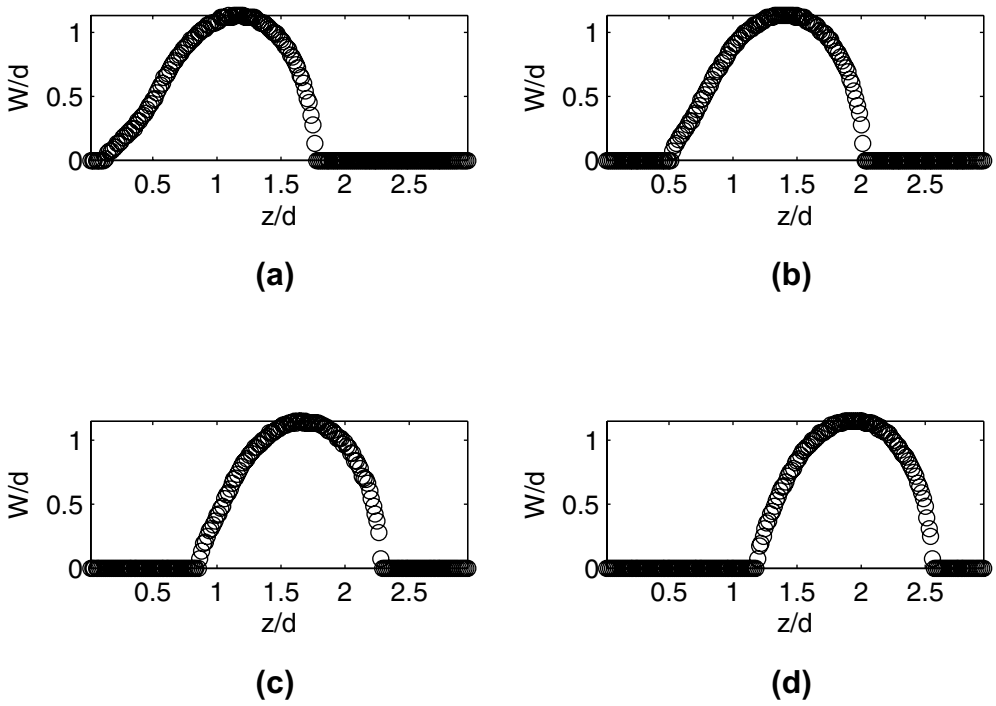

Figure 11: The measured width profile of the drop after pinch-off for (a) $t_0 - t = -0.002$ s, (b) -0.004 s, (c) -0.006 s, and (d) -0.008 s.

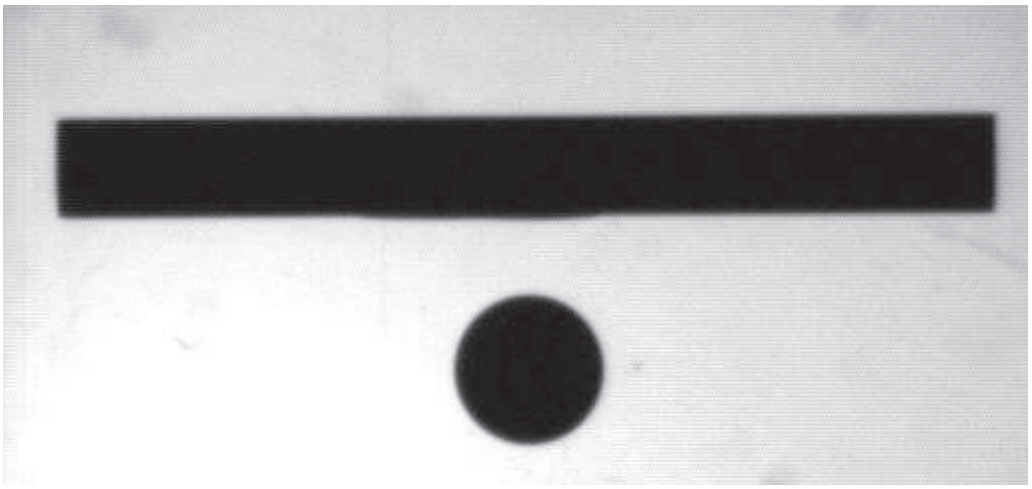

Figure 12: Photograph of the two standards (a spherical metal ball and a length of cylindrical capillary tubing) used in assessing the accuracy of the data analysis technique. Th metal ball has diameter $D = 4.77$ mm and the capillary tube has length $L = 29.88$ mm and diameter $d = 3.17$ mm. The values determined using the experimental analysis protocol were $L = 29.85$ mm and $D = 4.73$ mm.

known size and analyzed using the experimental protocol outlined above. A photograph of the objects used is shown in Figure 12. The two objects were a spherical metal ball with diameter $D = 4.77$ mm and a section of cylindrical capillary tubing of length $L = 29.88$ mm and diameter $d = 3.17$ mm.

Using the capillary diameter, d, as the length standard (as in the actual experiments) the experimental analysis technique measured $L = 29.85$ mm and $D = 4.73$ mm. The relative errors in the two measurements are 0.1% and 0.9% for the length and diameter determinations, respectively.

CHAPTER 3

PENDANT DROP FORMATION I: PINCH-OFF STRUCTURE, DROP SIZE, AND SATELLITE DROP GENERATION

In this chapter experimental results of particulate effects on drop formation for suspensions of various ϕ are presented. The results are divided into three areas: development of the liquid thread during necking and the subsequent pinch-off structures formed, formation of the primary drop, and satellite drop generation after pinch-off. A discussion of the results and their key implications follows in which we will focus on interpreting the experimental results with the goal of developing a broader understanding of the role of the particles in the pendant drop formation process.[1]

3.1 Development of the liquid thread and pinch-off structure

Here, we address the motion of the forming drop after surface tension forces holding it to the tip of the orifice have been exceeded and the drop falls under its own weight. We examine particle motions in the developing liquid thread for a low-ϕ suspension, followed by consideration of the pinch-off structures of various suspensions. Lastly, we describe the evolution of the liquid thread through pinch-off for a more concentrated suspension.

In this section we will present results for both drops forming into silicone oil and into air. Although the different cases should be clear from the context, Figure 13

[1]The work presented in this chapter is taken from Furbank & Morris (2004) [18].

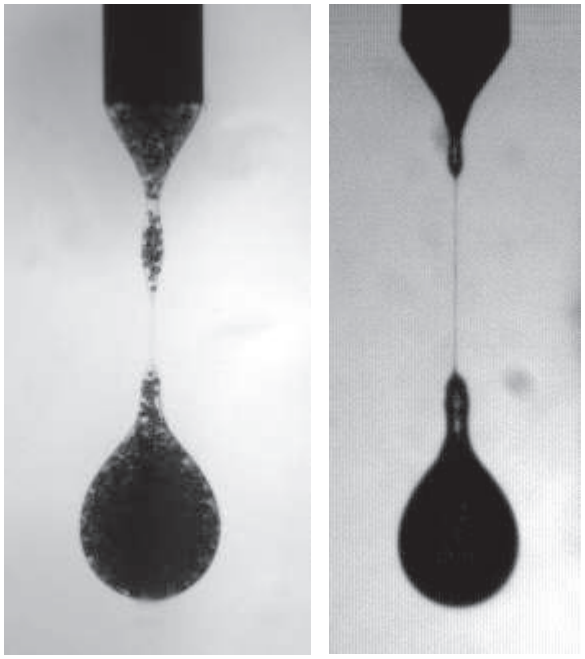

Figure 13: Pinch-off structures of a drop forming into ambient silicone oil (a) and into air (b) for $\phi = 0.20$, $d = 0.32$ cm, $d_p = 212 - 250$ μm.

contrasts the appearance of each for a suspension of $\phi = 0.20$. The primary difference between the two situations is that the particles are visible within the forming drop for drops forming into silicone oil while the entire structure is opaque for drops forming into air. In addition to the visible differences, the three-phase contact line in ambient silicone has more complex wetting behavior than in ambient air. Because of this the experiments performed into silicone oil are used exclusively for qualitative assessment of the drop formation process and to develop an understanding of the actual particle motions within the forming drop while those performed into air are used to generate quantitative information.

3.1.1 Particle motions during necking

Figures 14 and 15 illustrate the photographic results from a typical experiment in the vicinity of the pinching time for pure suspending liquid and a suspension of

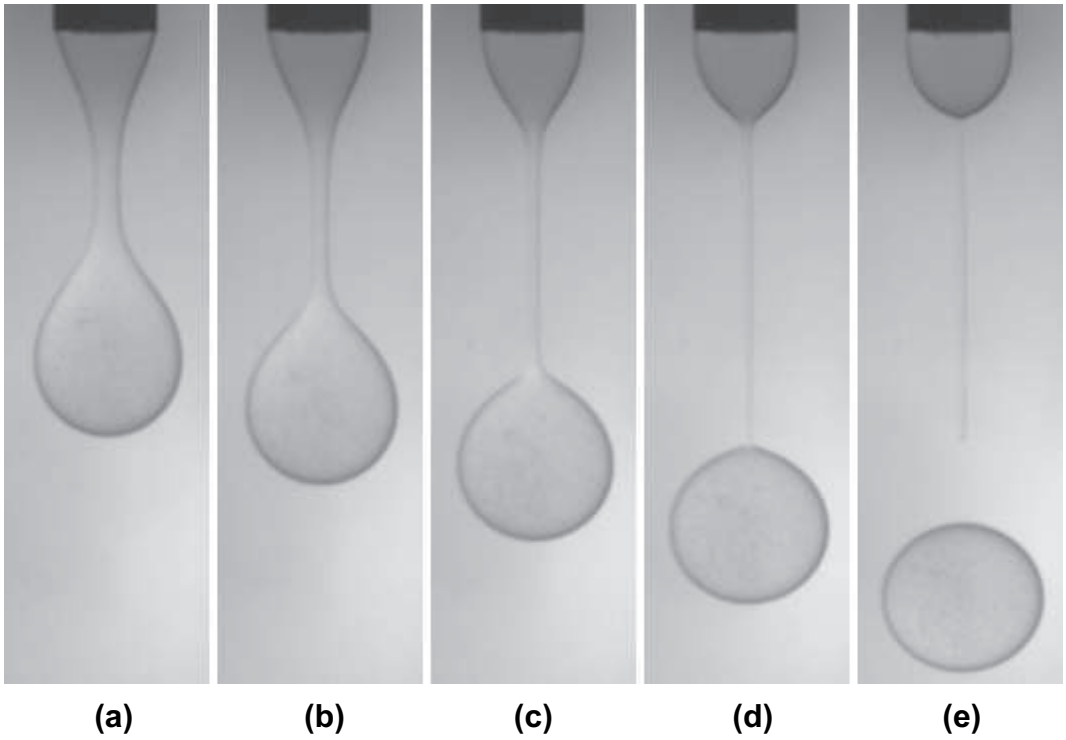

Figure 14: Evolution of the liquid thread up to and slightly beyond pinch-off for $\phi = 0$, $d = 0.32$ cm into silicone oil with $Q = 1.8$ cm^3/min ($Re = 0.04$). Time between frames is 1/30 s.

$\phi = 0.05$ ($d_p = 212 - 250$ μm) respectively for the same conditions ($d = 0.32$ cm, $Q = 1.8$ cm^3/min, $Re = 0.04$). The time between frames is 1/30 s. In both instances the drops are formed into silicone oil which slows the necking process (relative to flow into air) and allows for direct visualization of the particles.

In the case of the pure liquid (Figure 14) a thread is formed as the drop falls away from the orifice. This liquid thread continues to stretch and undergo necking, eventually rupturing near the trailing edge of the forming drop. This result is similar to that observed by numerous researchers of pure liquid drop formation [23, 37, 44, 55].

The particle-laden case is illustrated in Figure 15. The particles are initially randomly and uniformly distributed throughout the liquid as it flows through the orifice and into the hanging drop; the relative uniformity is illustrated by the first

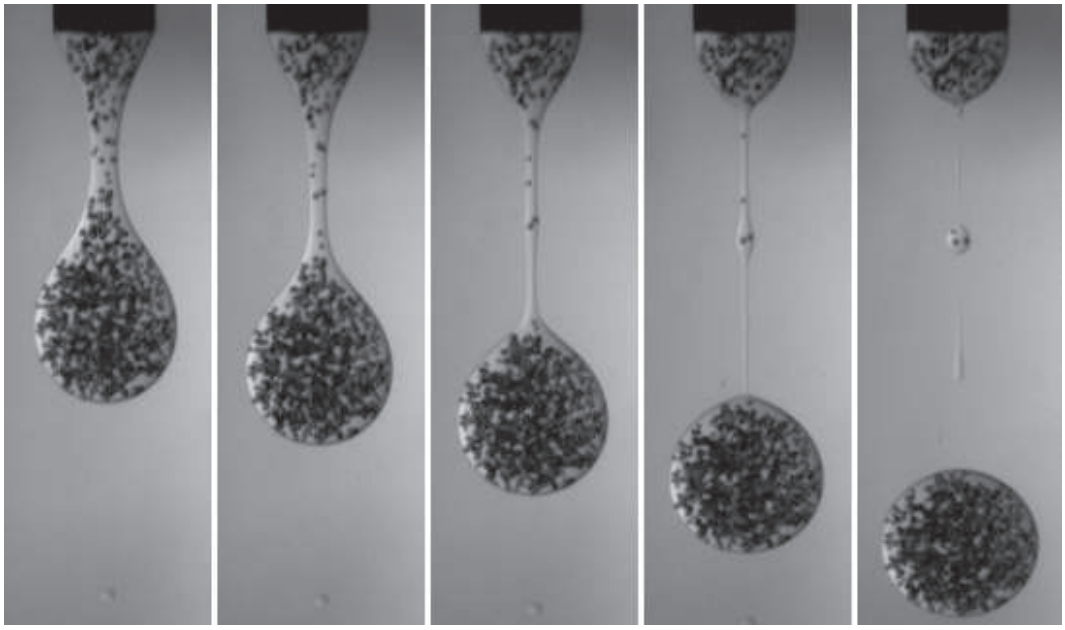

Figure 15: Evolution of the suspension thread up to and slightly beyond pinch-off for $\phi = 0.05$, $d = 0.32$ cm, $d_p = 212 - 250$ μm into silicone oil with $Q = 1.8$ cm^3/min ($Re = 0.04$). Time between frames is 1/30 s.

image, Figure 15(a), even though at this time it is clear that necking has already begun to influence the particle distribution. The early stage of necking occurs in a fashion similar to that observed for the pure liquid as may be seen from the similarity of the shapes in the two earliest photographs, (a) and (b), from each of Figures 14 and 15. However, the presence of the particles and their distribution within the forming thread introduce novel features not seen in pure liquids as the thread progresses toward rupture. Depending on the random distribution of particles in the liquid when necking begins many possibilities exist.

At a time very shortly following that of Figure 15(b) resistance to further narrowing by the two particles in the center of the liquid thread induces a bulging of the thread. Particles located below this point are completely swept into the forming drop before rupture while those above it are retracted towards the orifice—with a single exception. Surprisingly, the two particles located directly above the central pair move in opposite directions (Figure 15(c)-(d)). The particle slightly closer to the orifice actually returns to join the liquid at the tip of the orifice while the lower particle remains in nearly the same location, and is eventually incorporated into the satellite drop seen in (Figure 15(e)). This sequence is only one illustrative example for a low-ϕ suspension as the thread width approaches that of the particle size.

3.1.2 Pinch-off structure

The presence of particles in the liquid leads to pinch-off structures which are qualitatively different from those seen for the pure liquid. At low particle concentrations (up to $\phi \approx 0.10$) the macroscopic behavior of the structure near pinching is very similar to that of the pure liquid, as illustrated by Figure 16 where again drops are formed into silicone oil.

Notably, the shape of the forming drop is that of the "needle-sphere" configuration typical for pure liquids [23, 37, 44, 55] in which a slender, needle-like liquid thread

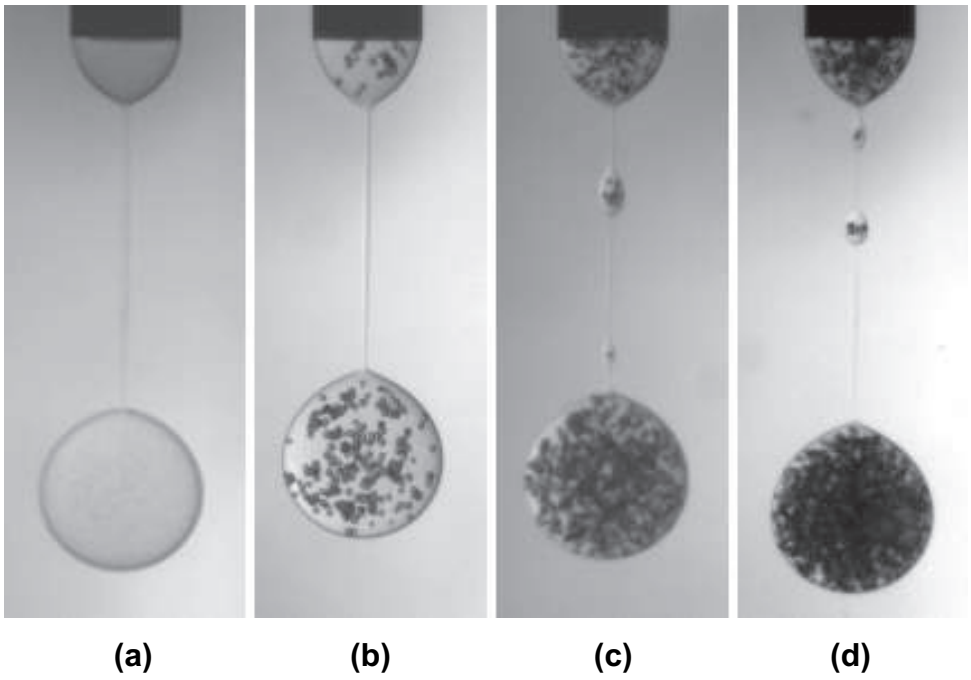

Figure 16: Representative pinch-off structures for the pendant drop formation of suspensions of (a) $\phi = 0$, (b) 0.02, (c) 0.05, and (d) 0.10 into ambient silicone oil for $d = 0.32$ cm, $d_p = 212 - 250$ μm, $Q = 0.35$ cm^3/min ($Re = 0.007$).

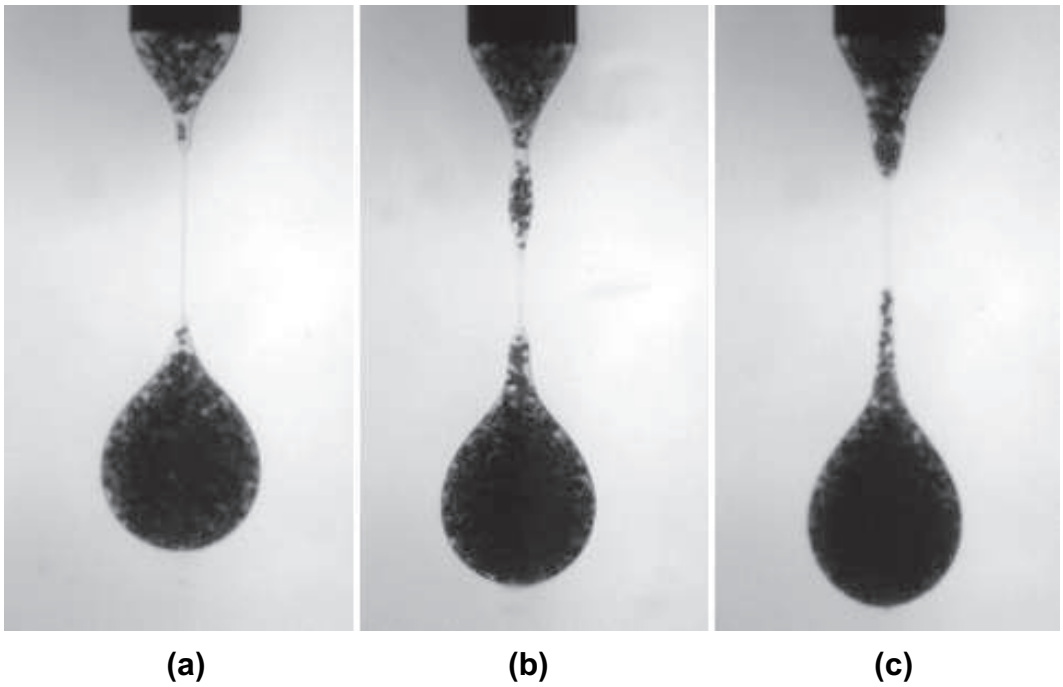

Figure 17: Representative pinch-off structures for the pendant drop formation of suspensions of (a) ϕ=0.15, (b) 0.20, and (c) 0.25 into ambient silicone oil for d = 0.32 cm, $d_p = 212 - 250$ μm, $Q = 0.35$ cm^3/min ($Re = 0.007$).

connects the liquid at the tip of the capillary orifice to the nearly spherical drop. The subsequent rupture occurs near the point of attachment of the thread to the drop. Although the overall pinch-off shape up to moderate ϕ is similar to that of the pure liquid, the presence of the particles leads to fundamentally different behavior simply because individual or groups of particles may be captured in the thread during necking. In this event, more common at higher ϕ but observed even at $\phi = 0.02$, single particles or groups of particles resist stretching and prevent further thinning of the thread. This leads to the generation of satellite drops not observed for pure liquid, as illustrated by Figure 15 in the preceding subsection.

As the particle concentration is increased beyond $\phi \approx 0.10$, as illustrated in Figure 17 for drops into silicone oil, larger numbers of particles are present in the liquid thread during the early stages of necking. As necking proceeds, these particles are

forced out of the thinning thread back up towards the capillary tip and down into the forming drop. These particle motions create new structures, which are thicker and more cone-shaped than observed for the pure liquid. These structures at the ends of the liquid thread result in a more gradual transition from the thread to the liquid at the capillary tip and at the tail of the forming drop. We term these structures "spindles" due to this descriptive term used for similar structures observed in electrohydrodynamic sprays [25] although obviously under very different conditions. These spindles are also similar to particle structures observed by Schaflinger & Machu [40] and Nicolas [32] who have examined dense suspensions falling under gravity into the suspending liquid and hence in the absence of interfacial tension. These authors describe particle tails developing behind the falling drops which appear similar to those observed here.

The spindle structures we observe become more pronounced with increasing ϕ, and the length of the region over which final necking occurs is much shorter than that observed for pure liquid and lower ϕ ($L_N \approx 0.6$ for $\phi \leq 0.10$ and decreases to $L_N \approx 0.3$ for $\phi = 0.25$). In addition, at higher ϕ pinch-off occurs higher on the thread away from the edge of the forming drop, the shape of which has become more pear-like than spherical. The presence of the particles also leads to significant variability in the ultimate location of pinch-off along the thread depending on the size of the spindles which develop.

Pinch-off from two additional orifice diameters (0.16 and 0.64 cm) was also examined using the same suspension of d_p = 212-250 μm. In both instances, the overall trends with increasing ϕ are similar to that presented above for the 0.32 cm orifice (Figures 18 and 19). The number of particles captured in the neck at pinch-off does, however, depend strongly on the orifice size. The smallest orifice is characterized by very short necks with particles rarely captured in the neck. As d increases, the pinch-off length and number of particles in the neck both increase.

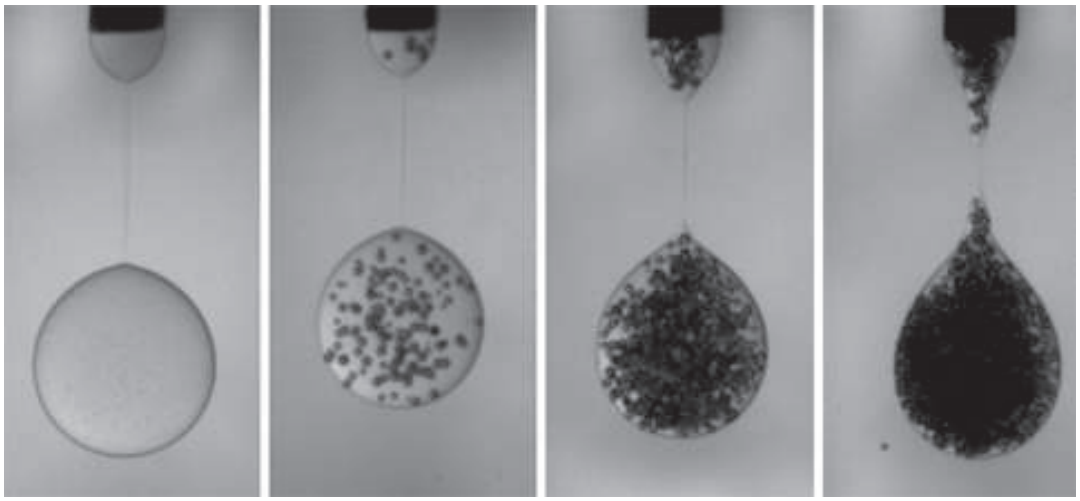

Figure 18: Pinch-off structures for the pendant drop formation of suspensions of (a) $\phi = 0$, (b) 0.02, (c) 0.10, and (d) 0.25 into ambient silicone oil for $d = 0.16$ cm, $d_p = 212 - 250$ μm, $Q = 1.8$ cm^3/min ($Re = 0.08$).

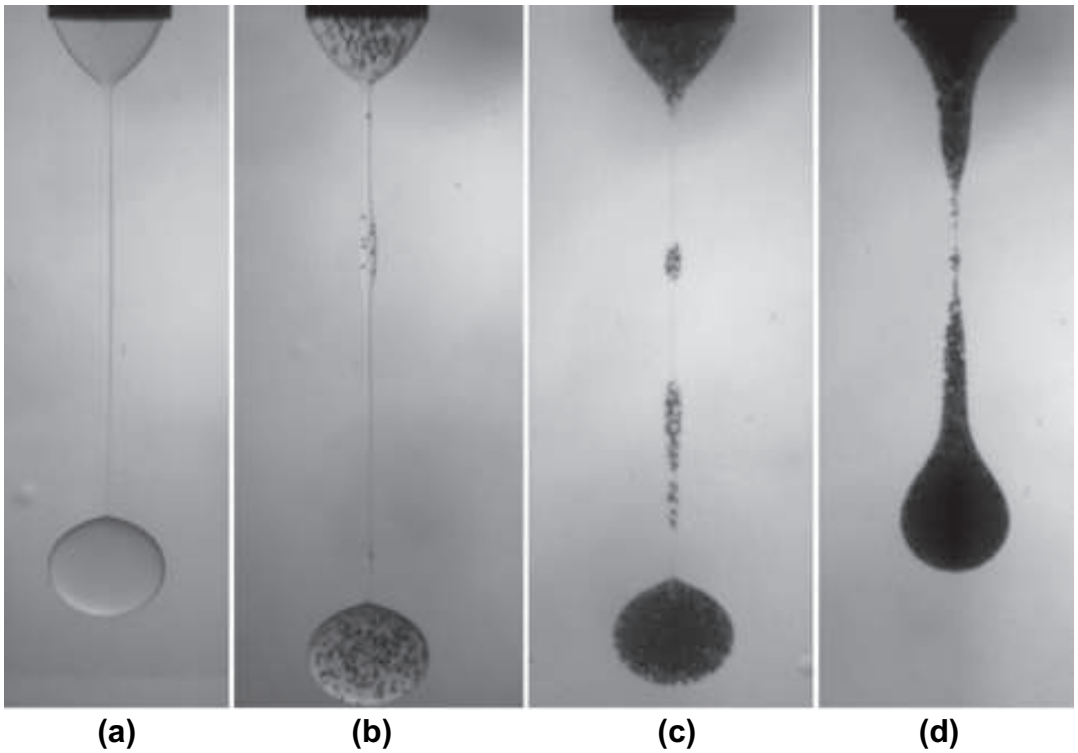

Figure 19: Pinch-off structures for the pendant drop formation of suspensions of (a) $\phi = 0$, (b) 0.02, (c) 0.10, and (d) 0.25 into ambient silicone oil for $d = 0.64$ cm, $d_p = 212 - 250$ μm, $Q = 1.8$ cm^3/min ($Re = 0.02$).

3.1.3 Evolution of the thread at higher ϕ

In addition to qualitatively altering the shape of the structure at pinch-off, the particles also lead to much different behavior of the developing thread as the drop falls away from the tip of the capillary. In contrast to the results presented above, those presented here are for drops forming into air. The forming drops are thus dark in the photographs.

In Figure 20, the evolution of the thread up to and beyond rupture for the pure liquid and a suspension of $\phi = 0.20$ are compared. The time between consecutive frames is 1/250 s. The two photographic sequences are arranged such that the frames just before pinch-off (marked with asterisks) in each case are aligned.

In the case of the pure liquid a nearly symmetrical neck rapidly develops (second or third image in Figure 20(a)) which narrows uniformly as it undergoes elongational stretching and finally ruptures at either end forming a single satellite drop. Immediately after rupture the drop is very nearly spherical and the liquid remaining at the tip of the orifice resembles a hemispherical cap.

The high-ϕ suspension presents a significant contrast, as necking occurs more slowly and appears to occur in two stages. The initial necking stage is characterized by a relatively thick, particle-laden neck which develops essentially symmetrically about its midpoint. This stage is similar to that of the pure liquid although the neck is wider and elongation occurs more slowly. Final necking begins in image seven or eight of Figure 20(b), where a fluctuation in ϕ is evident. It is in the region of this concentration fluctuation that final necking occurs, as a slender, particle-free region develops into a pure liquid thread which rapidly stretches and breaks. The suspension also shows the characteristic spindle structures, with the upper spindle much more pronounced in this example. The spindles retract slowly following rupture resulting in a situation much different from that described above for the pure liquid: here we see a non-spherical drop with a "tail" and a long retracting spindle near the orifice.

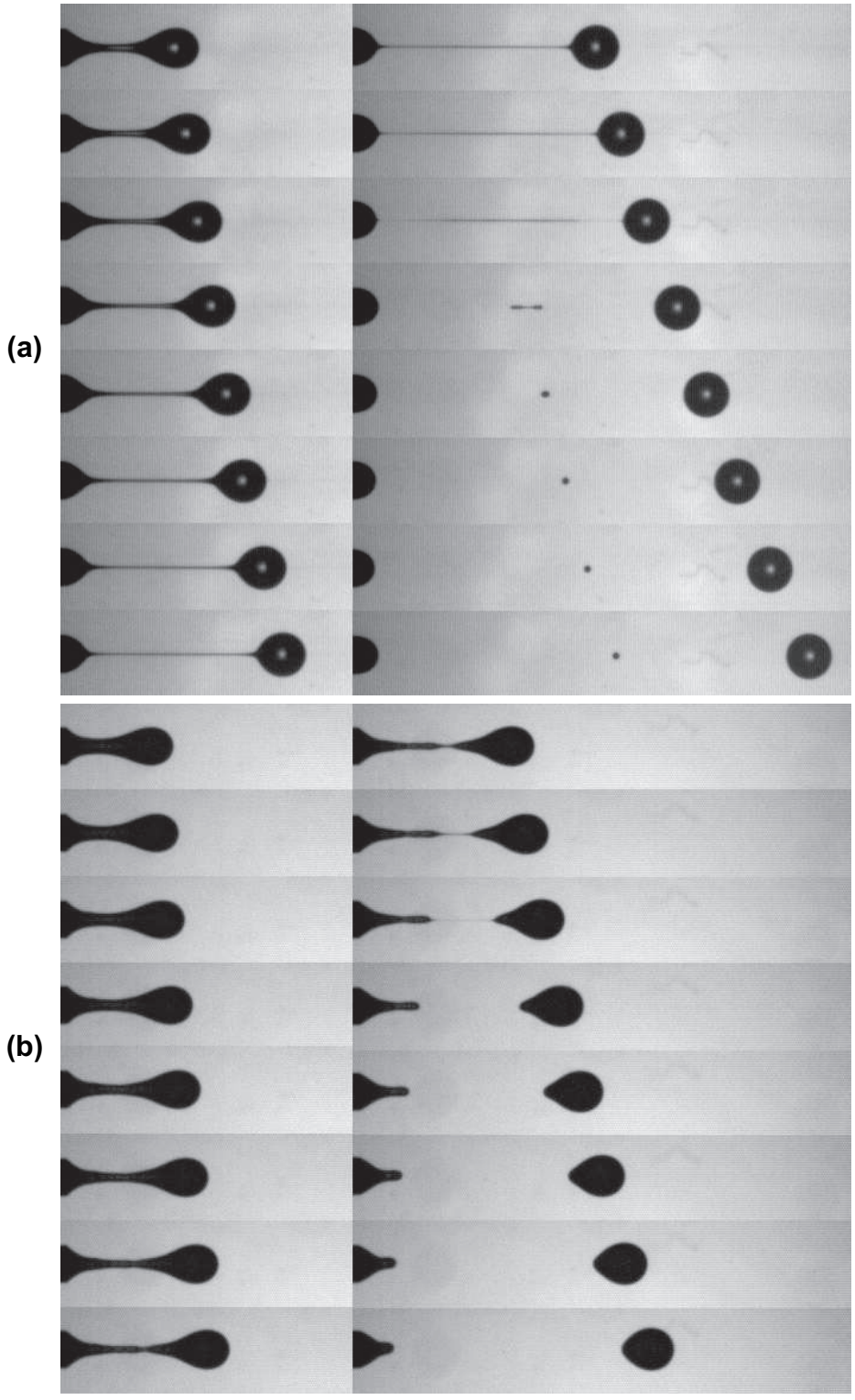

Figure 20: Evolution of the liquid/suspension thread during necking through pinching for pure liquid (a) and suspension ($\phi = 0.20$) (b) into ambient air for $d = 0.32$ cm, $d_p = 212 - 250$ μm, $Q = 0.5$ cm^3/min ($Re = 0.01$). Time between frames is 1/250 s. Gravitational acceleration is to the right.

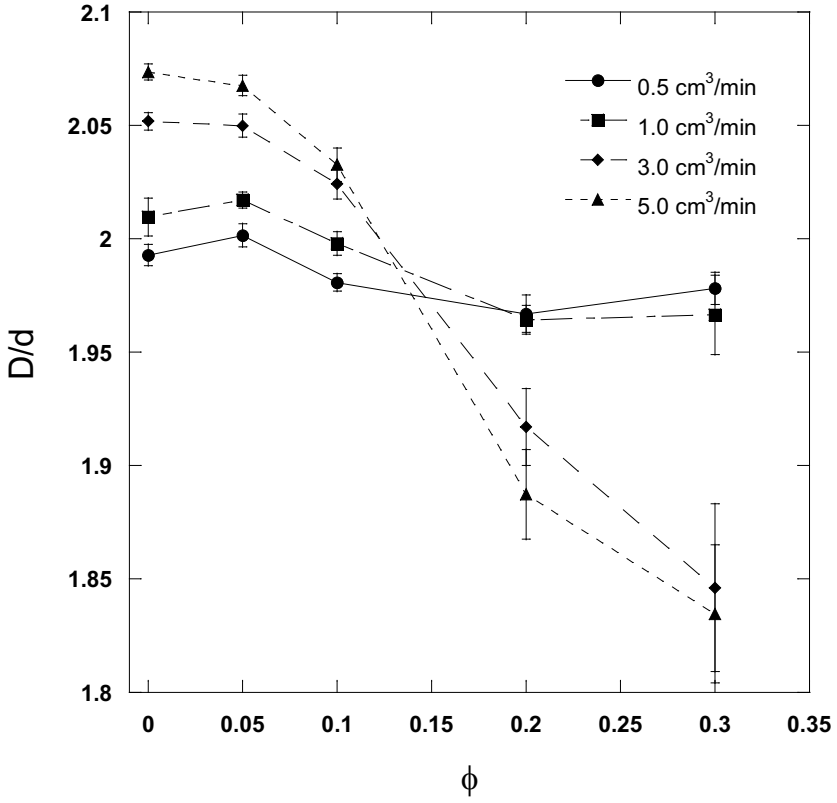

Figure 21: Dimensionless primary drop size (D/d) for drops forming into ambient air as a function of ϕ for $d = 0.16$ cm, $d_p = 212 - 250$ μm.

The necking dynamics described here is the focus of the next chapter in which this process will be investigated more thoroughly.

3.2 Drop formation and satellite drop generation

Following pinch-off of the liquid thread a primary drop is formed. This formation may be accompanied by subsequent breakup of the retracting thread into smaller, satellite drops. In order to assess the influence of suspended particles on this process, measurements were made of the primary drop size as well as the number and size of satellites formed as a function of ϕ for a range of Q. In these experiments Q was sufficiently low that drops are formed pendantly for $\phi = 0$.

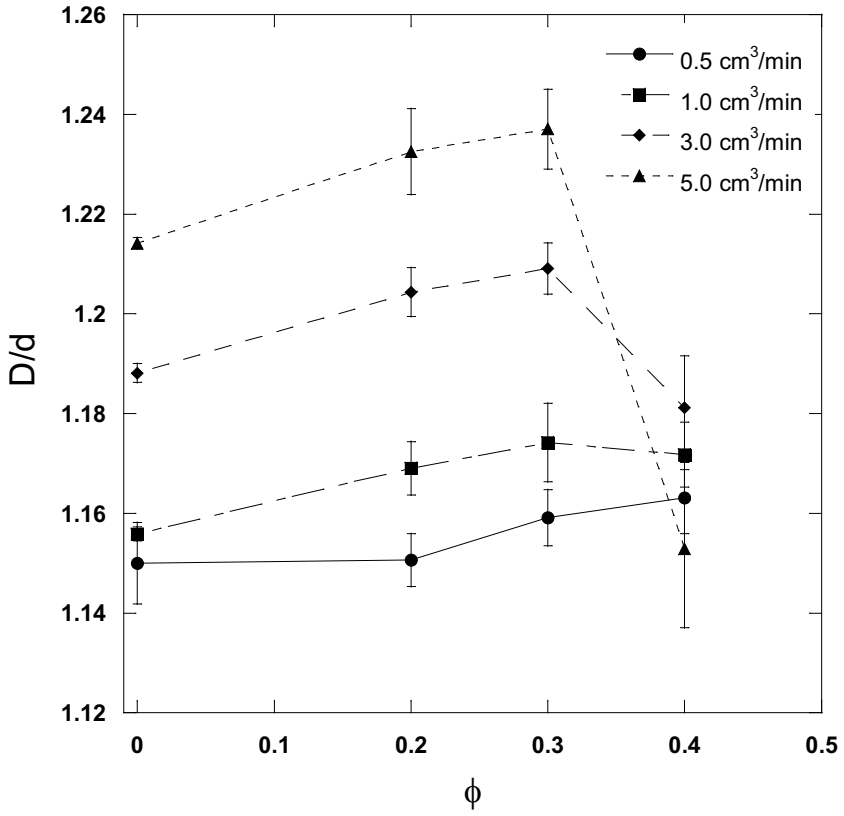

Figure 22: Dimensionless primary drop size (D/d) for drops forming into ambient air as a function of ϕ for $d = 0.32$ cm, $d_p = 212 - 250$ μm.

3.2.1 Drop size

Figures 21 and 22 illustrate how the primary drop size changes with ϕ for two orifice sizes: $d = 0.16$ and 0.32 cm. For each flow rate the dimensionless drop size (D/d) is plotted against ϕ. The drop size was determined using the MATLAB image analysis toolbox to detect the edge of the drop from photographs and, assuming axisymmetry, the volume was computed (as described in Chapter 2) as $V_{\text{drop}} = \pi \int [R(z)]^2 dz$ where R is the detected radius of the drop and z is in the direction of gravity; the effective diameter was determined by solving $V_{\text{drop}} = (1/6)\pi D^3$ for the diameter. This approach was required to assess the size of non-spherical drops prevalent at the imaging location for higher ϕ; the drops relax to spherical as they fall. The diameters of the pure liquid drops measured here agree well with those predicted using the Harkins-Brown factor [22] as well as the correlation developed by Scheele & Meister [41], being consistently slightly (from 1–6%) smaller than predicted in this case. This is consistent with results reported by Zhang & Basaran [55] and serves to validate our technique.

At low flow rate, $Q = 0.5$ and 1 cm^3/min, little effect of ϕ on drop size is observed for either the $d = 0.16$ cm (Figure 21) or $d = 0.32$ cm (Figure 22) orifice. Although there appears to be a slight decrease with ϕ for the smaller orifice and a slight increase for the larger these changes are small compared with the changes at higher flow rates. For $Q = 3$ and 5 cm^3/min, both orifices show a marked decrease in drop size with increasing ϕ. The results indicate that the decay of drop size with ϕ depends upon the orifice size or its ratio to the particle size: the decay begins at higher ϕ for the larger ($d = 0.32$ cm) orifice and is less pronounced than in the case of the small orifice, while decay begins essentially at $\phi = 0$ for the smaller ($d = 0.16$ cm), with the largest decrease occurring as ϕ is increased from 0.10 to 0.20. Accompanying this increase in concentration is a change in behavior to one in which higher flow rate no longer corresponds with larger drop size; this is counter to the observed trend for the pure

liquid and lower concentrations.

The negligible changes in drop size at the lowest flow rates for both orifices indicate that the particles have a negligible effect on the balance between surface tension and gravity. At these low flows the Harkins-Brown theory for predicting drop sizes is still valid based on these measurements. The observed decrease at higher flow rates indicates that the particles are inducing more jet-like behavior and that the drops are no longer forming in a purely pendant manner. This effect will be further examined in Chapter 5 when we investigate the transition from dripping to jetting.

3.2.2 Satellite drop formation

An unanticipated result of these experiments is the inhibition of satellite drop formation with increasing ϕ. As presented in Figure 16 and remarked upon in section 3.1 the presence of particles in the neck at the time of thread rupture could be expected to lead to the generation of more satellite drops than that of the pure liquid. This does, in fact, seem to be true for suspensions of very small ϕ (Figure 23) where a slight increase in the number of satellite drops formed is observed for some flow rates. The behavior at high ϕ is markedly different. As the particle concentration increases, satellite drop generation falls off rapidly.

Although Figure 23 indicates that the average *number* of satellites decreases quite dramatically with ϕ it tell us nothing of the *size*. The size information is presented in Figure 24 which contains plots of the total volume of satellite drops formed for each pinch-off event observed during the course of an experiment; satellite drop volume was assessed by direct measurement of diameter after the drops became spherical. The pure liquid forms a nearly constant volume of satellite drops (≈ 0.5 mm^3) for each primary drop. This behavior is changed quite radically by the addition of even a small particle fraction, as seen for the results at $\phi = 0.02$ where the satellite-drop volume becomes scattered. As ϕ is increased, the instances in which even a single

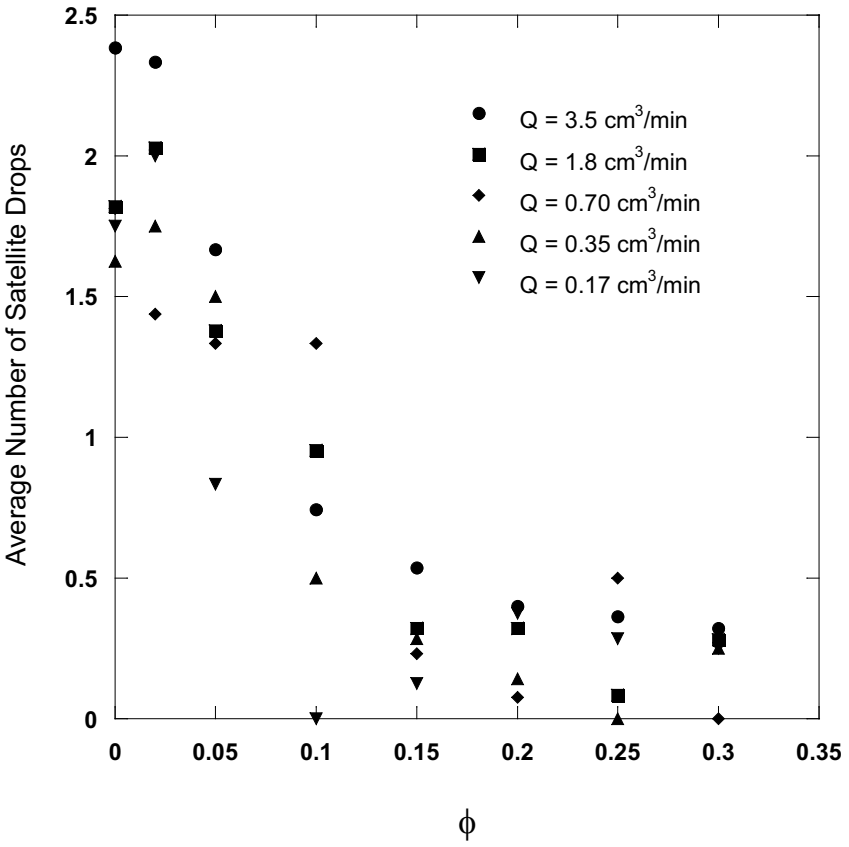

Figure 23: Average number of satellite drops formed as a function of ϕ for drops forming into ambient air for $d = 0.32$ cm, $d_p = 212 - 250$ μm.

satellite drop is formed become relatively few, but these few are much larger than observed for pure liquid.

The manner in which satellite formation is affected by suspended particles is illustrated in Figures 25 and 26, which compares the evolution of the suspension column and subsequent thread rupture for two drop formation events for a concentrated suspension of $\phi = 0.40$. In the first case (Figure 25), pinch-off occurs near the middle of the thread with two long spindles eventually retracting without generation of satellite drops. This case occurs most frequently and results from final necking and pinching in a single location, usually near the center of the thread. The other case (Figure 26) is the result of nearly simultaneous pinching in two separate locations near the ends of the thread. This rare dual pinching leads to the formation of a large, concentrated satellite drop.

3.3 Discussion

In the preceding two sections, our goal was to present, with limited interpretation, the results of many experiments to illustrate the pinch-off behavior of particle-laden liquids in the dripping (or pendant drop) mode. Here, we discuss the experimental results with a focus on elucidating the effects introduced by the particles, with the primary goal of gathering certain ideas which provide insight to general features of particulate influence on the drop formation processes we have studied. Critical to this goal is an examination of the drop formation process both for dilute suspensions, where the process occurs in a manner similar to that of the pure liquid with some notable differences, and for more concentrated suspensions, where the process as a whole is different. We will also address the inadequacy of a continuum description of the mixture during drop formation due to finite-size effects of individual particles.

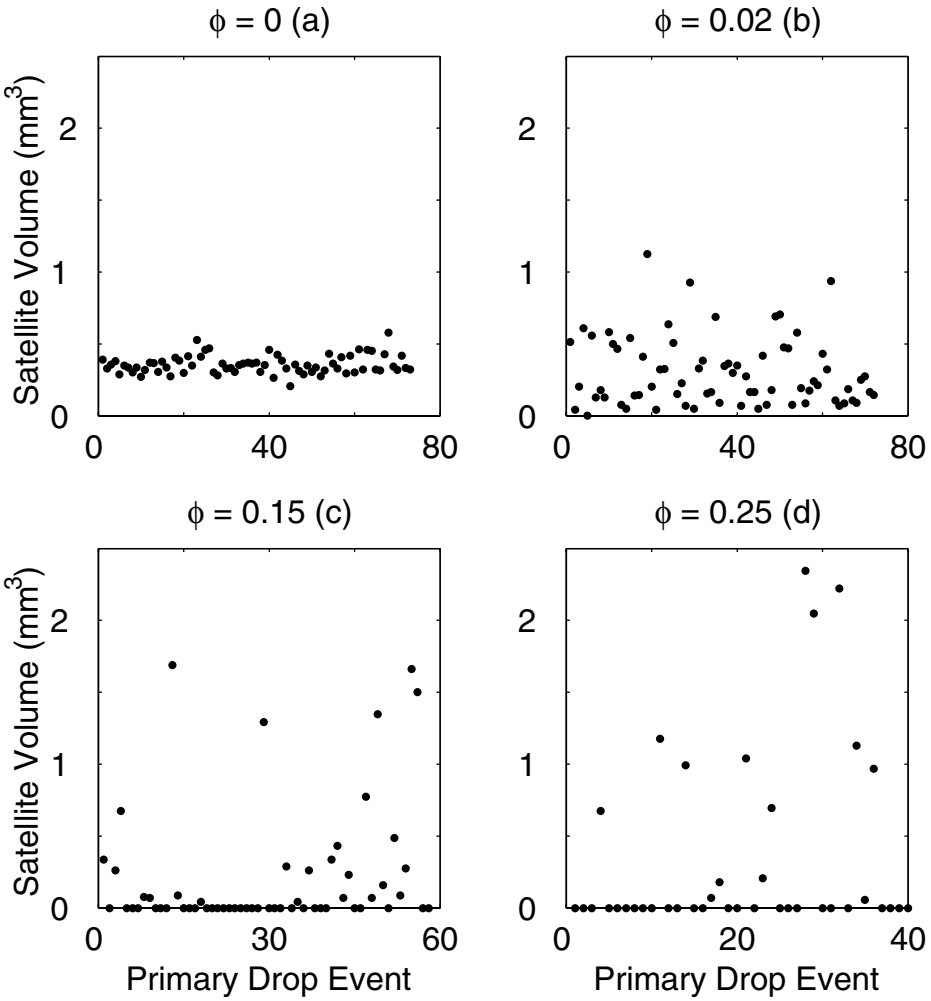

Figure 24: Total volume of satellite drops formed for (a) ϕ=0, (b) 0.02, (c) 0.15, and (d) 0.25 into ambient air for $d = 0.32$ cm, $d_p = 212 - 250$ μm, $Q = 3.5$ cm^3/min ($Re = 0.07$). The abscissa represents the number of primary drop events observed over the course of an experiment (for example, for $\phi = 0$ slightly less than 80 primary drops were observed).

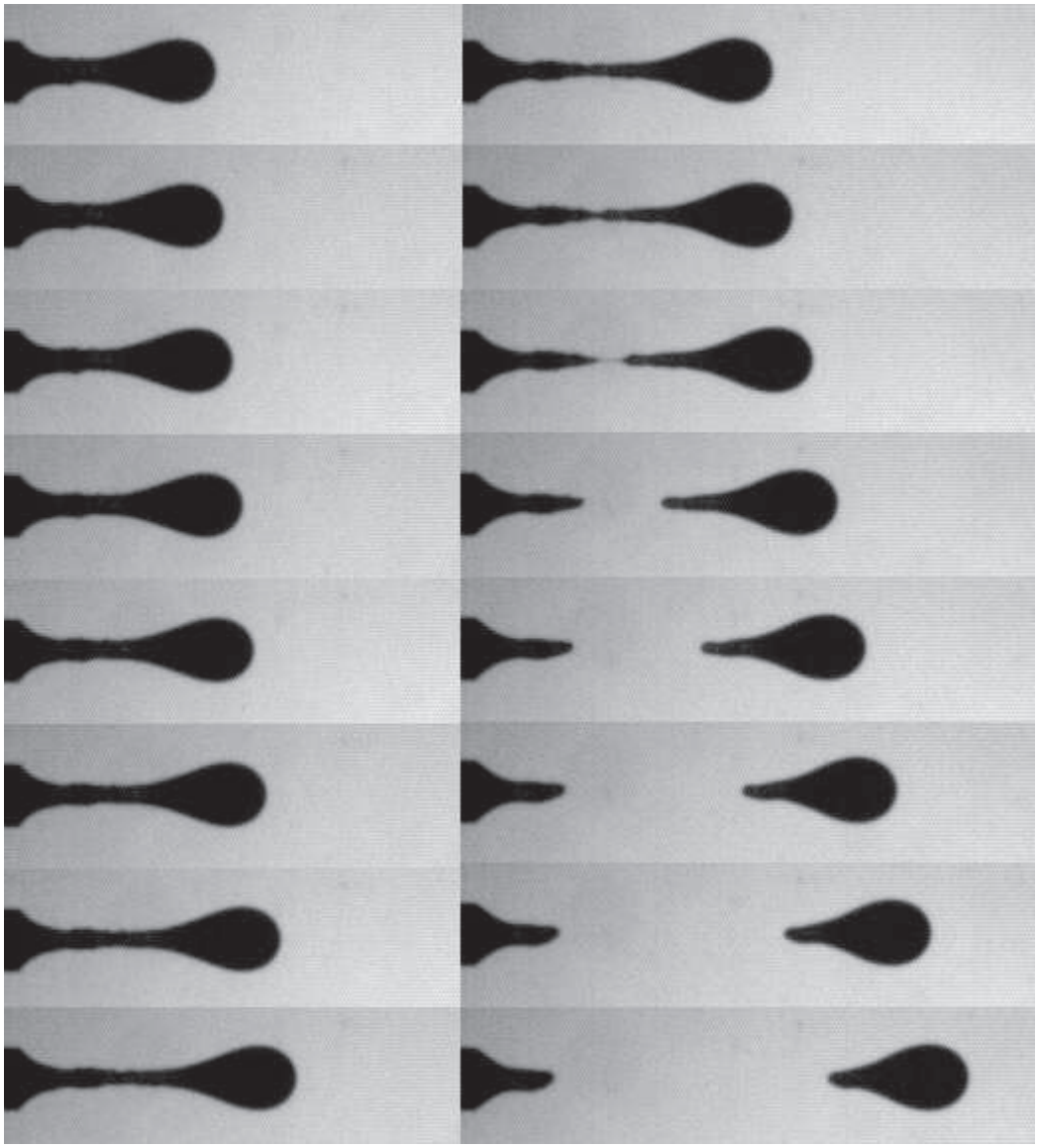

Figure 25: Evolution of the thread through pinching for $\phi = 0.40$ into ambient air for $d = 0.32$ cm, $d_p = 212 - 250$ μm, $Q = 0.5$ cm^3/min ($Re = 0.01$) illustrating the case where satellite drops are suppressed due to a single pinch-off event with stable retraction of the top and bottom spindles.

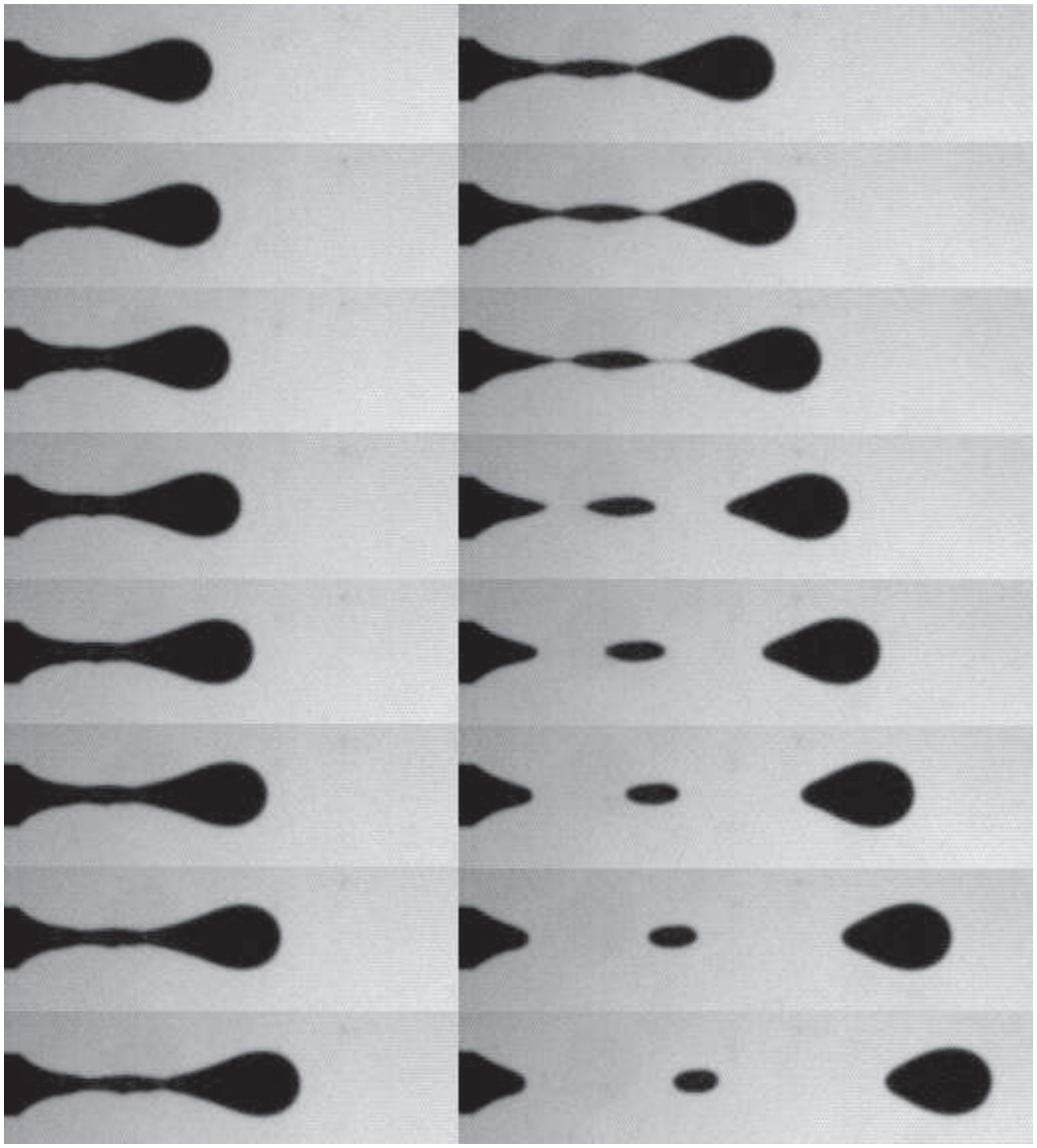

Figure 26: Evolution of the thread through pinching for $\phi = 0.40$ into ambient air for $d = 0.32$ cm, $d_p = 212 - 250$ μm, $Q = 0.5$ cm^3/min ($Re = 0.01$) illustrating the case where a single, large satellite drop is produced due to nearly simultaneous double pinching.

3.3.1 Particle fraction dependence in the dripping mode: low- and high-ϕ behavior

Although the drop formation process in the dripping mode continuously changes with increasing ϕ, it is illustrative to examine the two extreme ϕ studied here. Consider the behavior exhibited by the $\phi = 0.05$ suspension presented in Figure 15. Although initially the particles are apparently uniformly distributed in the forming drop, the determining factor in how the eventual drop is formed is the location of the particles within the thread once necking begins. Just before necking begins, the particles have a certain configuration and it is this configuration which ultimately determines whether particles are captured in the neck at thread rupture. If particles are captured in the liquid thread there are two consequences. First, the thread will be unable to attain the same length as in the case of the pure liquid, because continued uniform thinning of the stretching thread beyond the particle size is impossible. Second, the breakup of the thread following initial rupture will occur differently than is observed in secondary breakup of a pure liquid thread. These two effects at low ϕ can be interpreted as particles causing a destabilization of the liquid thread.

For $\phi = 0.40$, as shown in Figures 25 and 26, the process proceeds differently. Just prior to necking, there are many more particles present than in the low-ϕ case. The motions of these particles are restricted within the developing thread by their close proximity to neighbors. This contrasts with the low-ϕ case, where particles are nearly free to move within the thread until the thread width has thinned to a few particle diameters. The close packing of particles at $\phi = 0.40$ results in a resistance to necking, making it difficult for the particles to rearrange and accommodate further stretching. We observe that for thread rupture to occur a particle-free cross-section of the thread must develop, and as noted above, the location of rupture is dependent on the distribution of particles when necking begins and can occur anywhere

along the length of the thread. It appears most likely the rupture results at a position determined by existing (as opposed to dynamically-induced) fluctuations in ϕ which become more pronounced relative to the mean—with consequently large material property fluctuations—as the thread diameter becomes small. Following thread rupture the large number of particles present in the top and bottom spindles resist necking to the small scales necessary for secondary rupture and the accompanying generation of satellite drops. Both this and the initial resistance to necking lead us to conclude that large ϕ provides a stabilizing effect on the liquid thread, whereas small ϕ induces large fluctuations which are destabilizing. The cross-over is in the vicinity of $\phi = 0.10 - 0.15$ for the situations probed by our work.

3.3.2 Continuum breakdown

One typical technique employed in modelling the flow of suspensions is to neglect the discreteness of the solid particles and account for the particulate phase through an increased effective mixture viscosity, such as the well-known Krieger [26] form

$$\mu_{\text{eff}}(\phi) = \mu(1 - \phi/\phi_{\max})^{-1.82} \tag{8}$$

with μ the suspending liquid viscosity and $\phi_{\max}$ an empirically determined maximum packing fraction (throughout this work we will use the Krieger equation to approximate the suspension viscosity and have made no attempt to optimize the formula). We find, not unexpectedly, that the continuum approach breaks down at small thread diameters and, more surprisingly, that the use of an effective viscosity does a very poor job of explaining the L/d behavior at pinch-off in the dripping mode.

Comparing our results for pinch-off structures with those of Shi *et al.* [44], we observe a similarity between our concentrated suspensions (Figure 17) and their high viscosity pure liquid (glycerin, $\mu = 12$ P). Specifically, these authors noted a change in pinch-off structure with increasing viscosity similar to that observed here due to increasing ϕ: the structures changed from needle-and-sphere configurations to the

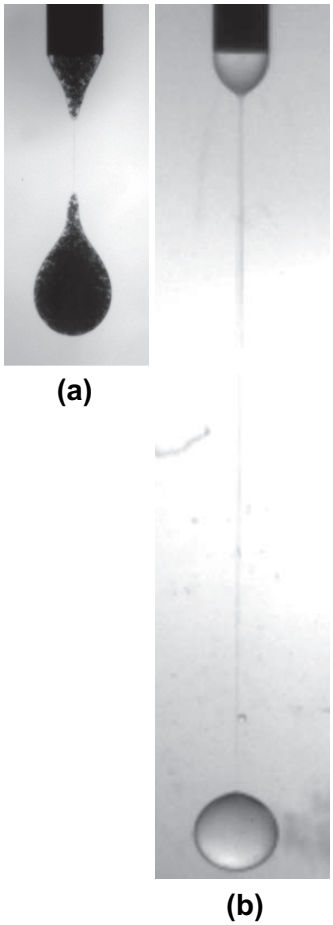

Figure 27: Comparison of the pinch-off structure of a suspension of $\phi = 0.25$, $d_p = 212 - 250$ μm (a) and that of a pure liquid mixture with the same components as the suspension although with different quantities such that the resulting viscosity is ≈ 10 P equal to the effective viscosity of the suspension (b). The ambient fluid is silicone oil in both cases and $Q = 0.35$ cm^3/min.

pear-shaped drops described previously for high-ϕ suspensions. Motivated by this similarity, a suspending liquid mixture of the same three components (in different proportions than described in section 2.2) was prepared such that the viscosity was $\mu \approx 10$ P. This viscosity is nearly equivalent to the effective viscosity obtained using the Krieger empirical correlation for the $\phi = 0.25$ suspension in the $\mu = 4$ P suspending liquid used in our other experiments, assuming $\phi_{\max} = 0.64$. Drops were formed into silicone oil using this more viscous pure liquid and compared with the results from the previous, particle-laden, experiments (Figure 27).

From Figure 27 it is clear that the effective viscosity of the suspension does not determine the behavior at pinch-off. At pinching neither the overall thread length attained nor the structure are at all similar. The higher viscosity pure liquid has a much longer thread length and a structure more similar to that of the pure liquid lower viscosity mixture than the concentrated suspensions. Liquid viscosity is apparently governing the thread length at pinch-off. The change in thread length caused by increasing solid fraction from $\phi = 0$ to $\phi = 0.25$ is negligible compared with the change from increasing the viscosity of the pure liquid.

The pinch-off structures formed are also not similar. The concentrated suspension pinch-off structure is pear shaped, while the equivalent viscosity pure liquid retains the needle-sphere structure. (This may appear to be a contradiction of the results of Shi *et al.* [44], but is, in fact, not because the drops formed here were into silicone oil rather than air as in the cited work.) This indicates that it is not simply a contribution to the effective shear viscosity of the mixture made by the particles which governs the pinch-off shape of the suspension. The discrete size of the particles as they are forced out of the liquid thread during necking apparently also plays a role due to clustering of particles in regions at either end of the thread. The clustered particles are unable to rapidly integrate into the liquid cap at the orifice or into the forming drop. This causes the formation of the spindles and thus alters the geometry at pinch-off.

Both of these observations seem to preclude the use of standard effective viscosity descriptions in modelling particle-laden drop flows in accounting for the complete process. However, it may be possible to break the process down into two stages for the more concentrated suspensions where the use of an effective viscosity may be warranted in the first stage. These two stages will be referred to here as initial necking and final necking. Initial necking occurs while the thread width is large relative to the particle size. During this stage, the concentration of particles within a segment of thread apparently remains nearly uniform and the main role of the particles seems to

be resisting further thinning and stretching of the thread. Final necking begins once the thread width has thinned to several particle diameters and a significant fluctuation in the concentration is sampled. Once this happens a particle-free region develops and thread rupture rapidly occurs. In this portion of the process, the substantial literature on pure liquid drop formation should be applicable.

3.4 Concluding remarks

In this chapter we have presented an investigation of the formation of pendant drops from suspensions of varying concentration and specifically probed the pinch-off structures formed, the size of the resulting drops, and the generation of satellite drops.

The pinch-off structure of the forming drops change quite dramatically with increasing particle concentration and new structures, termed spindles here, are observed to form at either end of the thread attaching the drop to the capillary orifice. These new structures are the result of particles motions within the thread and are formed when the particles are forced out of the collapsing thread during necking. When this occurs, the particles are unable to rearrange themselves sufficiently to become fully incorporated into either the liquid remaining at the tip of the orifice or into the forming drop.

The evolution of the thread has also been investigated and we have proposed a two-stage model for the necking of concentrated suspensions. In this view, the first stage of necking occurs in a manner similar to that of pure liquids, with an added resistance introduced by the presence of the particles. In this stage a continuum description of the material may be possible and the contribution of the particles accounted for by a change in the effective bulk viscosity. The second stage occurs when the thread has thinned sufficiently that individual particles become important and a region of pure liquid forms along the thread where the ultimate rupture occurs. This model is based on the observations presented in this chapter and will be the focus of the

investigations presented in the next chapter.

Drop size as a function of particle concentration has also been investigated in this chapter with the result that for purely pendant drops the change in size is negligible. There is, however, a marked decrease in the drop size for cases where the flow rate is slightly elevated. This result will be further explored in Chapter 5 where the transition from dripping to jetting is explored; this increase in drop size appears to be due to a new transitory regime between purely pendant drops and fully developed jets which develops at large particle concentrations.

Lastly, we have found that the satellite drop generation is affected by increasing particle concentration and that fewer, but larger, satellite drops are formed at elevated concentrations. This result indicates that the particles have a stabilizing effect on the liquid thread after the initial rupture. The large number of particles within the thread form large spindles which can stably retract into both the liquid at the orifice and forming drop without undergoing secondary rupture. However, in some instances rupture can occur nearly simultaneously along the length of the thread and lead to a single, large satellite drop.

CHAPTER 4

PENDANT DROP FORMATION II: THREAD DYNAMICS

In this chapter we present an investigation of the particle effects on the dynamics of the thread during necking. The results presented in this chapter are from a set of experiments performed separately from those presented in Chapter 3, with increased resolution of the necking area; the resolution is still sufficient to capture the entire pinch-off event within the camera field of view. The goal of these experiments was to examine the necking region more closely than in those previously conducted in order to generate quantitative measurements of the thinning of the thread during necking and as pinch-off is approached.

In the preceding chapter we introduced the idea that the necking process of solids-laden suspensions could be viewed as occurring in two distinct stages. The first stage, termed "initial necking," begins just after the forming drop becomes unstable and starts to fall away from the capillary tip due to gravity. In this stage it appears that the particles' main effect is to slow the process by resisting the thinning of the thread. This observation—that the particles increase the resistance to the thinning and stretching of the thread—indicates that an effective viscosity treatment may possibly account for this added resistance in this first stage.

The second necking stage in the two-stage process we envision for the suspension mixtures, termed "final necking", involves times much closer to the eventual thread rupture. At these times the thread is much thinner and is of the same order as individual particles. A continuum treatment of the mixture in this stage is obviously

Table 4: Parameters for which experiments were performed.

d(cm)	$d_p(\mu$m)	d/d_p	ϕ	Re	Ca	Bo
0.16	106-125	12.8	0-0.30	0.01	0.01	0.6
0.32	106-125	25.6	0-0.40	0.01	0.07	2.4
0.32	212-250	12.8	0-0.40	0.01	0.07	2.4

not possible. In this chapter we explore the applicability of this two-stage necking model and assess several methods to identify the transition between the stages as well as to understand the particulate effects throughout.

4.1 Experiments performed

These experiments focused on examining the low-flow behavior for a wide range of particle concentrations ϕ, for two orifice diameters, $d = 0.16$ and 0.32 cm, and for two particle size distributions, $d_p = 106 - 125$ and $d_p = 212 - 250$ μm (Table 4). The flow rate, Q, in each experiment was fixed so that drops were formed very slowly (≈ 3.5 s between drops) with $Q = 0.25$ cm^3/min for the smaller orifice and $Q = 0.50$ cm^3/min for the larger one so that $Re = 0.01$ throughout. The experimental apparatus is that described in Chapter 2 and the general procedure outlined there is unchanged.

4.2 Thread thinning and stretching

In performing these experiments the primary information sought was the thinning and stretching of the thread as necking occurred. This data was obtained using the measurement techniques described in Chapter 2 to determine both the thread length, $L(t)$, and the minimum thread radius, $R(t)$, as functions of time. These quantities are then made dimensionless by meaningful length scales; the capillary diameter, d, for thread length, and the particle radius, a, for minimum thread radius. The upper bound of each particle size distribution was used in scaling the radius (*i.e.* $2a = 125$ μm or 250 μm). The minimum thread radius at a given time is

determined from the detected width profile of the forming drop ($W(z,t)$), as described in Chapter 2. The minimum thread radius, R, could also have been scaled by the capillary diameter, as is customarily done in pure liquid research, however, the particle radius was chosen in this case in order to focus on the influence of the size of individual particles as thinning progresses toward thread rupture. Figure 28 shows a typical set of L/d and R/a data for a suspension of $\phi = 0.10$ through an orifice of $d = 0.32$ cm with $d_p = 212 - 250$ μm. The photographs in Figure 28 correspond to the times on the x-axis below which they appear.

In Figure 28 both L/d and R/a are plotted as functions of time measured backwards from the pinch-off time, t_0, which is defined as the last picture captured at a given frame rate (500 fps in all the work presented in this chapter). Note that the thread radius for the last three images (corresponding to $t_0 - t \leq 0.004$ s) has fallen below the detection limit. This will, however, not be of great importance since at times very near pinch-off the thread is composed of only liquid and is assumed to thin, and ultimately rupture, in the same manner as pure liquids. Our primary interest will lie further away from pinching (although after necking has begun) where we will attempt to develop an understanding of how the particles effect necking.

4.2.1 Necking data

In this section we present the results for the necking experiments both graphically and photographically. For each experimental condition (d and d_p) the L/d and R/a curves as well as a corresponding photographic sequence of the process are presented for a number of different particle concentrations. The L/d and R/a data from a number of experiments and representative photographic sequences of the drop forming near pinch-off are presented in Figures 29-38. In each graph the results from five separate drop formation events are shown (with one exception: for $\phi = 0$ in Figure 32 only three drop experiments were performed). These graphs are presented in order to

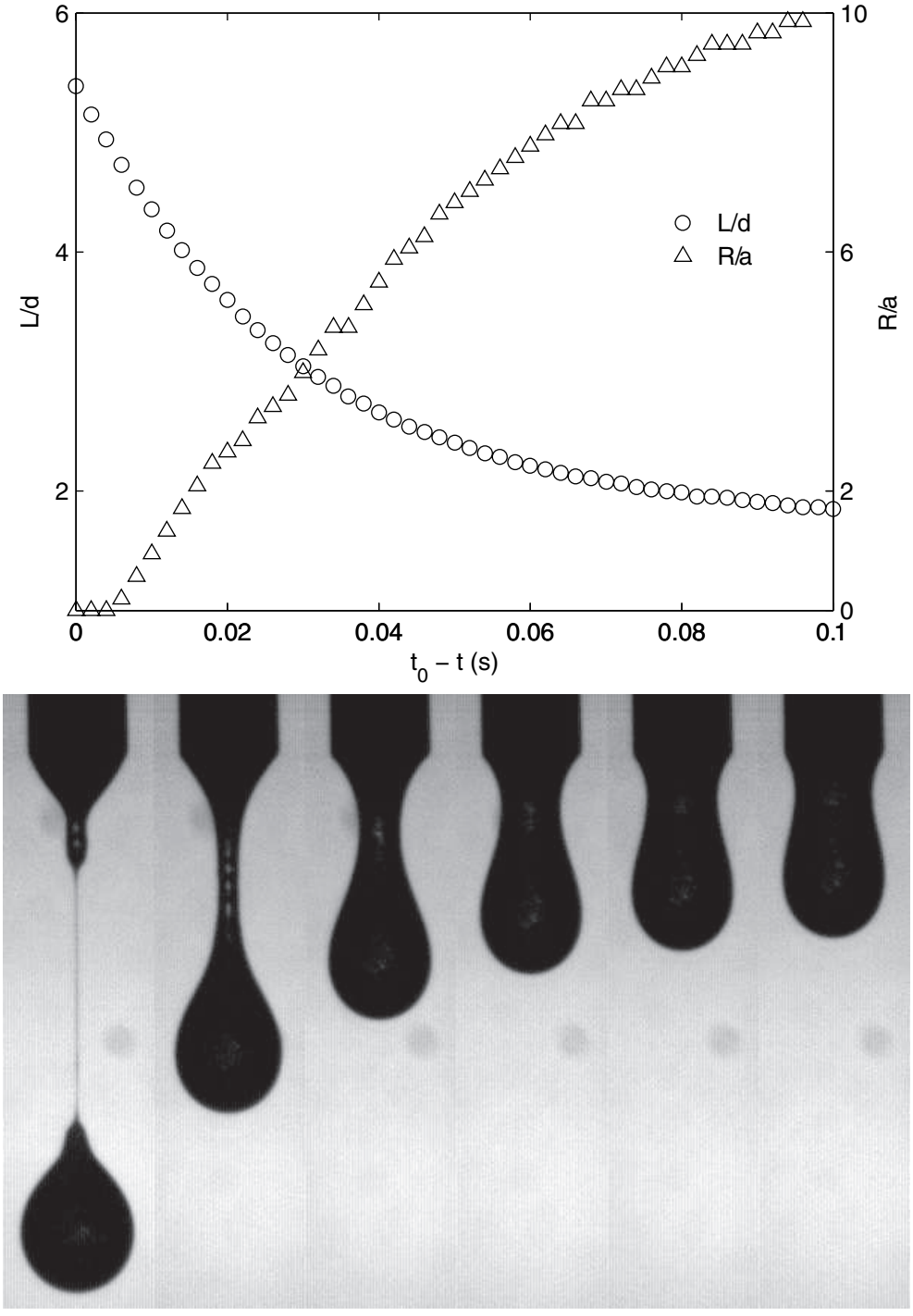

Figure 28: Example of the L/d and R/a curves for $\phi = 0.10$, $d = 0.32$ cm, and $d_p = 212 - 250$ μm. The photographs correspond with the times below which they appear.

describe the necking behavior of the various suspensions examined and to introduce the idea of particle-induced fluctuations. While the L/d and R/a curves in each graph show the results from a number of different experiments, the photographic sequences only present one drop event and are used to illustrate the qualitative changes resulting from concentration changes.

4.2.1.1 Smaller orifice ($d = 0.16$ cm)

In Figure 29 the L/d and R/a curves show the behavior for the smaller of the two orifices examined, $d = 0.16$ cm with $d_p = 106-125$ μm, for the pure liquid, $\phi = 0$, and the most concentrated suspension investigated for this orifice, $\phi = 0.30$. The primary effect of the particles on the L/d curve is to introduce increased variability as pinch-off is approached. This is clearly evident from the L/d curve for $\phi = 0.30$. The ultimate pinch-off length, however, is only mildly affected by the addition of particles with a slight decrease observed. The R/a data for the two cases illustrate some key differences between the pure liquid and the concentrated suspension. As seen for the L/d data, the addition of particles introduces increased fluctuations in the thread radius which become most pronounced at $t_0 - t \leq 0.04$ s. The highly concentrated suspension thread thinning also differs significantly from the pure liquid at either end of the R/a curve. Near pinch-off, the slope of the R/a curve for the $\phi = 0.30$ suspension becomes quite steep, which is a marked contrast from that observed for the pure liquid. At the other end of the R/a curve, away from pinch-off, the effect of the particles is to depress the curve and decrease the slope.

Figures 30 and 31 present photographic sequences for the two conditions shown in Figure 29. In these figures the drop formation event is shown for times before pinching ($t_0 - t \leq 0.028$ s) as well as for a short time after pinch-off ($t_0 - t \geq -0.010$). Comparing these figures it is easy to see the effects of the particles relative to the pure liquid case near pinch-off. As pinch-off is approached, the $\phi = 0.30$ suspension

has a much thicker neck than the pure liquid and the final thread thinning, and its eventual rupture, occurs at a localized region along the length of the thread. This final necking rate is much faster for the concentrated suspension, as shown in the R/a data for these two conditions. After rupture of the thread in the $\phi = 0.30$ case we see the characteristic stable retraction of the large spindle structures without the formation of any satellite drops. This retraction following pinch-off occurs asymmetrically, apparently due to the particle distribution within the spindle structures, and induces a side-to-side motion in the spindle as it retracts.

4.2.1.2 Larger orifice ($d = 0.32$ cm)

For the larger orifice diameter, $d = 0.32$ cm, we observe similar trends in the L/d and R/a behavior with increasing particle concentration, with a few notable exceptions. The results for this orifice are presented in Figures 32-37 for $d_p = 212 - 250$ μm and Figure 38-40 for $d_p = 106 - 125$ μm.

In Figure 32 the pure liquid is compared with a low-ϕ suspension ($\phi = 0.05$). For the pure liquid there is very little variability in either the L/d or R/a curves for the different drop events. As with the smaller orifice, the thread thins below the level of detection before it ruptures. Once particles are added, in this case a small amount such that $\phi = 0.05$, the increased variation in the data is evident, as is the steepening of the R/a curve near pinching. One difference from the behavior observed for the smaller orifice is that the particles lead to a large decrease in L/d at pinch-off. This effect continues as the particle concentration is increased (Figure 35) although it is less pronounced than the initial decrease observed when particles are first introduced ($\phi = 0.05$). At higher concentrations, $\phi = 0.20$ and 0.40 as shown in Figure 35, the variability in both the thinning and stretching of the thread increases and the slope of the R/a curves becomes gradually steeper near pinch-off and flatter away from it in a similar manner to that observed for the smaller capillary.

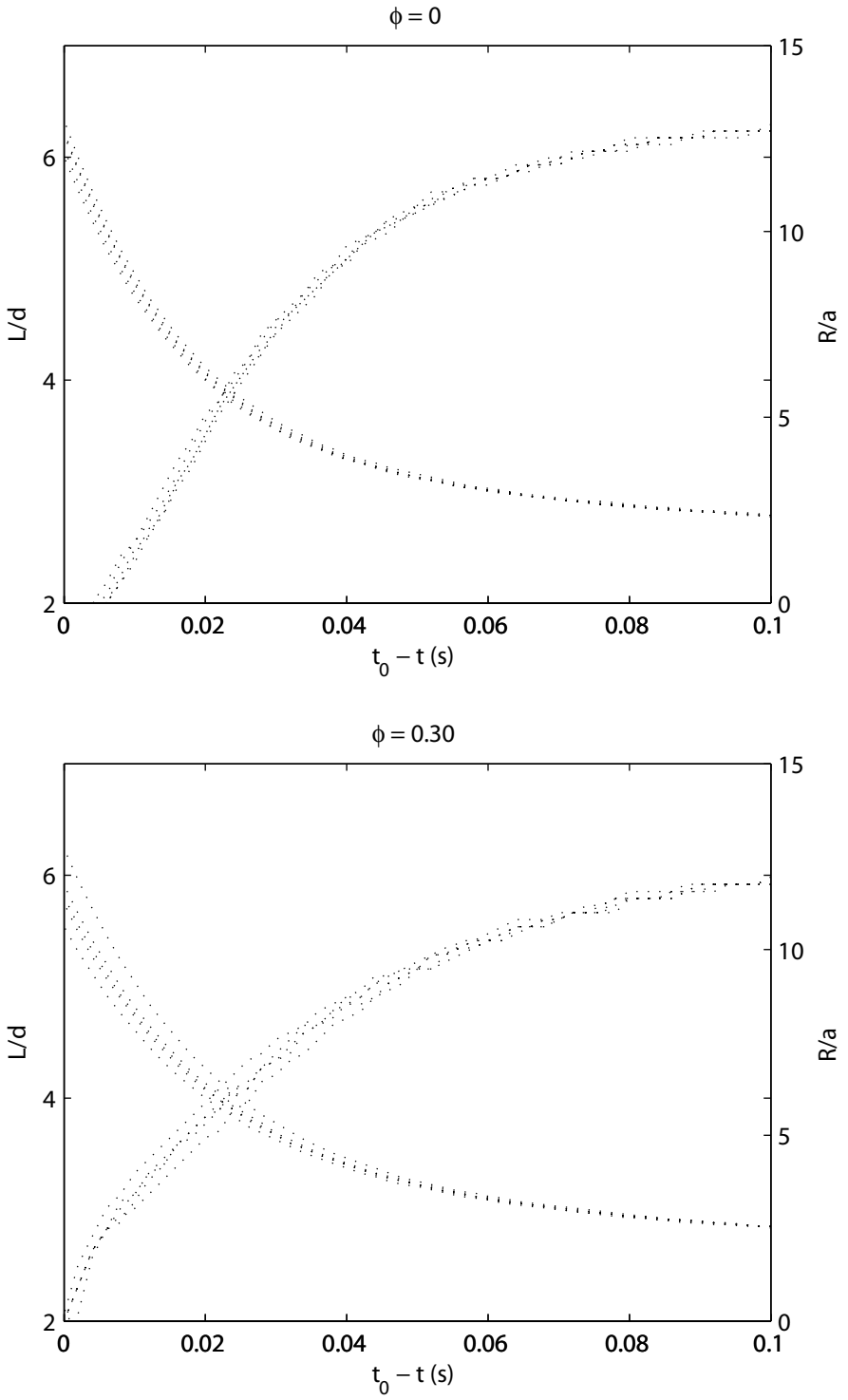

Figure 29: L/d and R/a measurements for $\phi = 0$ and $\phi = 0.30$, $d = 0.16$ cm, $d_p = 106 - 125$ μm.

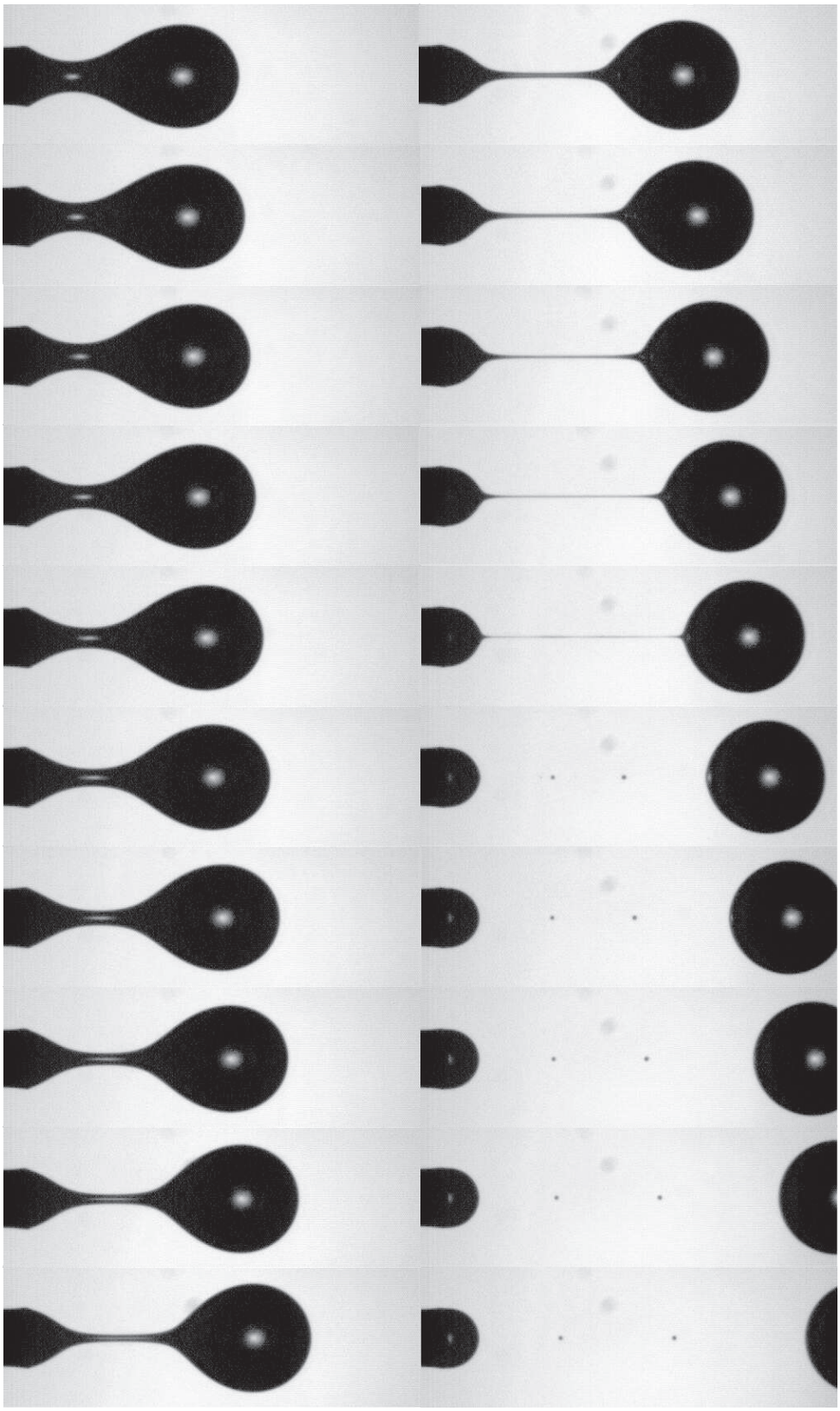

Figure 30: Photographic sequence for $\phi = 0$, $d = 0.16$ cm. The time between frames is 1/500 s and the time range is -0.010 s$\leq t_0 - t \leq 0.028$ s.

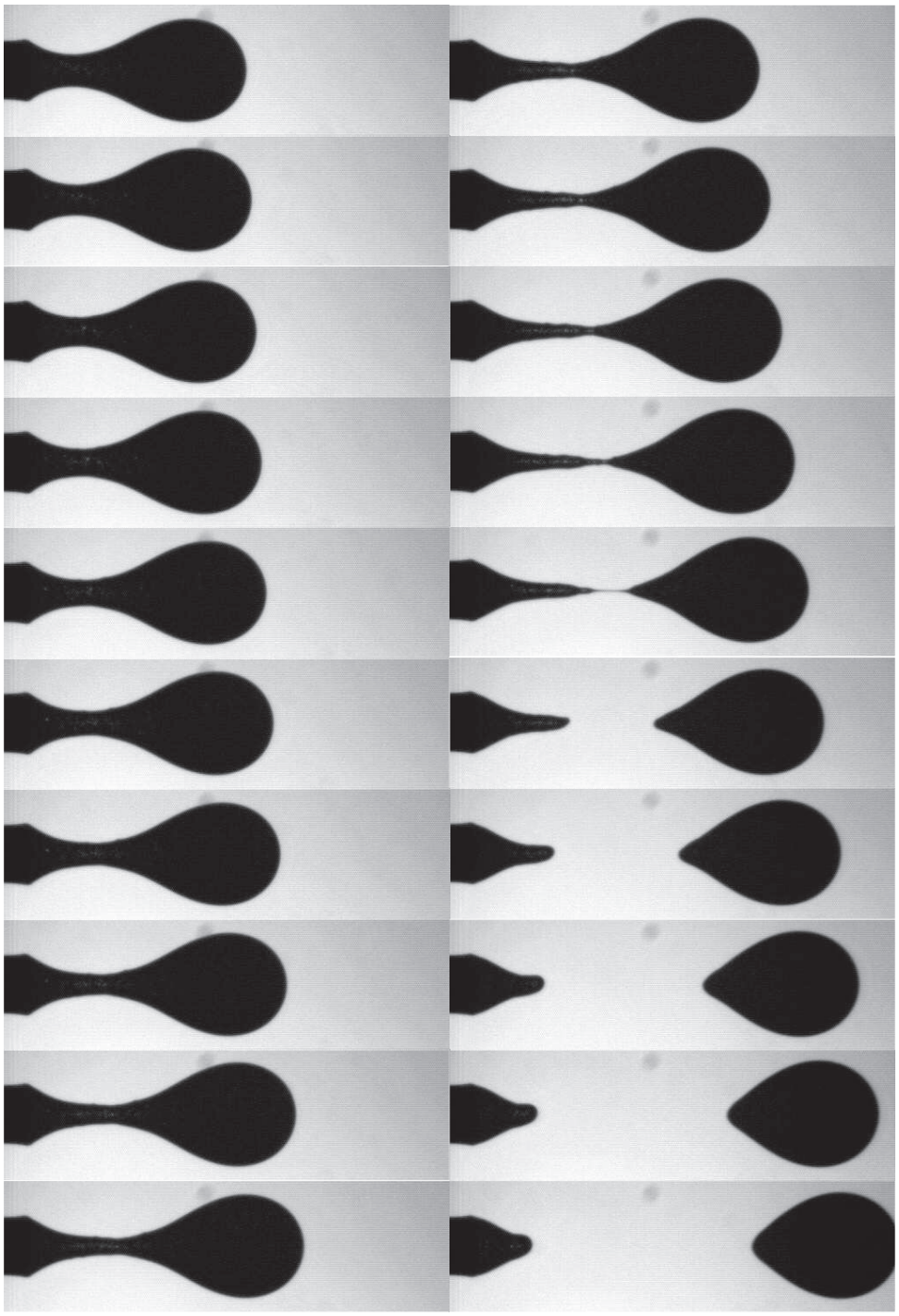

Figure 31: Photographic sequence for $\phi = 0.30$, $d = 0.16$ cm, $d_p = 106 - 125$ μm. The time between frames is 1/500 s and the time range is -0.010 s$\leq t_0 - t \leq 0.028$ s.

These changes in the L/d and R/a data with increasing ϕ are clearly evident in the photographic sequences for these conditions presented in Figures 33 and 34 for the pure liquid and the low-ϕ suspension and in Figures 36 and 37. Increasing ϕ increases the size of the spindle structures formed near pinch-off which leads to a decrease in the length the thread can attain before rupture. Also, the effect of thicker necks at times near pinch-off are evident for increasing ϕ which leads to the greater thinning rates observed for these conditions.

Figure 38 shows the L/d and R/a data for the $d = 0.32$ cm orifice with smaller particles, $d_p = 106 - 125$ μm for suspensions of $\phi = 0.10$ and 0.40. The behavior of both L/d and R/a are very similar to that of the larger particle suspensions for the same size orifice although the fluctuations at the highest ϕ are not as pronounced. The photographic sequences for the smaller particles (Figures 39 and 40) also show very similar behavior to those for the larger particle suspensions although the thickness of the spindle structures at moderate ϕ are smaller for the smaller particles. Also, the asymmetric retraction of the spindle structure for the $\phi = 0.40$ suspension (Figure 40) is quite pronounced although this is likely not an effect due solely to particle size since similar effects are observed for the larger particle suspensions as well.

4.2.2 Average necking behavior

The mean of the data presented above are used to characterize the average behavior for a given condition and to compare the different curves. The average L/d and R/a curves for selected particle concentrations are shown for $d = 0.16$ cm with $d_p = 106 - 125$ μm (Figure 41), $d = 0.32$ cm with $d_p = 212 - 250$ μm (Figure 42), and $d = 0.32$ cm with $d_p = 106 - 125$ μm (Figure 43). The average behavior more clearly indicates the particle effects on the thinning and stretching of the thread during necking than the data curves presented in the previous section. In these figures only the pure liquid, a low-ϕ suspension, and a high-ϕ suspension are presented in order

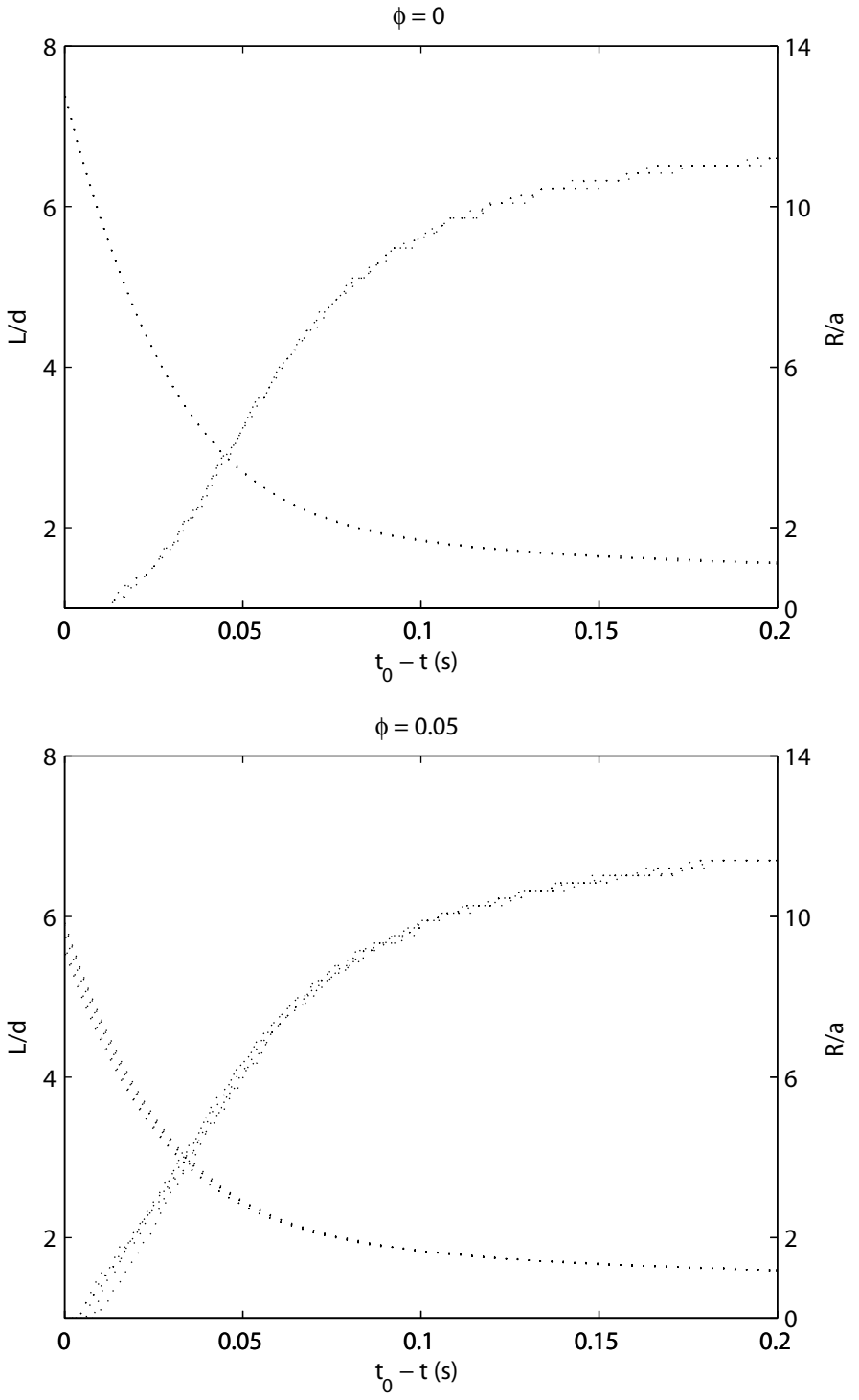

Figure 32: L/d and R/a measurements for $\phi = 0$ and $\phi = 0.05$, $d = 0.32$ cm, $d_p = 212 - 250$ μm.

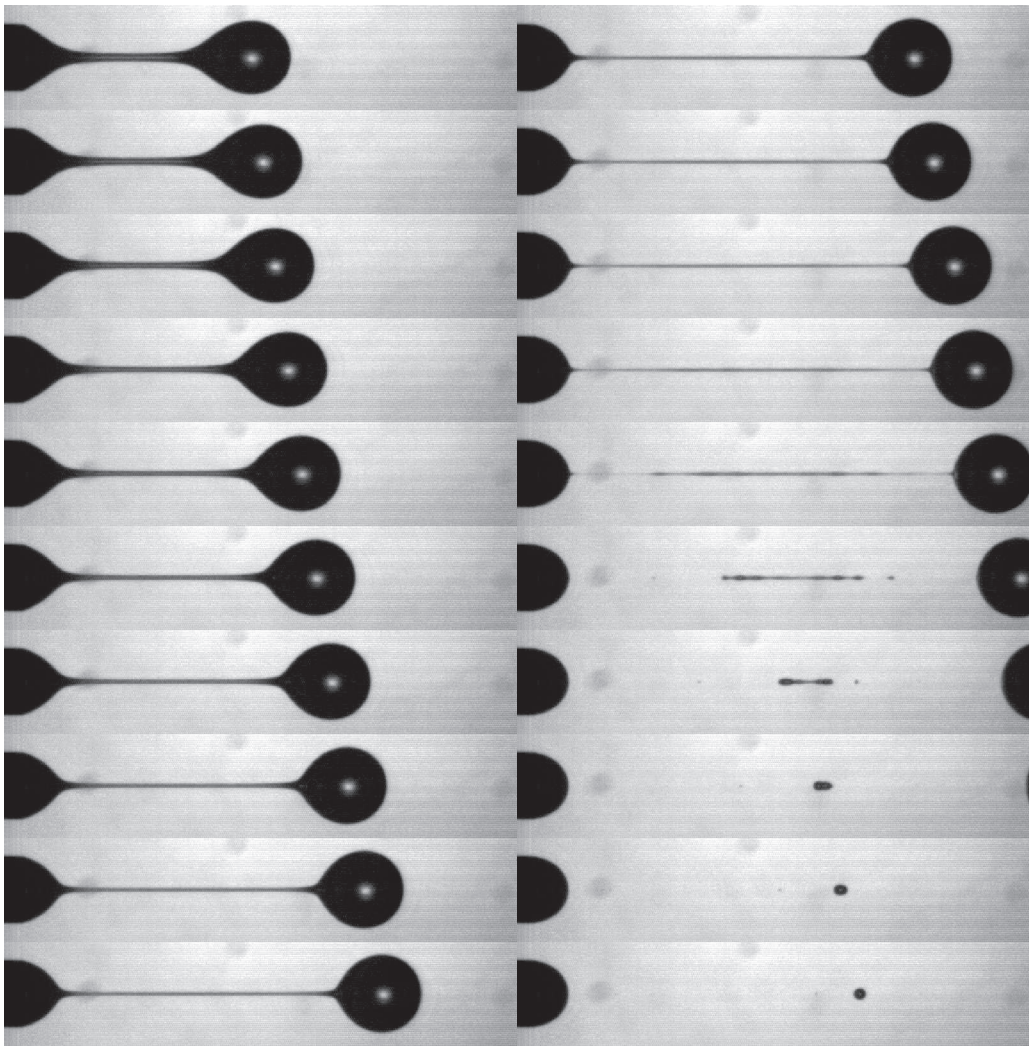

Figure 33: Photographic sequence for $\phi = 0$, $d = 0.32$ cm. The time between frames is 1/500 s and the time range is -0.010 s$\leq t_0 - t \leq 0.028$ s.

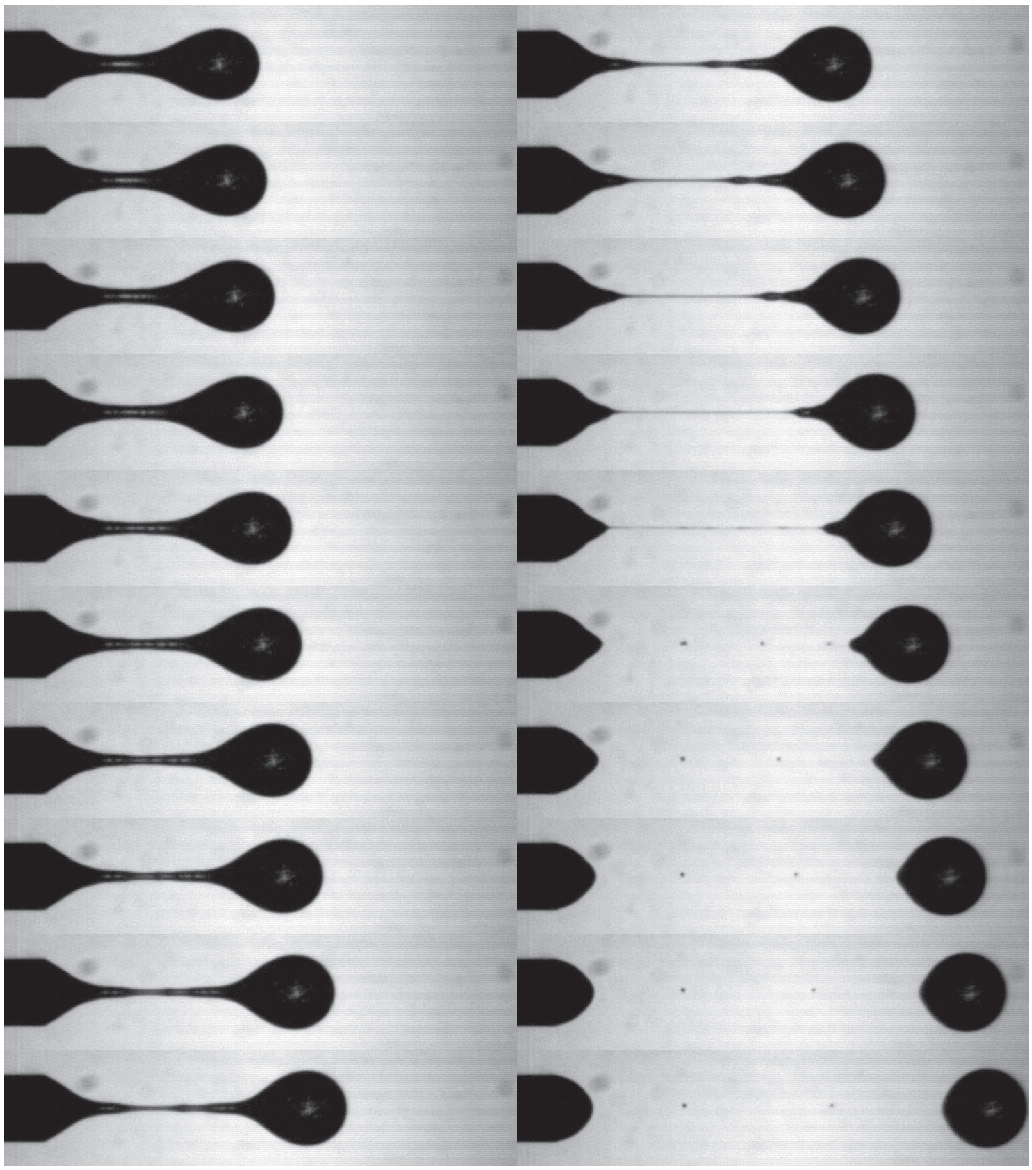

Figure 34: Photographic sequence for $\phi = 0.05$, $d = 0.32$ cm, $d_p = 212 - 250$ μm. The time between frames is 1/500 s and the time range is -0.010 s$\leq t_0 - t \leq 0.028$ s.

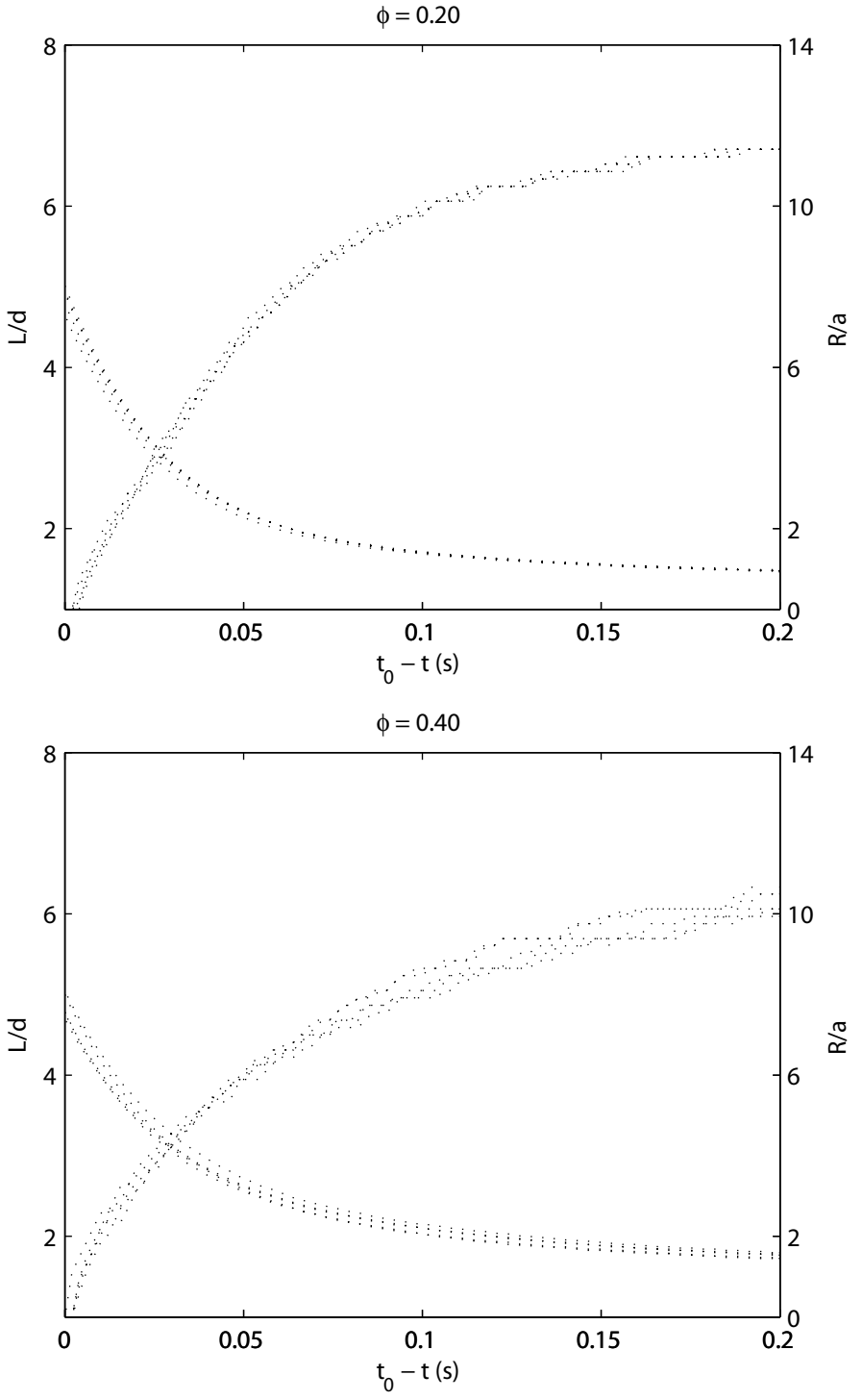

Figure 35: L/d and R/a measurements for $\phi = 0.20$ and $\phi = 0.40$, $d = 0.32$ cm, $d_p = 212 - 250$ μm.

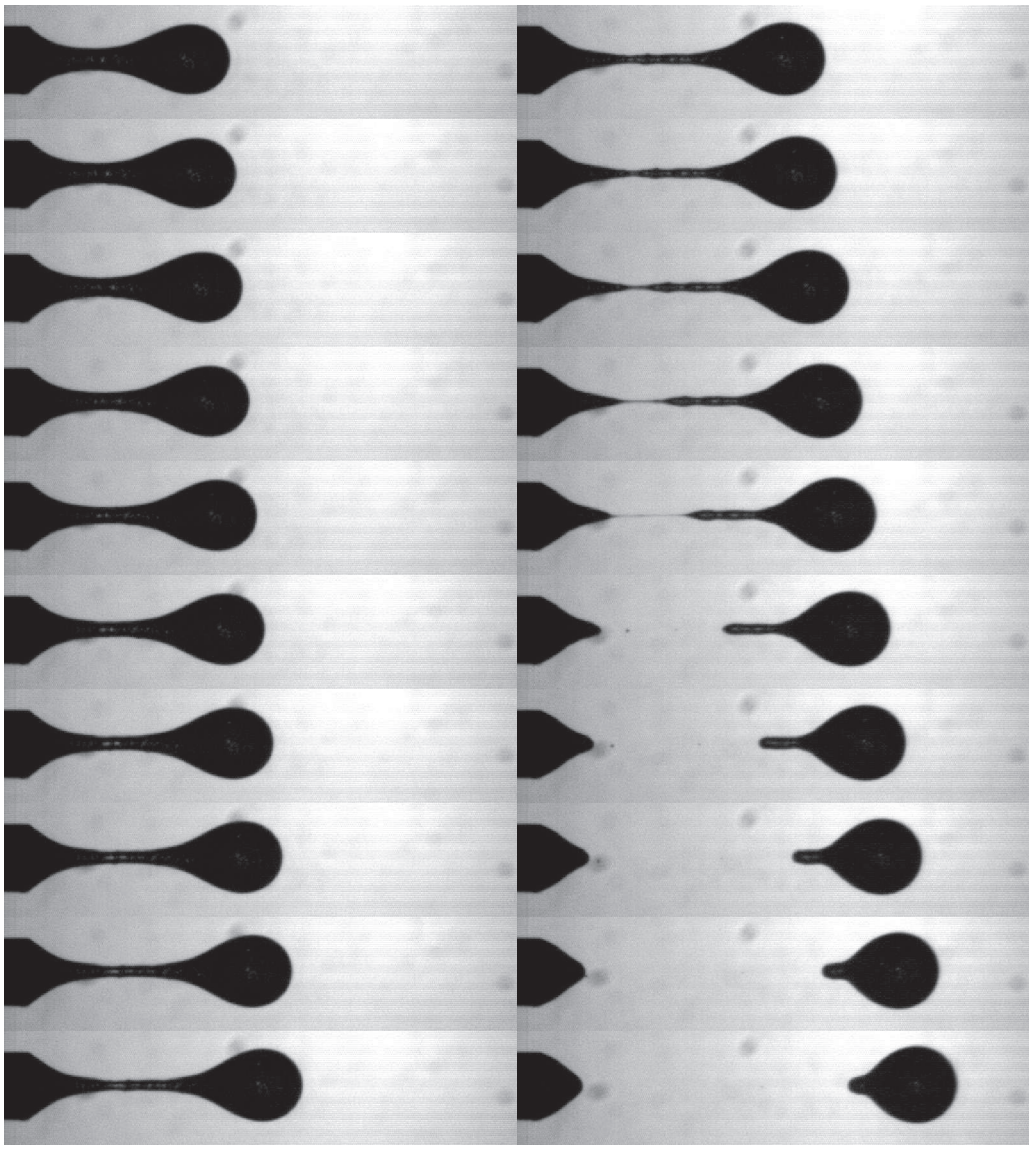

Figure 36: Photographic sequence for $\phi = 0.20$, $d = 0.32$ cm, $d_p = 212 - 250$ μm. The time between frames is 1/500 s and the time range is -0.010 s$\leq t_0 - t \leq 0.028$ s.

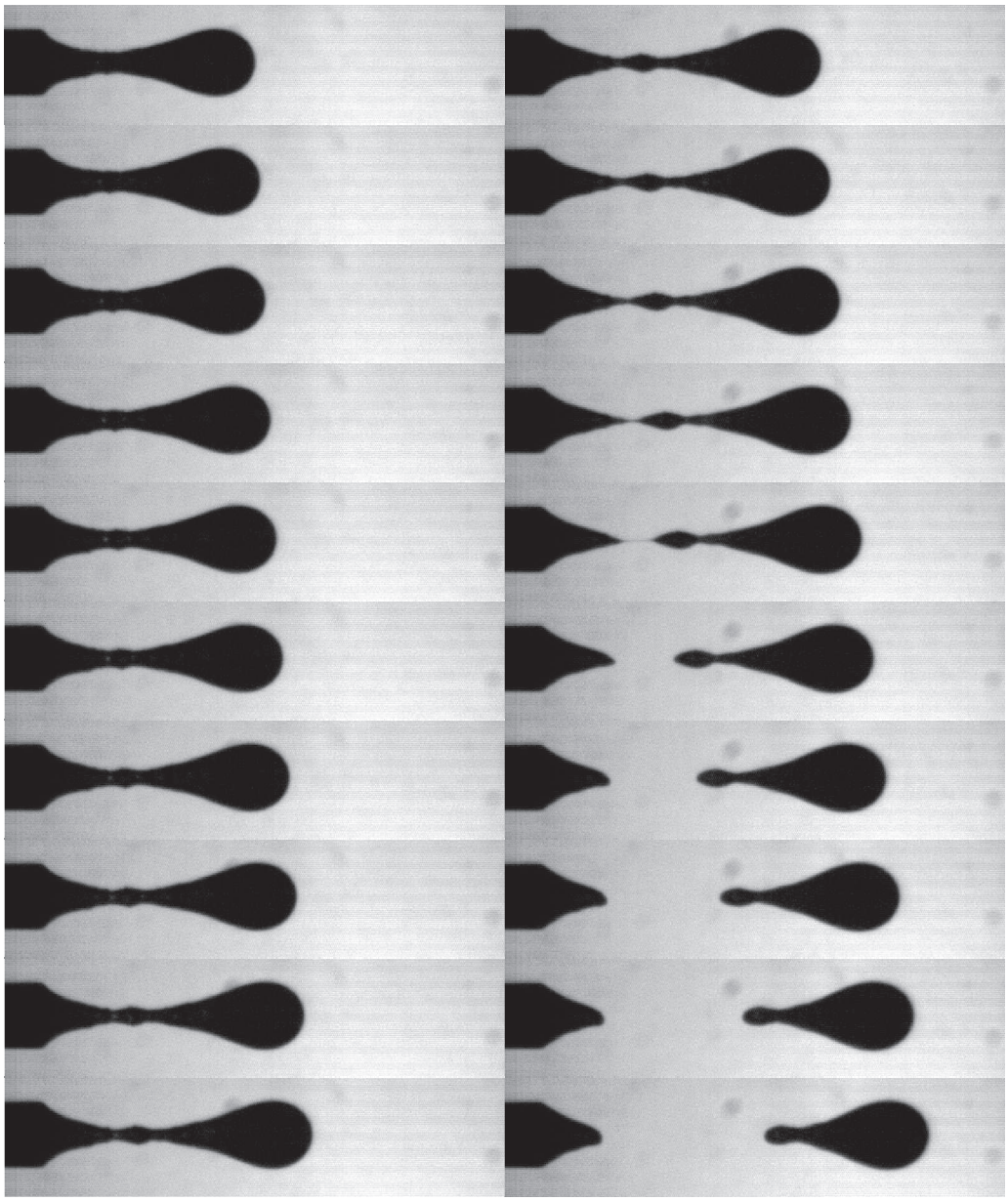

Figure 37: Photographic sequence for $\phi = 0.40$, $d = 0.32$ cm, $d_p = 212 - 250$ μm. The time between frames is 1/500 s and the time range is -0.010 s$\leq t_0 - t \leq 0.028$ s.

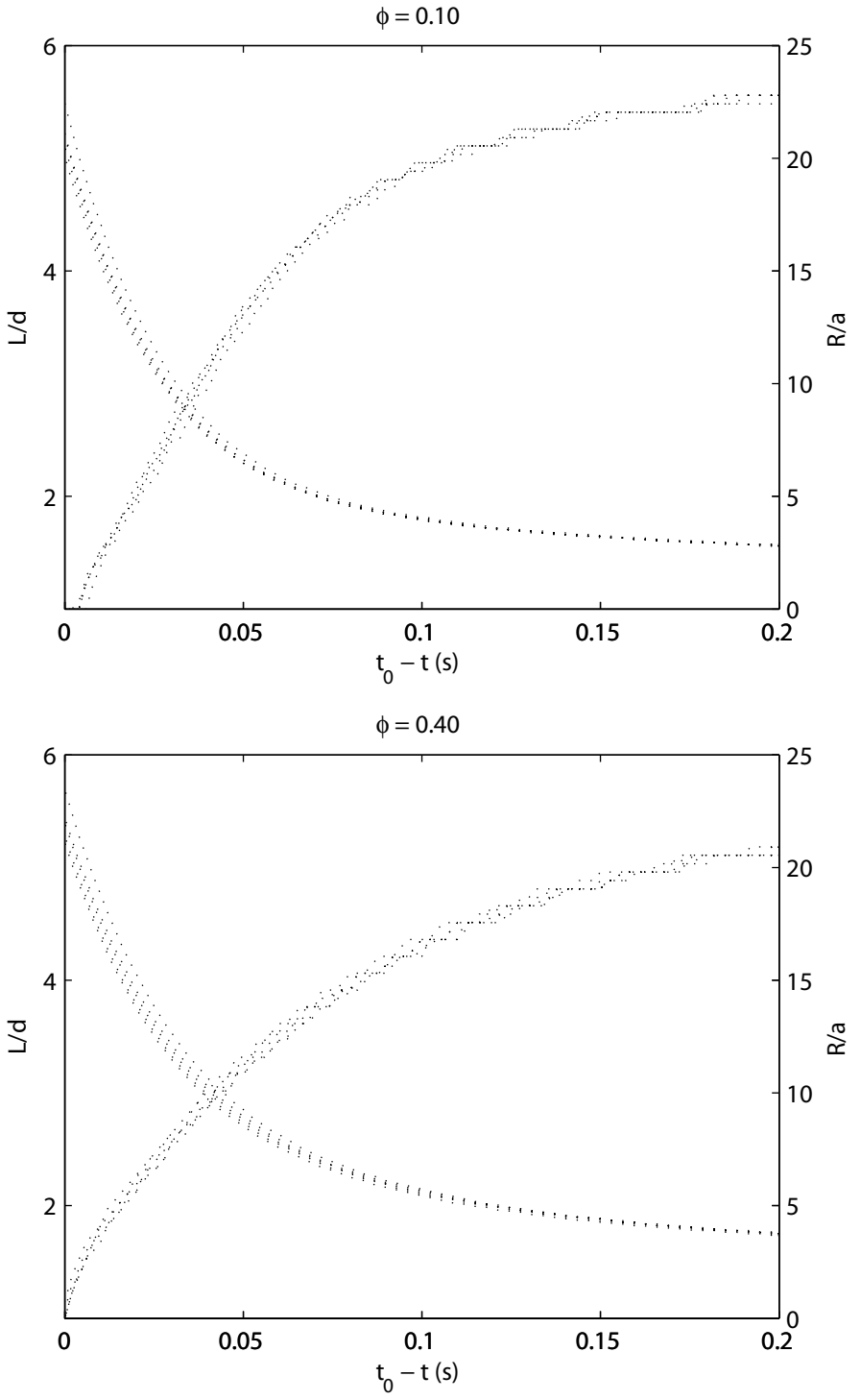

Figure 38: L/d and R/a measurements for $\phi = 0.10$ and $\phi = 0.40$, $d = 0.32$ cm, $d_p = 106 - 125$ μm.

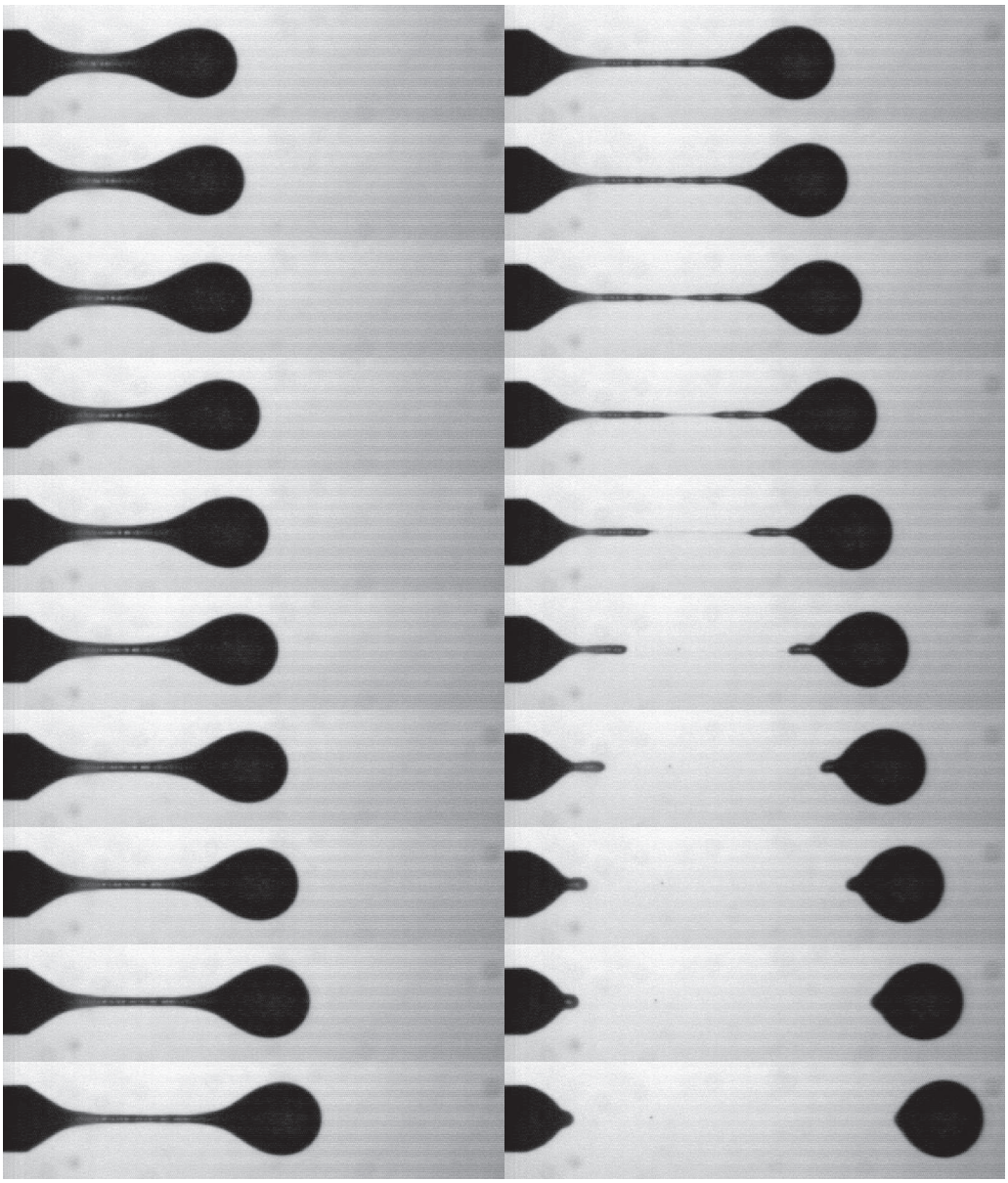

Figure 39: Photographic sequence for $\phi = 0.10$, $d = 0.32$ cm, $d_p = 106 - 125$ μm. The time between frames is 1/500 s and the time range is -0.010 s$\leq t_0 - t \leq 0.028$ s.

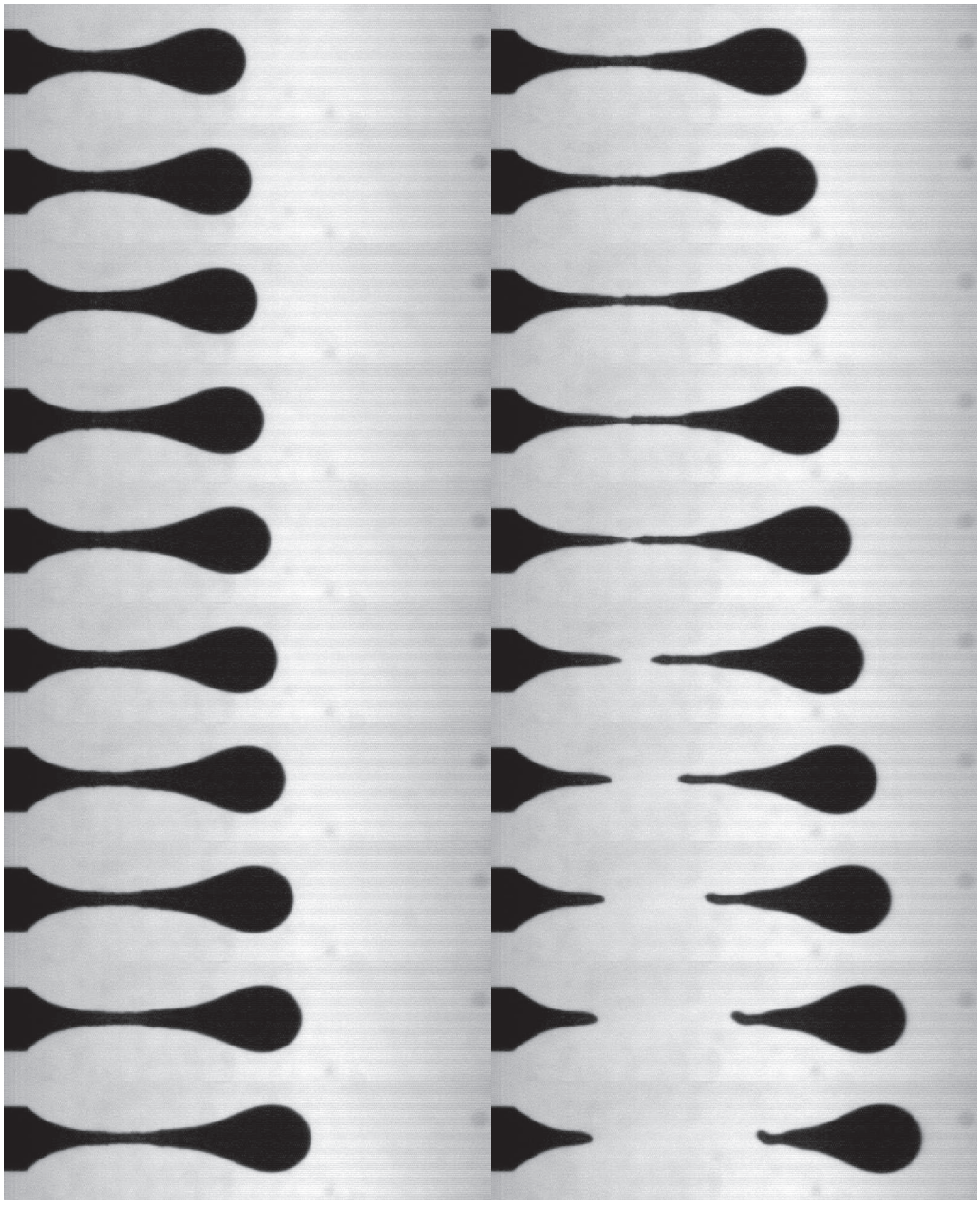

Figure 40: Photographic sequence for $\phi = 0.40$, $d = 0.32$ cm, $d_p = 106 - 125$ μm. The time between frames is 1/500 s and the time range is -0.010 s$\leq t_0 - t \leq 0.028$ s.

to highlight the particulate effects at the different extremes.

Figure 41 presents the average necking behavior for the smaller orifice (d = 0.16 cm) for ϕ = 0, 0.05, and 0.30. From the L/d graph it appears that the particles have little effect. At pinch-off both suspensions have a shorter length than the pure liquid but the effect is not great ($\sim$ 6%). Away from pinch-off the L/d curves of the pure liquid and the $\phi = 0.05$ suspension are indistinguishable while the $\phi = 0.40$ suspension L/d data is slightly greater, possibly indicating an earlier onset of necking.

The differences in the thread thinning R/a between the pure liquid and the suspensions are more pronounced than the L/d behavior for the d = 0.16 cm orifice. Away from pinch-off, during the early stages of necking, the pure liquid and the ϕ = 0.05 suspension are nearly identical while the ϕ = 0.30 suspension is already significantly thinner. This indicates that increasing ϕ does in fact lead to the onset of earlier necking. This is somewhat misleading since the particles do not actually affect the balance of surface tension and gravity which governs when necking begins in pendant drop formation. Since all the curves presented in analyzing this process are measured using the pinch-off time as the reference, the effect of increasing ϕ is actually to increase the length of the overall necking process. So the particles are actually resisting the thinning and extending the time scale over which necking occurs.

Near pinch-off, as described in the previous section, the effect of the particles is to increase the slope of the R/a curve. For the pure liquid the thread thins more slowly, with the final necking occurring after the thread has thinned below the detection level possible here. This steepening of the slope is evident for even the lowest-ϕ suspension examined for this orifice, ϕ = 0.05 but becomes more pronounced at the highest concentrations.

The average necking L/d and R/a data for the larger orifice, d = 0.32 cm, are presented in Figures 42 and 43 for the two particle size distributions of $d_p = 212 - 250$ μm and $106 - 125$ μm, respectively. In these two figures the trends with increasing

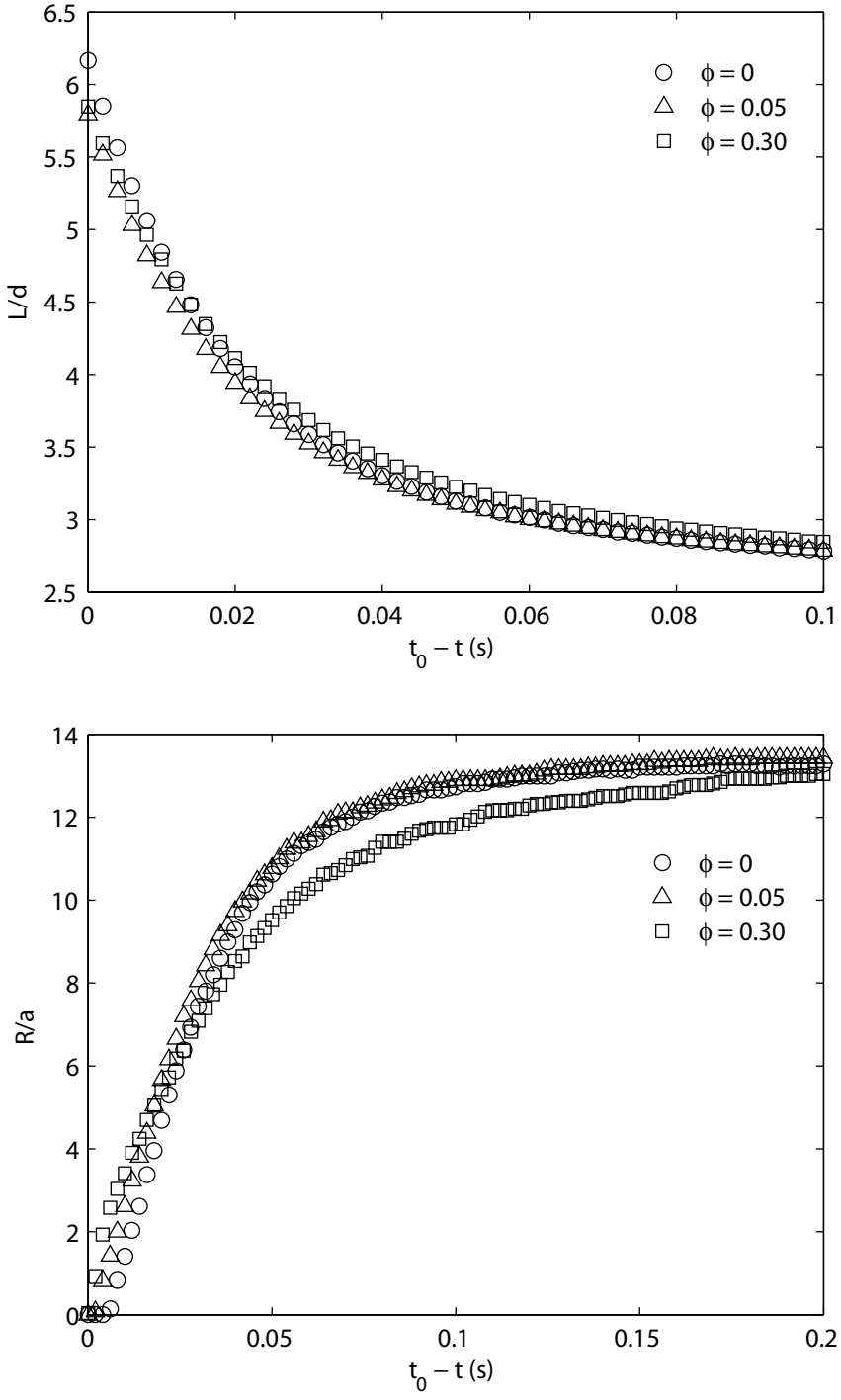

Figure 41: Average L/d and R/a curves for $\phi = 0$, 0.05, and 0.30, $d = 0.16$ cm, $d_p = 106 - 125$ μm.

ϕ are very similar for both particle sizes and the effect of d_p on the process appears to be negligible from this data. The data for the larger orifice exhibit similar trends to that observed for the smaller one with more pronounced effects. The addition of particles causes a large decrease in the pinch-off length ($\sim$ 22%) and, while this decrease continues with increasing ϕ, the effect is greatest in going from $\phi = 0$ to finite ϕ. An increase in L/d away from pinch-off is also evident at the highest ϕ and is indicative of the particles increasing the overall necking times as discussed previously for the smaller orifice. This lengthening of the necking interval is also evident from the thinning curves for $d = 0.32$ cm where the R/a values of the concentrated suspensions, $\phi = 0.40$ are significantly less than those of the pure liquid or the low-ϕ suspensions at times away from pinch-off. As pinch-off is approached, however, this trend is reversed and the necks of the concentrated suspensions are thicker and thin much more rapidly.

4.3 Effect of viscosity on the thread dynamics

In order to assess the impact of viscosity on the necking dynamics two additional pure liquid samples were prepared and analyzed. The liquids consisted of the same three components as the suspending liquid ($ZnCl_2$, H_2O, UCON) but with a greater percentage of UCON, the highly viscous component. The two additional samples prepared were: a 35% UCON mixture ($\mu = 520$ cP) and a 40% UCON mixture ($\mu = 870$ cP). The suspending liquid was a 30% UCON mixture ($\mu = 310$ cP). The results for the experiments with the higher viscosity pure liquids and their comparison with the suspending liquid are presented in Figures 44-47.

Figure 44 shows the L/d and R/a curves for the three different viscosity mixtures through the smaller orifice ($d = 0.16$ cm) and Figure 45 shows photographic sequences of the forming drops of the mixtures. Increasing viscosity causes the necking to begin at earlier times relative to pinch-off and leads to a large increase in the pinch-off length. For the $d = 0.16$ cm orifice the 40% UCON mixture has a pinch-off L/d

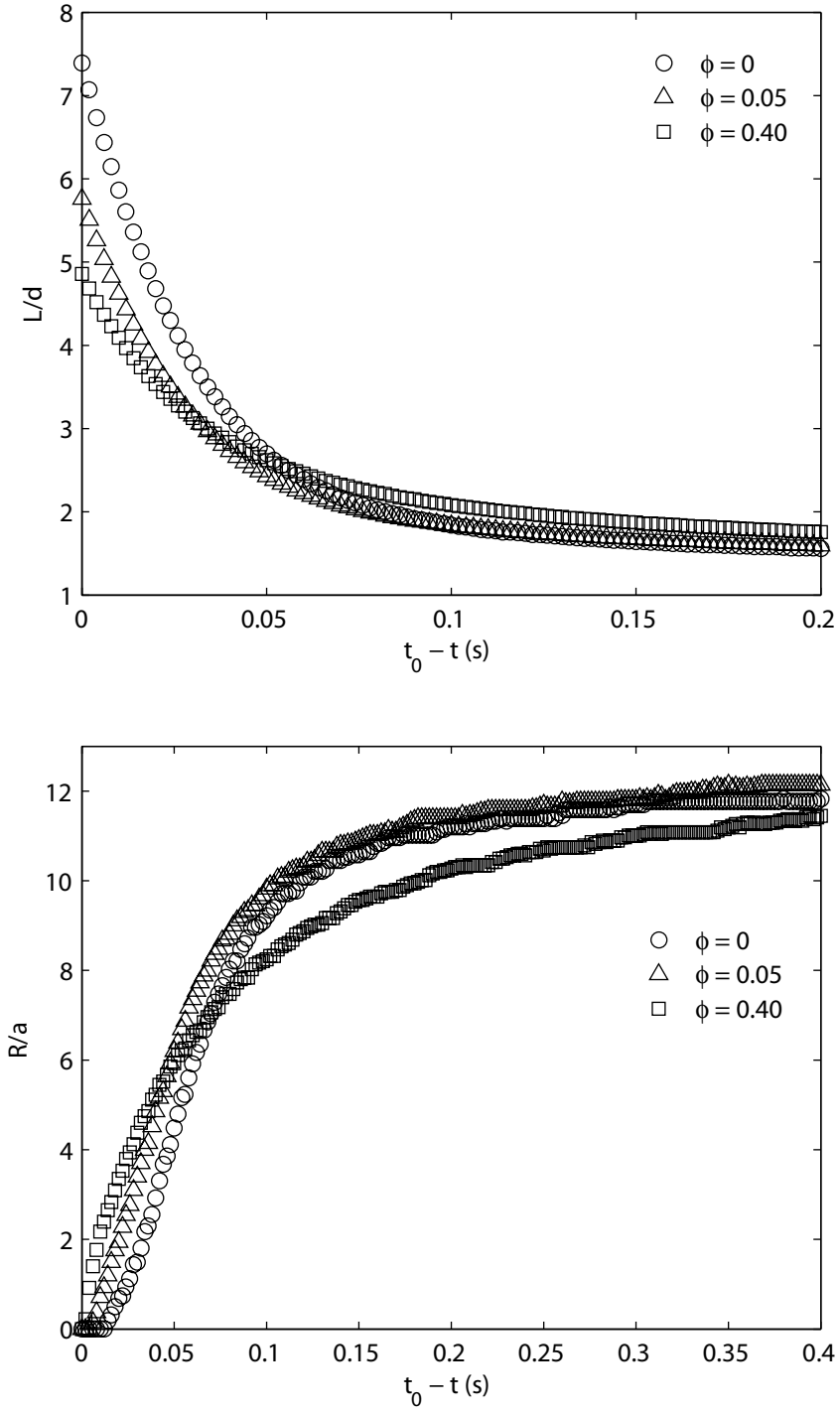

Figure 42: Average L/d and R/a curves for $\phi = 0$, 0.05, and 0.40, $d = 0.32$ cm, $d_p = 212 - 250$ μm.

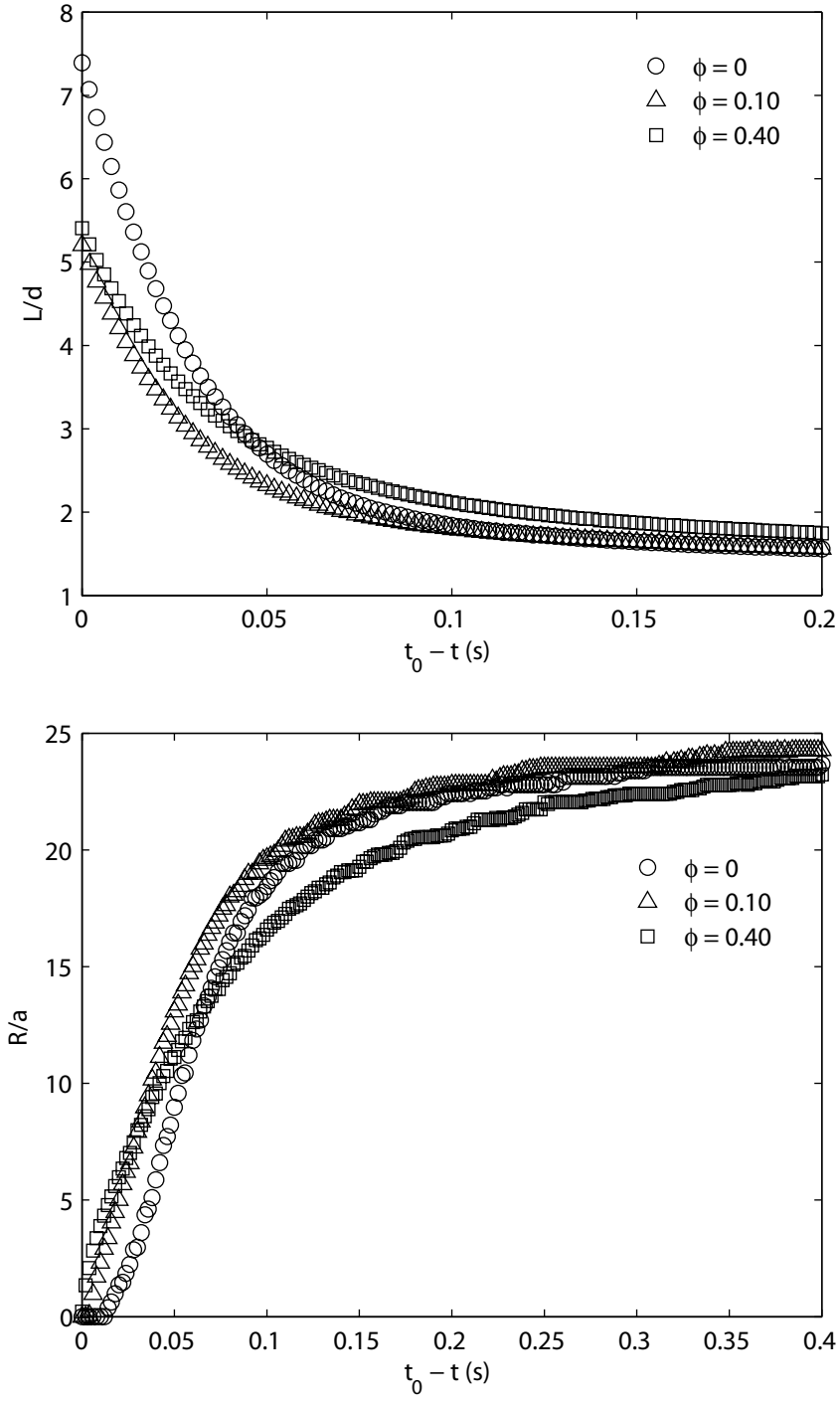

Figure 43: Average L/d and R/a curves for $\phi = 0$, 0.10, and 0.40, $d = 0.32$ cm, $d_p = 106 - 125$ μm.

of nearly twice that of the 30% mix. Since the necking time has increased with increasing viscosity the thinning also begins earlier and the slope of the R/a curves decrease with increasing viscosity. These trends are clearly seen in the photographic sequences where at a given time during necking increasing viscosity leads to longer and narrower threads.

The stretching and thinning behavior of the various mixtures through the larger orifice ($d = 0.32$ cm) is shown in Figure 46 with the corresponding photographic sequences for select times approaching pinch-off presented in Figure 47. As in the case of the smaller orifice, increasing the viscosity of the liquid leads to increases in the necking time with the corresponding increase in L/d and decrease in R/a at fixed times away from pinch-off.

From the data for the higher viscosity liquids we can draw several conclusions regarding the effect of viscosity on the necking dynamics and compare these effects to those observed for the suspensions in section 4.2.2. The primary effect of increasing the viscosity of the pure liquid is to increase the resistance to the necking process. This leads to longer necking times, slower thinning of the neck, and much longer thread lengths at pinch-off. Comparing these effects to those for the concentrated suspensions we see that there are similarities in the behavior as well as differences. The overall effect of increasing the necking time is common between both the higher viscosity liquids and the concentrated suspensions. This is consistent with the idea that the particles are increasing the bulk viscosity of the mixture, at least during a certain portion of the necking process. This increase in the necking time for the suspensions can be seen in the R/a curves away from pinch-off where the thinning is slowed relative to the pure liquid in a similar manner to that observed for the higher viscosity pure liquid mixtures. As pinch-off is approached, however, the behavior between the two cases is very different. Near pinch-off, thinning for the pure liquids occurs at slower rates for increasing viscosity while the opposite effect is observed for

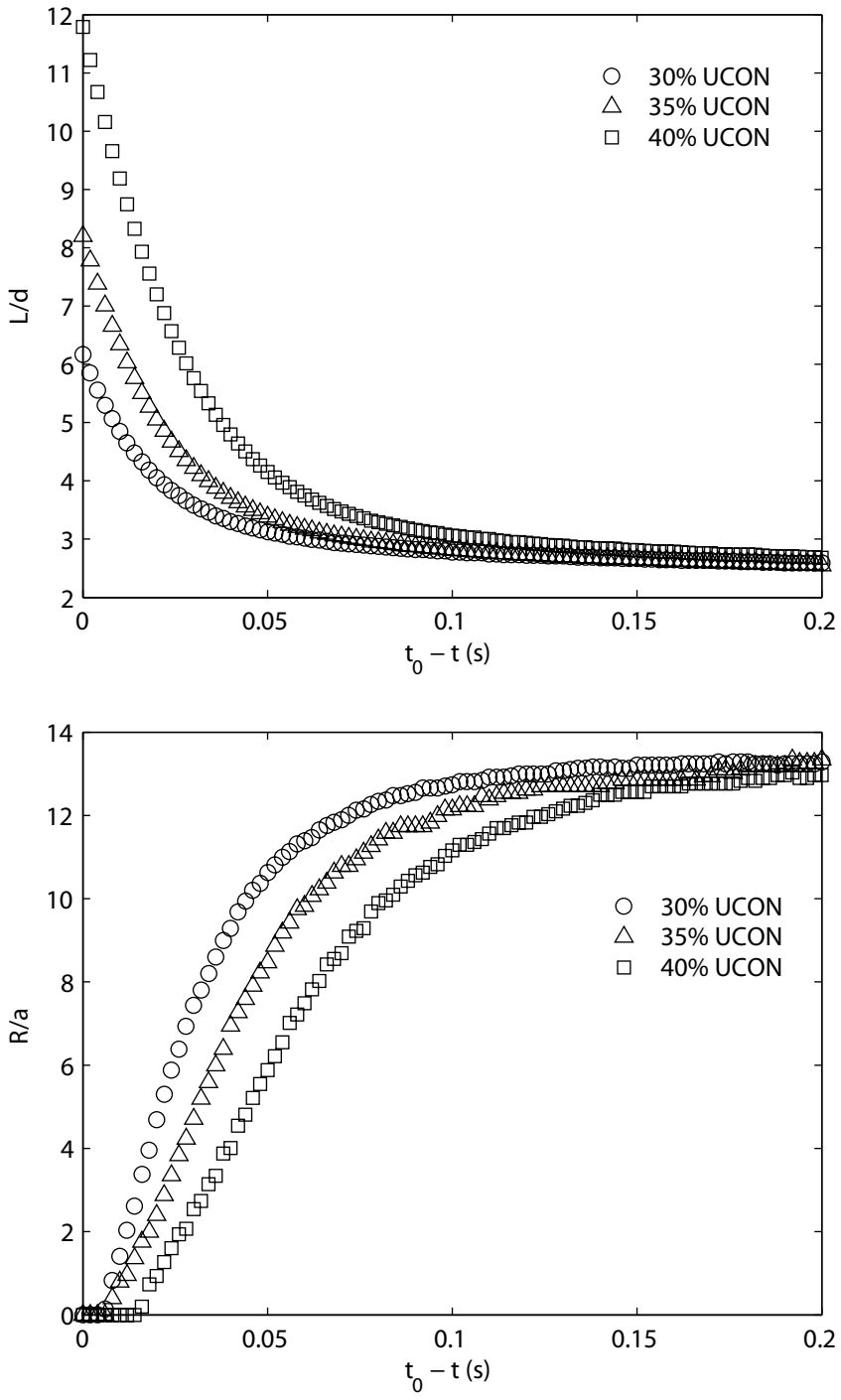

Figure 44: Average L/d and R/a curves for the $d = 0.16$ cm orifice for the varying viscosity pure liquids.

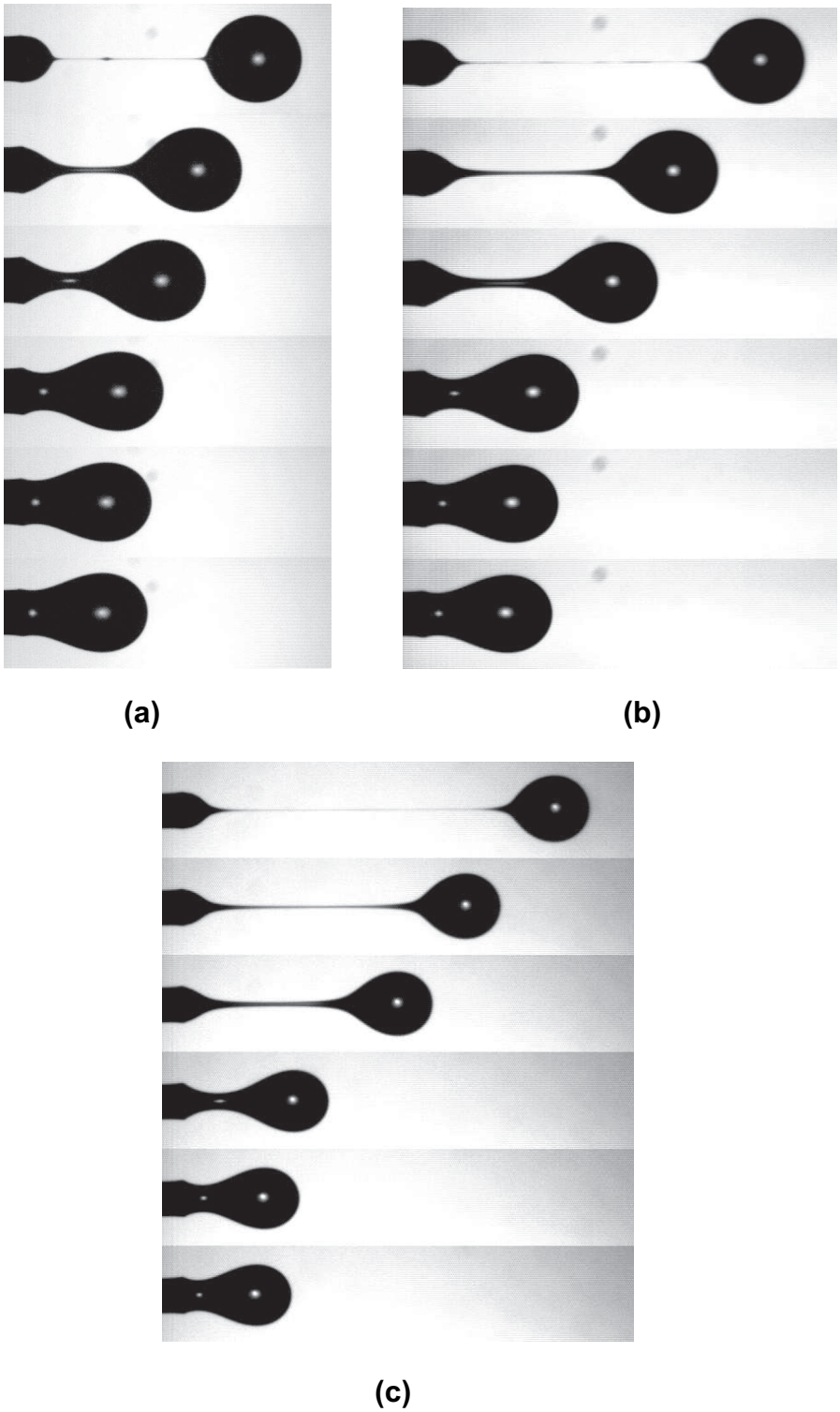

Figure 45: Photographs of the forming drop at various times before pinch-off for pure liquid mixtures of varying viscosity where (a) 30% UCON, (b) 35% UCON, and (c) 40% UCON for $d = 0.16$ cm. The times from the first picture in each sequence are $t_0 - t = 0$, 0.01, 0.02, 0.05, 0.08, 0.10 s.

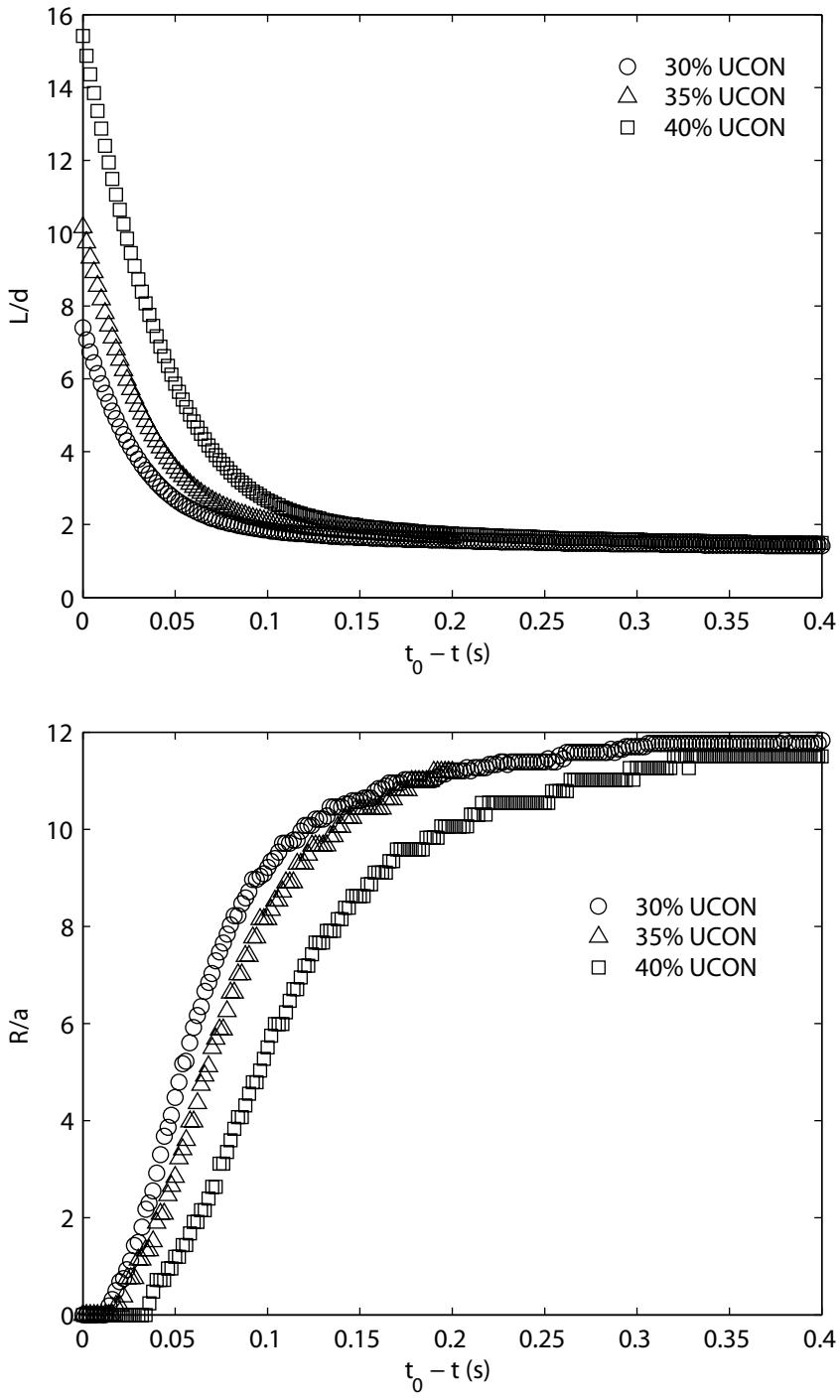

Figure 46: Average L/d and R/a curves for the $d = 0.32$ cm orifice for the varying viscosity pure liquids.

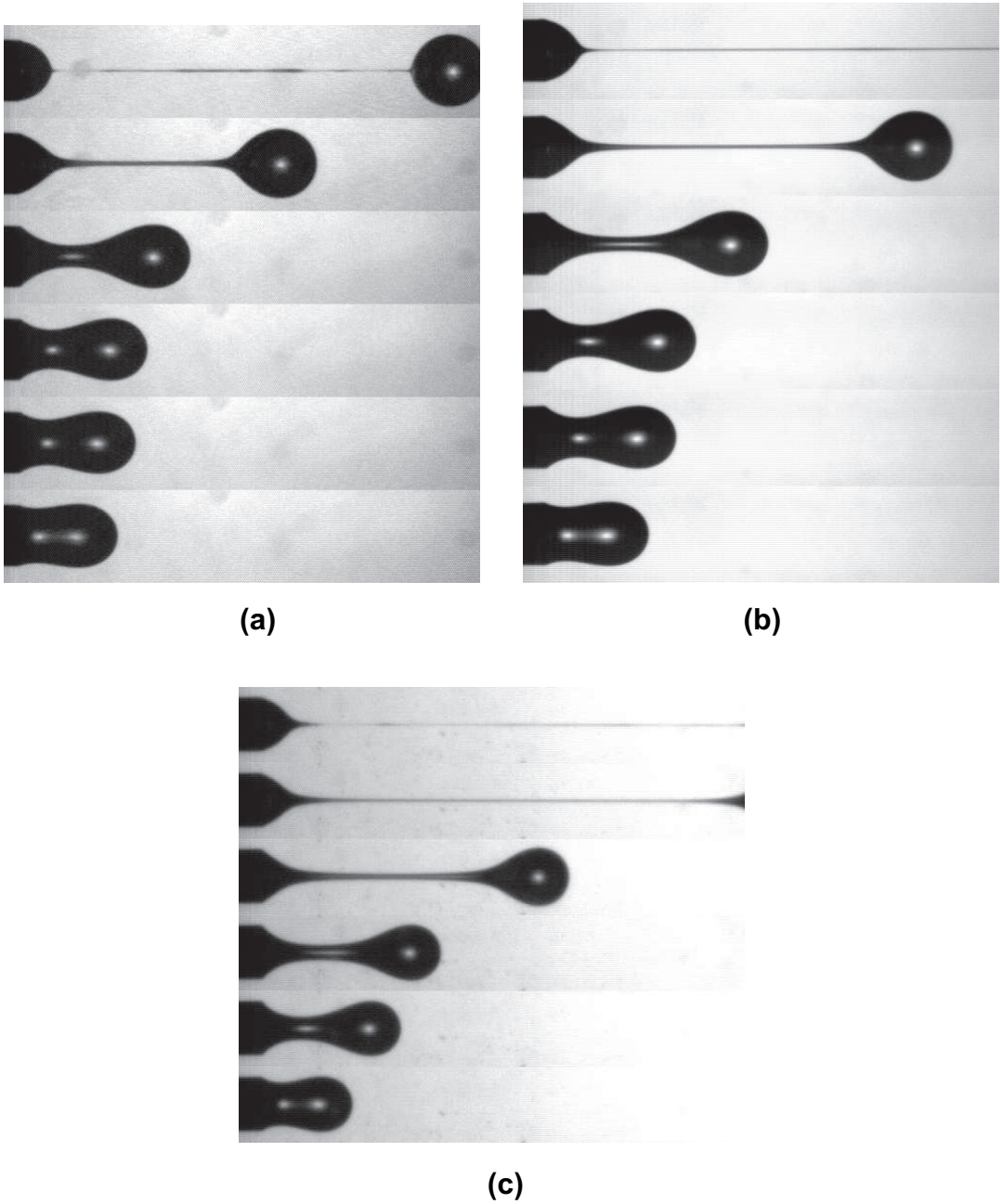

Figure 47: Photographs of the forming drop at various times before pinch-off for pure liquid mixtures of varying viscosity where (a) 30% UCON, (b) 35% UCON, and (c) 40% UCON for $d = 0.32$ cm. The times from the first picture in each sequence are $t_0 - t = 0$, 0.02, 0.05, 0.08, 0.10, 0.20 s. In the cases where pinch-off occurs outside the field of view, the thread length was determined from additional experiments in which the camera was repositioned.

increasingly concentrated suspensions. Finally, the increase in the lengthening of the thread at pinch-off with increasing viscosity is opposite that observed for increasing particle concentration.

4.4 A model for thread thinning

In order to quantify the effect of the added resistance of the suspensions to the thinning of the neck, we will attempt to develop a model equation which can be fit to the R/a data over some portion of the necking process. This investigation is motivated by the observations presented earlier in this chapter: that the concentrated suspensions exhibit similar behavior to that observed for the higher viscosity pure liquids during the early stages of necking. Recalling our earlier proposition that necking occurs in two separate stages for concentrated suspensions, this investigation seeks to determine whether the first stage of this process can be understood in terms of an effective viscosity treatment of the suspensions.

The thinning data for the thread has been fit to an exponential decay equation of the form

$$R/a = A(1 - e^{-B(t_0 - t)}) + C \tag{9}$$

where A is the value of R/a away from pinching, C is a constant required since the value of R/a reaches zero before $t_0 - t = 0$ (due to the limits of the detection algorithm), and B is the rate of exponential decay of the thread radius during necking. This equation was motivated by the work of Clanet & Lasheras (1999) [10] who used a similar form to examine the thinning rate of forming drops of water as a function of orifice diameter. In attempting to fit the R/a versus $t_0 - t$ data the goal is to understand how viscosity, and possibly particle concentration, affects the thinning of the thread in the early stages of necking.

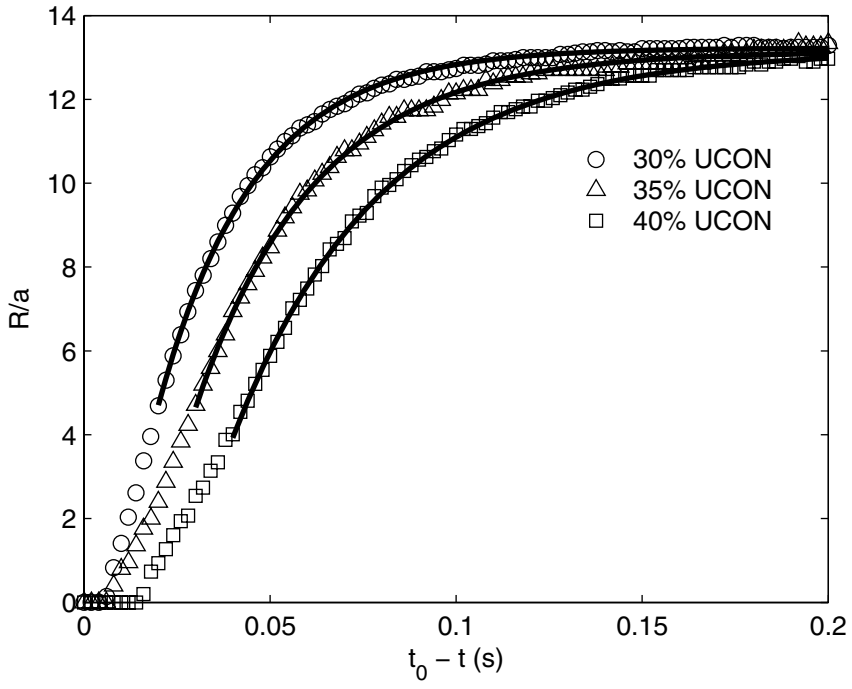

Figure 48: Fitted R/a data for varying viscosity pure liquids for $d = 0.16$ cm.

4.4.1 Fitting the R/a data of the pure liquids

The data for the pure liquid mixtures of varying viscosity presented in Figures 44 and 46 were used to determine if this fitting technique would be possible and, if it was, whether it could be used to back out information on the liquid viscosity. The fitted data are shown in Figures 48 and 49 and the fitting parameters are presented in Table 5. The fits to (9) are surprisingly good (the minimum adjusted R^2 value was 0.996) to all of the data as long as times near pinching are excluded. This was anticipated since the exponential decay form is not expected to describe the dynamics in this region [10].

The exponential term, B, in (9) provides a measure of the rate of the thread thinning during the first stage of necking and thus reflects the influence of viscosity, or mixture effective viscosity in the case of suspensions, in this region. As viscosity increases the value of B decreases, indicating that the resistance to the thinning is increasing with viscosity, as expected.

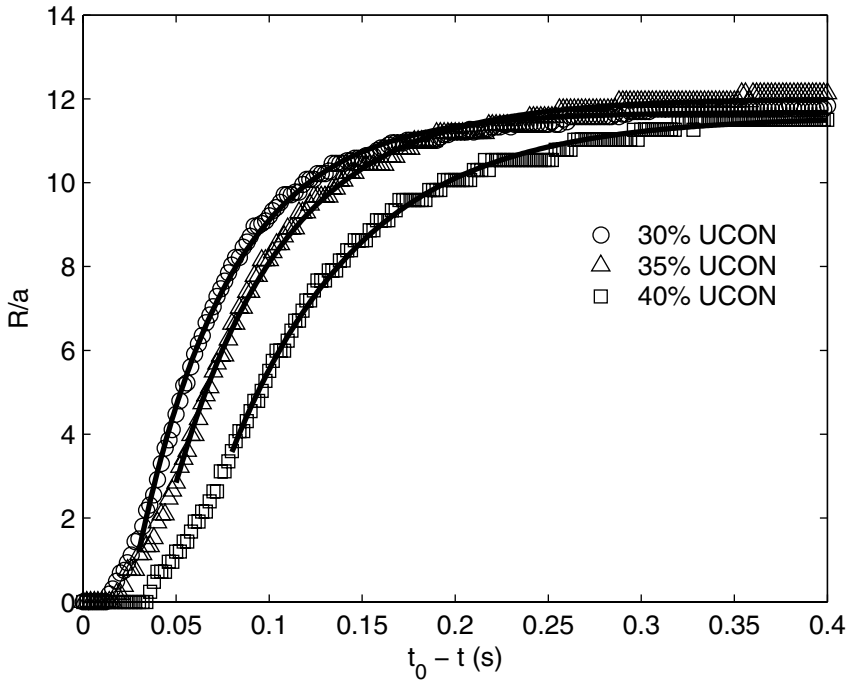

Figure 49: Fitted R/a data for varying viscosity pure liquids for $d = 0.32$ cm.

Table 5: Fitting parameters for Equation (9) for the pure liquid mixtures.

d(cm)	% UCON	μ(cP)	A	B(1/s)	C	R^2
0.16	30	310	18.4	38.4	-5.1	0.999
0.16	35	520	21.5	31.0	-8.4	0.998
0.16	40	870	25.1	25.0	-12.0	0.999
0.32	30	310	19.1	20.0	-7.4	0.997
0.32	35	520	21.5	17.0	-9.5	0.996
0.32	40	870	24.7	14.1	-13.2	0.996

Table 6: Fitting parameters for Equation (9) for the suspensions.

d(cm)	d_p (μm)	ϕ	A	B(1/s)	C	R^2
0.16	106-125	0.05	15.7	36.0	-2.3	0.999
0.16	106-125	0.10	14.5	34.6	-1.5	0.999
0.16	106-125	0.20	14.0	32.3	-0.8	0.999
0.16	106-125	0.30	12.4	25.1	0.6	0.999
0.32	212-250	0.05	14.8	19.0	-2.9	0.994
0.32	212-250	0.10	13.7	18.1	-1.5	0.994
0.32	212-250	0.20	12.5	17.5	-0.5	0.995
0.32	212-250	0.30	10.6	14.7	1.2	0.997
0.32	212-250	0.40	9.3	10.8	2.1	0.998
0.32	106-125	0.10	26.5	17.9	-2.7	0.993
0.32	106-125	0.20	24.8	17.9	-0.7	0.995
0.32	106-125	0.30	23.0	13.1	0.2	0.998
0.32	106-125	0.40	21.2	11.5	2.0	0.999

4.4.2 Fitting the R/a data of the suspensions

The averaged R/a data for the suspensions was also fit to the model equation in (9) and for all the suspensions the fit was found to be remarkably good. An example of the resulting fits for $\phi = 0.05$ and 0.30 for $d = 0.16$ cm are shown in Figure 50 and those for $\phi = 0.05$ and 0.40 for $d = 0.32$ cm in Figure 51. The various fit parameters for all of the suspensions are presented in Table 6.

As discussed briefly in the previous section the exponential term, B, in (9) provides a measure of the rate of thinning of the thread during the early stages of necking. For the suspensions, this rate is observed to decrease with increasing concentration (Table 6) for each orifice and particle size examined. This trend indicates that the added viscosity due to the particle phase is in fact contributing to the observed changes in the thinning rate during necking.

To try to understand how the changes in the thinning rate, B, correspond with increasing particle concentration, the measured values of the thinning rate are plotted

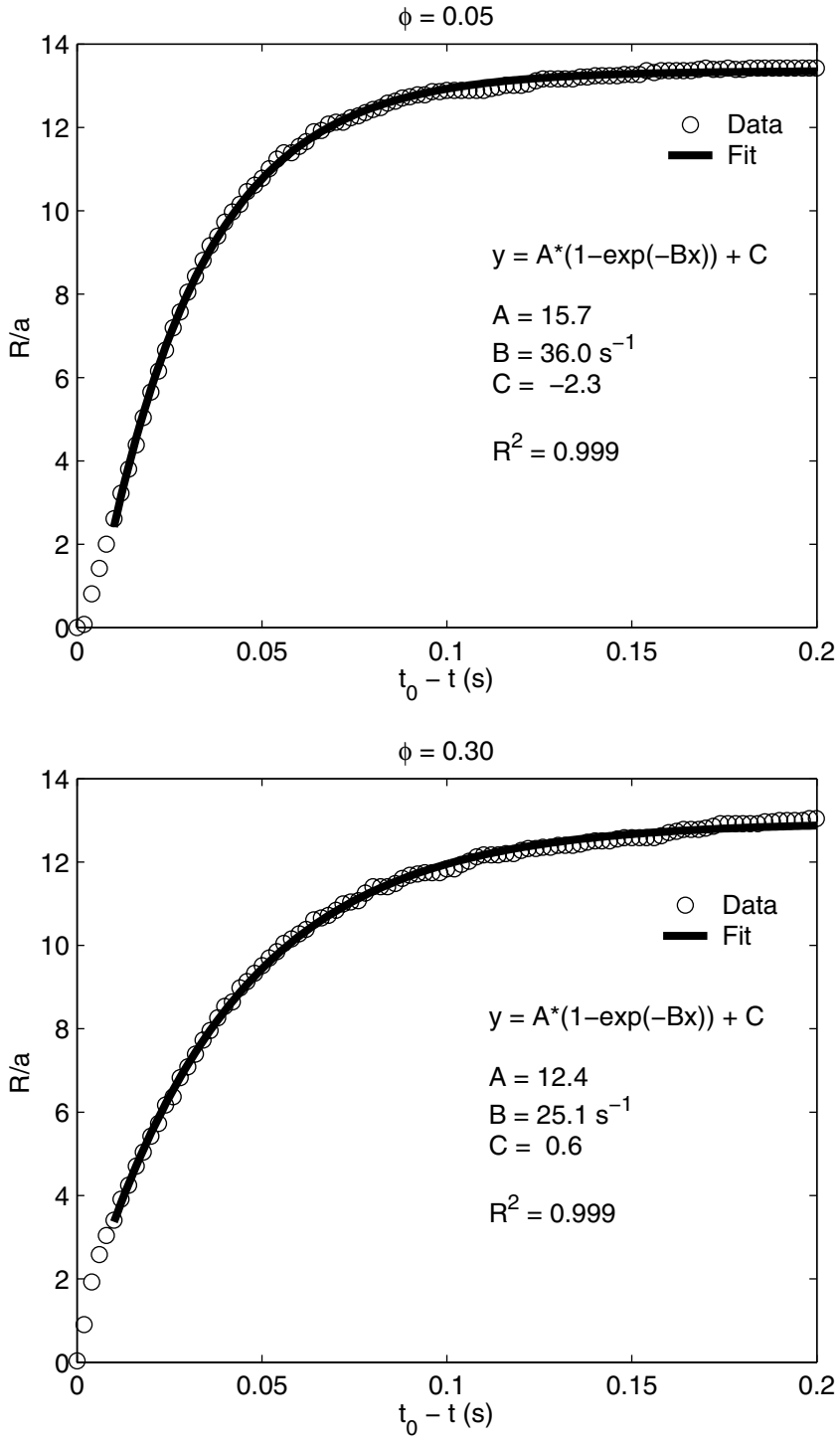

Figure 50: An example of the fitted R/a data for $\phi = 0.05$ and 0.30, $d = 0.16$ cm, $d_p = 106 - 125$ μm.

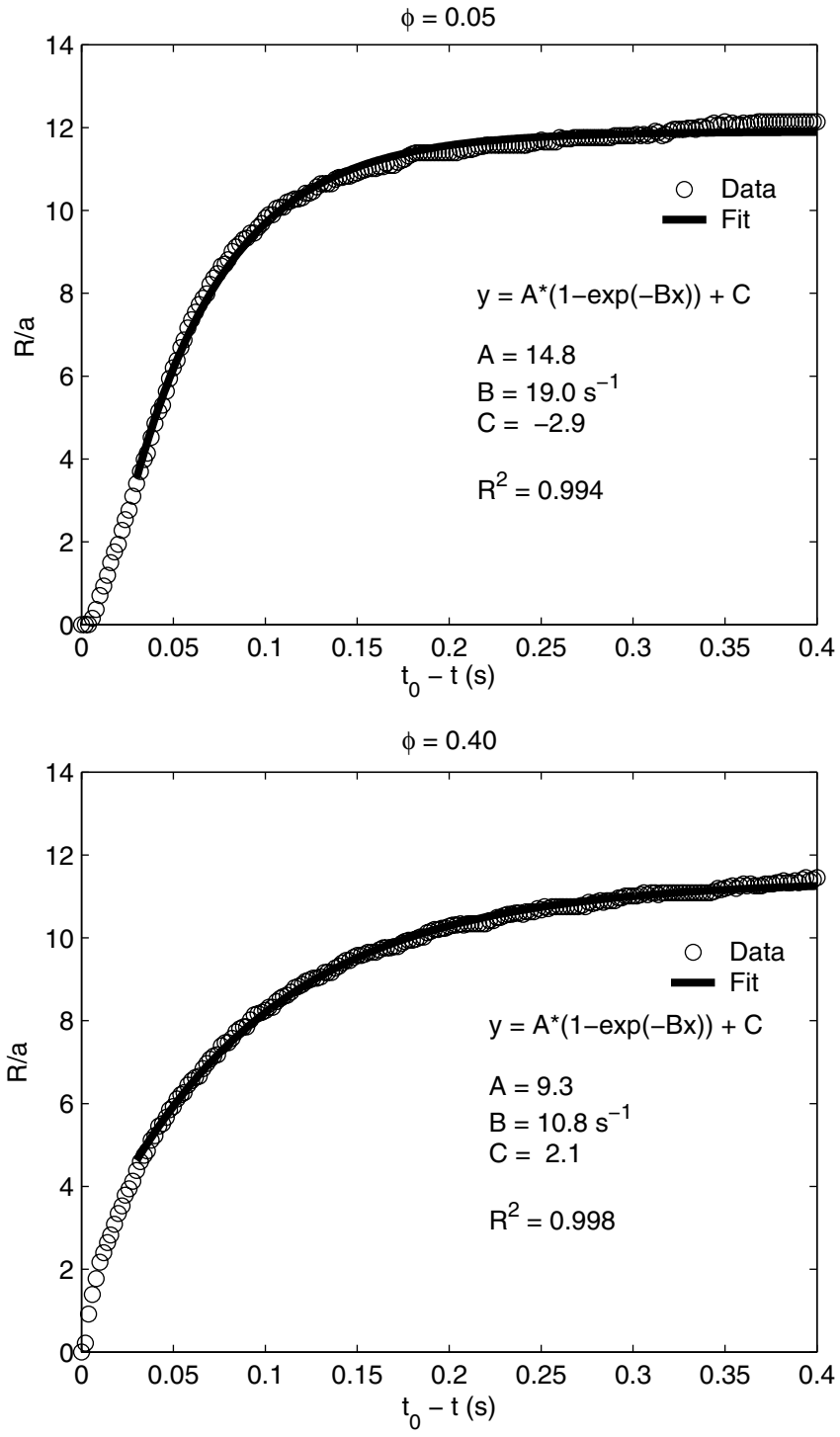

Figure 51: An example of the fitted R/a data for $\phi = 0.05$ and 0.40, $d = 0.32$ cm, $d_p = 212 - 250$ μm.

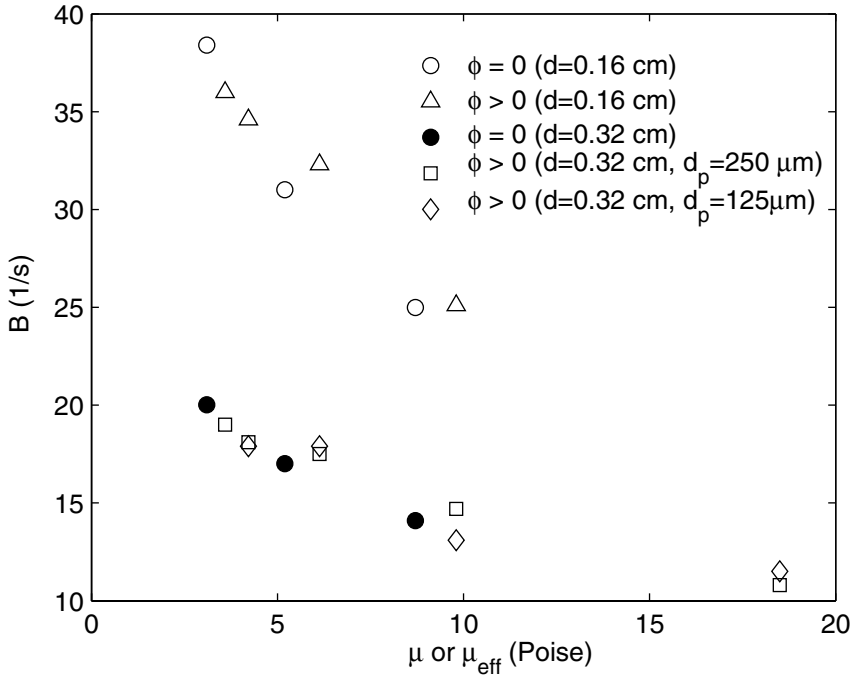

Figure 52: Thinning rate dependence on viscosity.

against the effective viscosity of the suspensions (Figure 52). The effective viscosity for the suspensions, μ_{eff}, is determined according to the Krieger viscosity formula

$$\mu_{\text{eff}}(\phi) = \mu(1 - \phi/\phi_{\max})^{-1.82} \tag{10}$$

The rates of thinning for the various viscosity pure liquids are plotted as well in order to assess the validity of this technique.

In Figure 52, the measured values of the thinning rate for the suspensions follow the same trend with increasing viscosity as that for the pure liquid mixtures for both of the orifices examined. This seems to indicate that the use of an effective viscosity in predicting the thinning rate during the early stages of necking is warranted and that the Krieger form is useful for this purpose even though it was obtained from shearing data while this is an extensional motion.

The thinning rate of the pure liquids and the suspensions is dependent upon the orifice diameter, the liquid properties, and the particle fraction. In these experiments

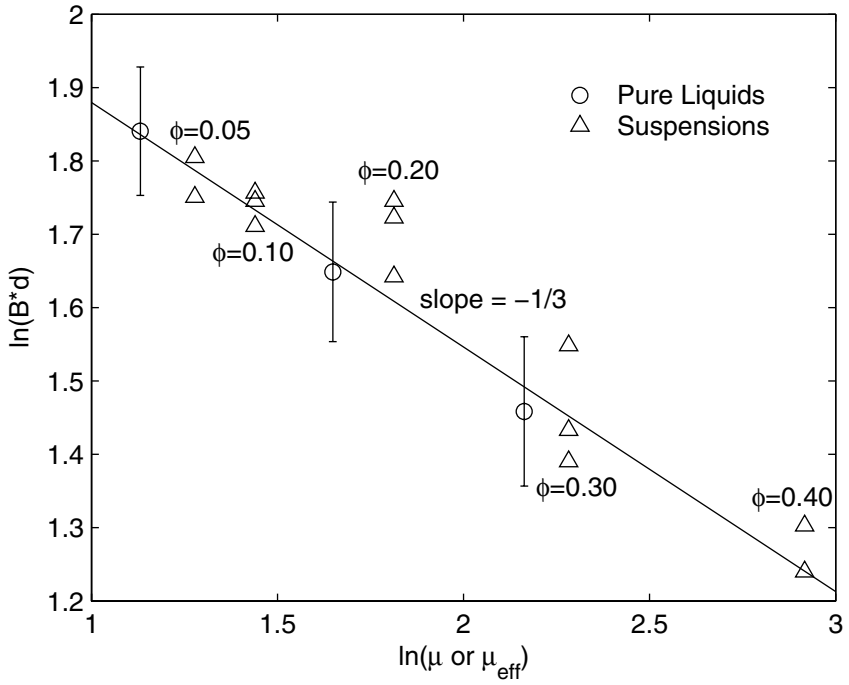

Figure 53: Thinning rate dependence on viscosity.

the only liquid property which changes is the viscosity since the surface tension of the different pure liquid mixtures is essentially constant. The viscosity is varied either directly—by changing the components in the cases of the different pure liquids—or by adding particles and changing the effective viscosity of the mixture. This leaves the thinning rate, B, as a function of only the orifice diameter and the mixture viscosity. From the data for the pure liquids it appears that $B \propto d^{-1}$ and the quantity Bd is a constant for a given mixture. Assuming this is the case, as supported by the experimental data, the quantity Bd becomes only a function of viscosity. Figure 53 plots the quantity Bd versus the viscosity (or effective viscosity in the case of the suspensions) in log-log form. The pure liquid data (the open circles in Figure 53) represent the average of the Bd values for both orifices and the error bars show the deviation. The solid line in the graph has slope $-1/3$ and seems to represent the data for the pure liquids and the suspensions quite well (with the exception of the data for the $\phi = 0.20$ suspension).

4.5 Particle-induced fluctuations

In this section we analyze the fluctuations introduced to the drop formation process by the particulate phase. In the previous sections these fluctuations have been noted and the increased variability of both the L/d and R/a behavior observed. Here we will investigate and quantify these effects.

A primary goal of this effort is to complete the picture of the two-stage necking model and develop a technique for identifying the transition between the two stages. The ability to fit the necking data at times away from pinch-off supports this idea and provides one measure of where this transition occurs. Since the fits are only possible for times above a certain $t_0 - t$ this time can be used as a lower bound for the range of times which encompass the first stage of necking. In this section we will develop another technique involving appropriate measures of the fluctuations introduced in the process by the particles and determining when these fluctuations become significant.

4.5.1 Averaging the shape of the forming drop

To develop a quantitative measure of the particle fluctuations, the shape of the forming drop for a number of different experiments is compared at times leading up to pinch-off. During necking the particles introduce increasingly large fluctuations as pinch-off is approached. At pinch-off these fluctuations are quite large and lead to the very different structures observed for identical conditions (*i.e.* ϕ, d, d_p). This is illustrated in Figure 54 which presents the pinch-off structures for five different experiments for a suspension of $\phi = 0.20$ with $d = 0.32$ cm and $d_p = 212 - 250$ μm. From this it is clear that the particle fluctuations have created large variability in the final structure of the forming drop at pinch-off. The idea in this technique is to determine a method for comparing these shapes at the same times, relative to pinch-off, and identify when the fluctuations become "significant" and then to use this time to

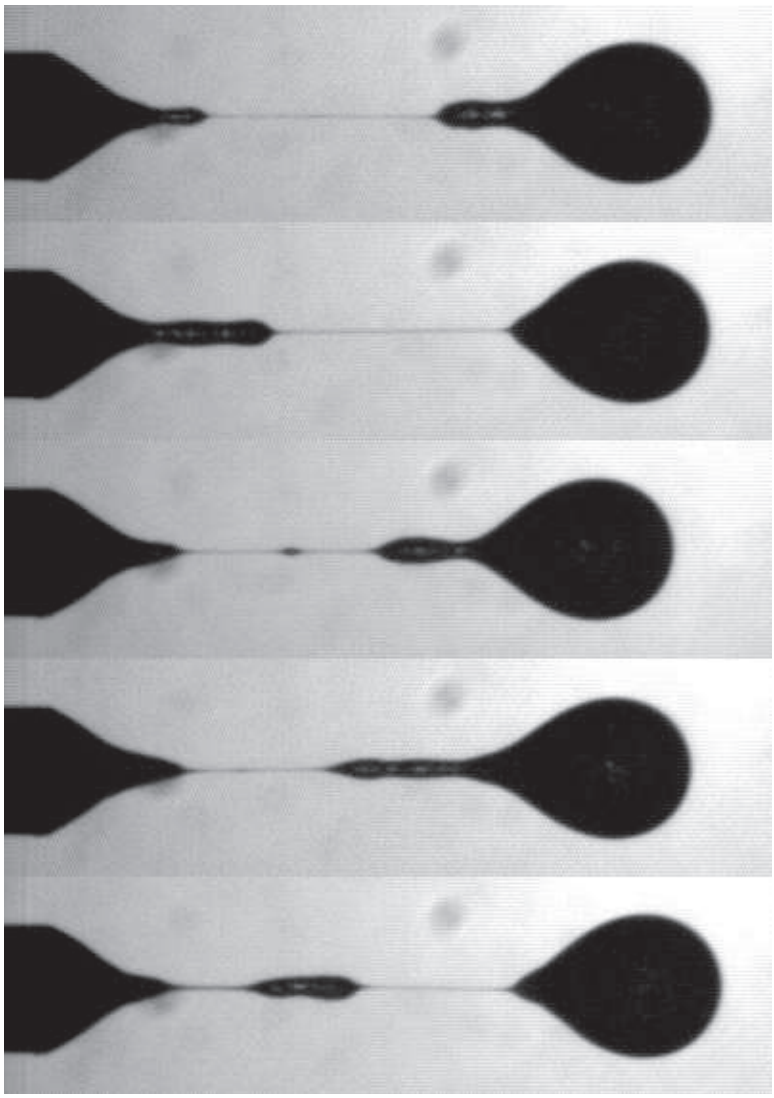

Figure 54: Pinch-off structures for five different experiments for $\phi = 0.20$, $d = 0.32$ cm, $d_p = 212 - 250$ μm.

identify the transition from stage-one to stage-two necking. Stated another way this approach seeks to determine if there exists a time before which all the drop shapes are essentially the same, regardless of the particle concentration, and if there is how it changes with ϕ.

The initial approach taken in analyzing the particle fluctuations was to average the shapes leading up to pinch-off. The deviation from the mean could then be used to determine how the particles were influencing the shape. The shapes for a suspension

of $\phi = 0.10$ at times approaching pinch-off are shown in Figure 55 and will be used to illustrate how the averaging scheme is implemented. In this figure the different curves represent the detected edge of the forming drop for five different experiments at the same conditions. At early times, $t_0 - t \leq 0.10\ s$, there is little or no deviation and the shapes of the forming drops are indistinguishable from one another. As thinning continues, however, the shapes start becoming noticeably different from one another ($t_0 - t = 0.05\ s$) with the axial deviation the most pronounced. As pinch-off is approached, this axial spreading of the shapes continues to increase and eventually radial fluctuations in the shapes become significant at times very near pinch-off. The resolution in Figure 55 is 1 pixel = 0.05 mm which corresponds to $R/a = 0.376$ and $z/d = 0.006$.

In attempting to average these shapes at a given time, the procedure was to take the mean of the various curves at a given axial position. The axial deviation in the curves introduced some difficulty in the process since near the end of the forming drop this averaging technique yields unrealistic values due to the large slopes. This problem could be alleviated through the use of a more sophisticated averaging technique involving the use of the gradients of the curves and averaging along directions normal to the curves at various points. However, the primary goal of this endeavor is to develop a measure of the difference between the curves and, from Figure 55, it is clear that the maximum deviation occurs in the axial direction at the end of the forming drop. This difference is nothing more than the difference in the thread lengths of the forming drops at a given time, $L(t)$. Using the deviation in L as the measure of difference of the shapes greatly simplifies the process (compared to the more complicated averaging technique) and also ensures that the maximum deviation in the shapes is used. This may be rationalized by considering that the particle effects should be greatest at L since the effects are cumulative over the length and integrated over the development time of the forming drop structure.

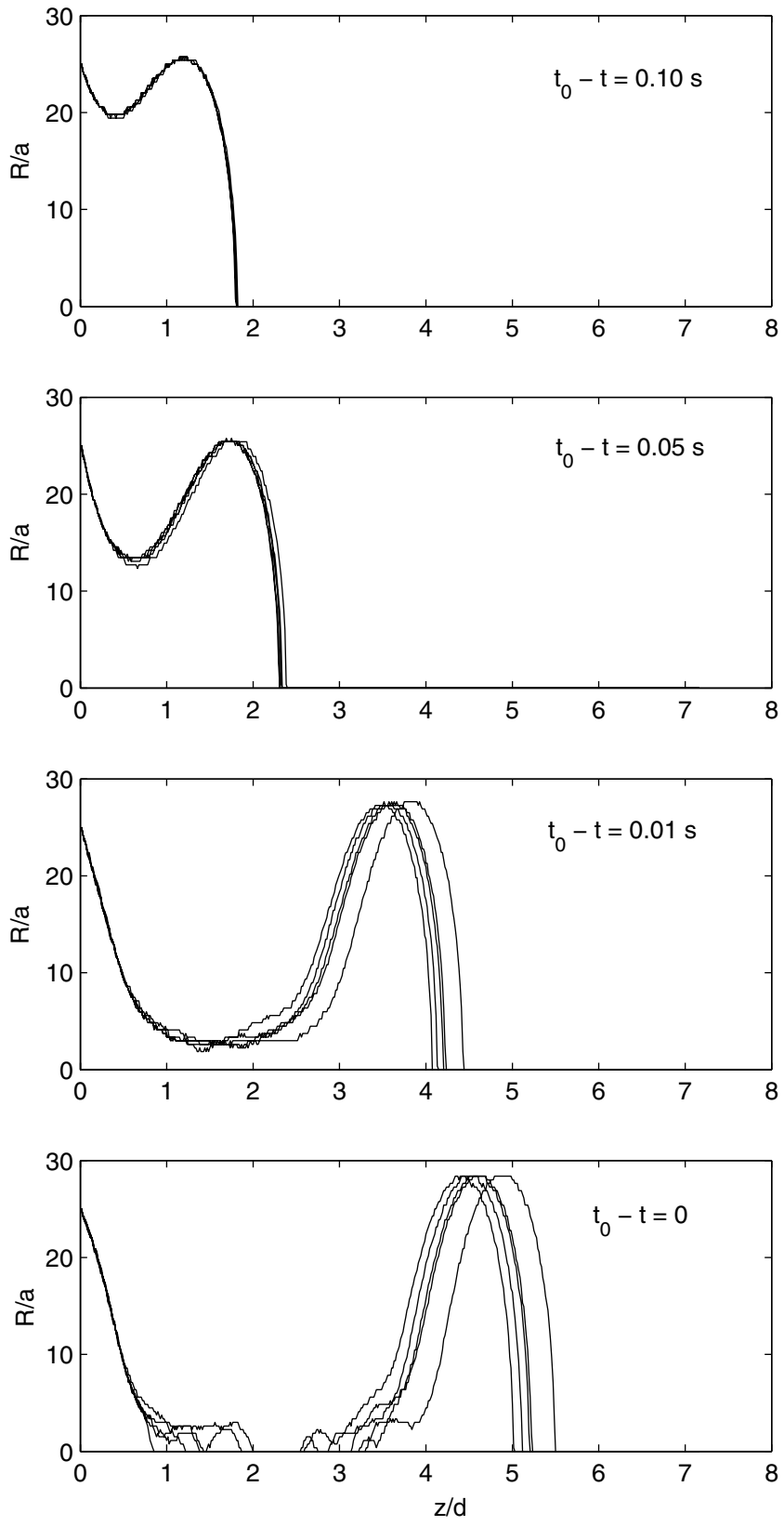

Figure 55: Shapes for the forming drop at various times before pinch-off for $\phi = 0.10$, $d = 0.32$ cm, $d_p = 106 - 125$ μm.

4.5.2 Deviation in L

As described in the previous section, the influence of the particle fluctuations is approximated by measuring the deviation in the $L(t)$ data. In this technique, the $L(t)$ curves are averaged and the standard deviation (ΔL) is used as the measure of the deviation. This method provides a measure of the maximum fluctuation in the shape of the forming drop.

The results of this analysis are presented in Figures 56-58 for the different experimental conditions investigated. In each of these figures the deviation in thread length, ΔL, is plotted as a function of time away from pinch-off, $t_0 - t$ where ΔL is scaled by the particle diameter to yield a measure of the deviation in terms of the number of particles. This scaling is somewhat arbitrary, in that a number of equally valid choices are possible (*e.g.* L or d), although it was chosen in order to determine if the deviation could be related to the thinning data, R/a, in which this scaling was already utilized. Also, as can be seen from the deviation data, this scaling results in order one deviations which is convenient.

Figure 56 presents the results for the case of the smaller orifice, $d = 0.16$ cm, with particles $d_p = 106 - 125$ μm. In this figure, ΔL for the pure liquid and the $\phi = 0.05$ and 0.10 suspensions are very similar with significant deviation in all three beginning at $t_0 - t \approx 0.05$ s and increasing to $\Delta L \approx 1.3$ just prior to pinch-off. The two highest concentrations, $\phi = 0.20$ and 0.30 start to show deviations earlier than the lower ϕ suspensions at $t_0 - t \approx 0.07$ s and the corresponding ΔL values at pinch-off are nearly twice as large. It is interesting to note that the maximum deviation at pinch-off occurs for $\phi = 0.20$ and not for the most concentrated suspension examined in this set. This trend holds for the other orifices examined as well and indicates that there exists a particle concentration which maximizes the fluctuations in L and that the fluctuations do not just increase monotonically with increasing ϕ. This result will

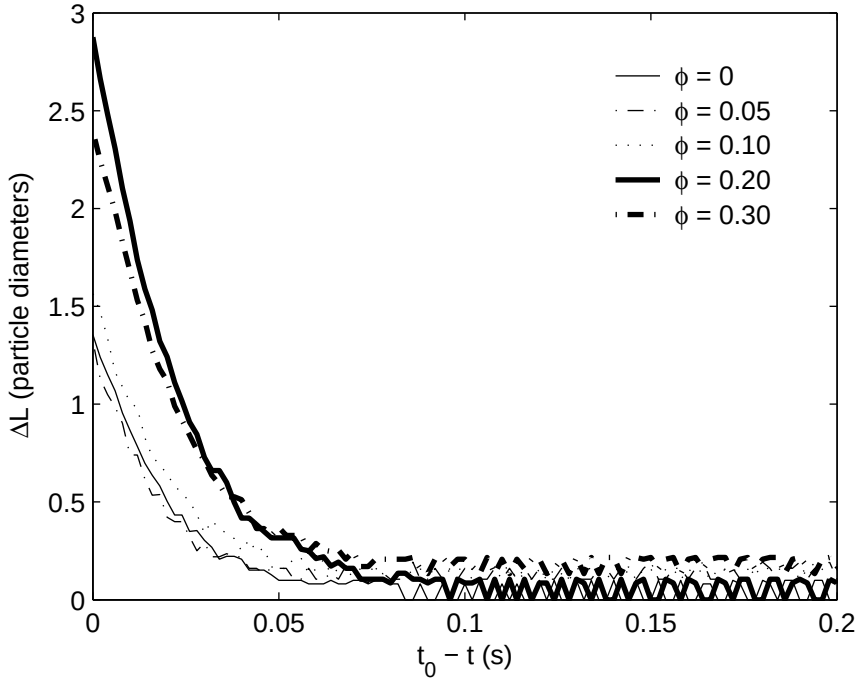

Figure 56: Deviation in L for $d = 0.16$ cm, $d_p = 106 - 125$ μm.

be explored further in the discussion section of this chapter. For all of the suspensions the deviations away from pinch-off are negligible and appear to characterize the noise in the experimental system. However, at the highest ϕ there does seem to be a slight increase in the deviation compared with the other suspensions which may indicate much earlier influence of the particles on the process at sufficiently elevated concentrations.

The deviation results for the larger orifice, $d = 0.32$ cm, with the smaller particles, $d_p = 106 - 125$ μm, are shown in Figure 57. For this orifice the ΔL values for the pure liquid are extremely small (< 1) throughout the process. This is quite different from the behavior of the pure liquid in the smaller orifice in which the deviations for the pure liquid and the low-ϕ suspensions are very similar. In this case the lowest-ϕ suspension, $\phi = 0.10$, has a deviation of ≈ 4.5. It is unclear why the behavior of the pure liquids are different in the two different orifices and the deviation is so much greater in the smaller orifice although it is possible that this results from the stronger

action of surface tension at the contact line of the smaller orifice. This would magnify any small imperfections in the surface of the capillary or changes in the wetting of the capillary tip from drop to drop and could result in the increased fluctuations in L observed. In any event, our primary interest in this endeavor is to understand the fluctuations introduced by the particles, especially for the highly concentrated suspensions in which the drop formation process is very different from the pure liquid case.

Other than the behavior of the pure liquid deviation, the ΔL behavior for the various small-particle suspensions through the larger orifice is very similar to that described previously for the smaller orifice. The maximum deviation occurs at pinch-off for each case and this value increases with increasing ϕ until $\phi = 0.30$ and then decreases quite markedly for the highest-ϕ suspension ($\phi = 0.40$). The values of ΔL are 2-3 times larger than those for the corresponding suspensions in the smaller orifice which indicates that the ratio d/d_p is relevant in understanding the fluctuations introduced by the particles. The times when the deviations start to increase are slightly greater than those observed for the smaller orifice. It is difficult to determine exactly when these fluctuations begin to become significant but it occurs in the range of $t_0 - t$ of 0.07-0.1 s with increasing ϕ leading to earlier fluctuations.

Figure 58 presents the data for the the ΔL fluctuations for the larger orifice, $d = 0.32$ cm, with the larger particles, $d_p = 212-250$ μm. In this case we observe some strikingly different behavior from either of the other two cases at the highest particle concentration although the lower-ϕ behavior is quite similar. The low-ϕ suspensions exhibit similar behavior to that of the smaller orifice in that the fluctuations of these suspensions are of similar magnitude (in this case directly comparable since the ratio d/d_p is the same) and start to increase near $t_0 - t = 0.07$ s. The big difference in behavior occurs for the $\phi = 0.40$ suspension. In this case ΔL is much larger than all of the other suspensions at times away from pinch-off. This behavior is not observed

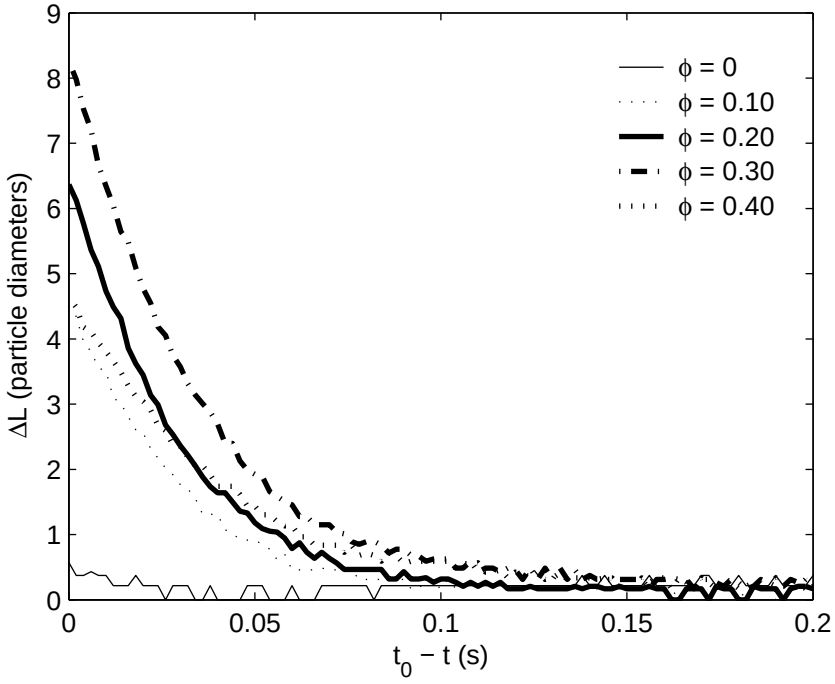

Figure 57: Deviation in L for $d = 0.32$ cm, $d_p = 106 - 125$ μm.

for either the smaller orifice or the same size orifice with the smaller particles. This indicates that this effect is due to the larger particle size although it is not clear why a similar effect is not observed for the smaller orifice since the particle to orifice diameter ratio is identical in both cases.

4.6 Discussion

In this chapter the thread dynamics have been investigated experimentally with the goal of developing a more detailed understanding of the particulate effects on the thinning and stretching of the developing thread during the drop formation process. Specifically, we have focused on investigating the proposition that the drop formation for concentrated suspensions can be thought of as occurring according to a 2-step process. In this endeavor we have also quantified various particle effects on the dynamics of the forming drop as well as the fluctuations introduced by the particles. In the remainder of this chapter we will discuss these experimental results in more

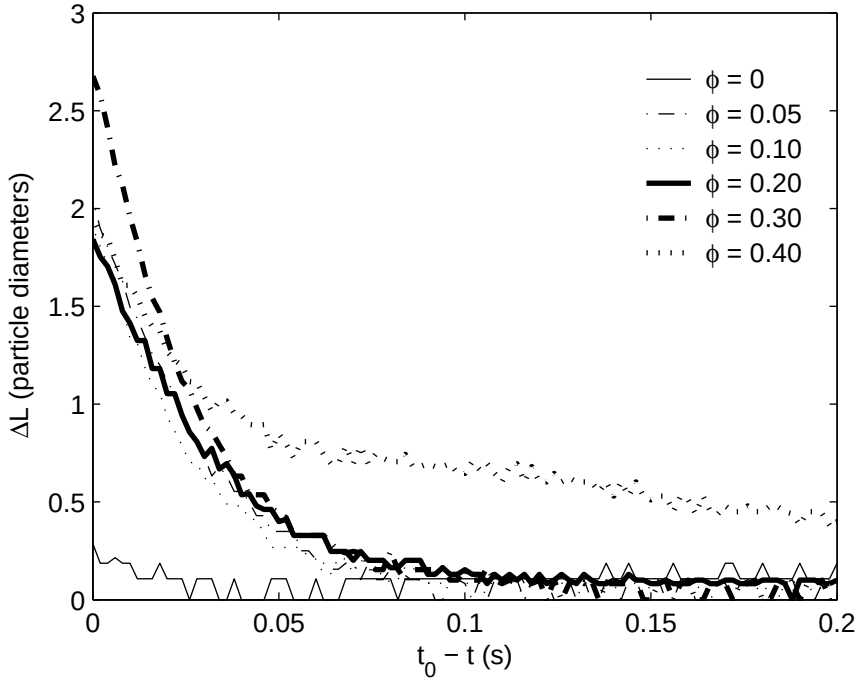

Figure 58: Deviation in L for $d = 0.32$ cm, $d_p = 212 - 250$ μm.

detail as well as probe the validity of the two-stage necking model.

4.6.1 Particle effects on the thread dynamics

The primary particulate effects on the thread dynamics are resisting the thinning and the lengthening of the thread, although these two effects have very different origins. The resistive thinning of the thread can be seen as an effective continuum effect while the length limiting quality of the particles is an effect of the discrete nature of the particles. In this section we will consider both of these effects and comment on each in turn.

The first effect can be seen in comparing the thinning curves for concentrated suspensions (Figures 41-43) and those for the higher viscosity pure liquids (Figures 44 and 46). In each of these, the thread thins more slowly than the pure suspending liquid and the result is due to the increase in either the pure liquid viscosity (in the case of the differing pure liquid mixtures) or the effective viscosity (in the case of the

suspensions). This effect is quantified in the thinning rate, as determined from the fits of the thinning data to the exponential form, (9). The thinning rate decreases with increasing viscosity and provides a quantitative measure of the effect of viscosity of the process.

This trend of slowing the thinning rate due to added particle concentration is reversed for times near pinch-off where we observe the rate of thinning to increase sharply with particle concentration. This effect is directly opposite to that of the increasingly viscous pure liquids, which thin more slowly throughout the necking process. To understand this result we recall the physical structure of the neck during these times. At this point the thread has thinned to $\sim 4-5$ particle diameters so the thread can be visualized as essentially a cylinder of liquid with a small number of particles spanning its cross-section. In this situation, individual particles are resisting the further thinning of the thread. This results in the thread being much thicker than the corresponding pure liquid (or any of the higher viscosity mixtures) at similar times away from pinch-off. At these times the particles must be considered discrete solid bodies and their unique arrangement within the thread dictates how necking proceeds. In order for the thread to rupture, the particles must be rearranged within the thread such that a particle-free region develops over which final necking occurs. This final necking—when the thread thinning transitions from thinning over a particle-rich to a particle-free region—is what leads to much steeper slopes in the R/a curves for increasingly concentrated suspensions. This process is somewhat analogous to the necking and rupture of solids where the material exhibits a yield stress at a weak point and then very rapidly ruptures at that location. The rearrangement of the particles within the thread during the later stage of necking can be viewed in these terms as developing a weak point within the cylindrical column and then rapidly rupturing at that point.

The transition in length scales—from d to d_p—is ultimately responsible for this

change in behavior and is the cause of both the steepening of the R/a curve near pinch-off and the reduced length of the thread. In the case for pure liquids there is no physical length scale other than the orifice diameter and the final necking is governed by the viscous length scale, L_μ, a quantity derived solely from the liquid properties. This viscous length scale, as proposed by Peregrine *et al.* [37], is defined as

$$L_\mu = \frac{\mu^2}{\rho\sigma} \tag{11}$$

This length scale is used in determining the range over which similarity solutions are possible for the shape of the forming drop. In our experiments $L_\mu = 1.7$ mm for the suspending liquid. Numerous researchers have utilized this technique to model the dynamics of the thread at times very near pinch-off [15, 44] although in the case of concentrated suspensions this technique is not feasible for two reasons. The first is the pinch-off structure itself. There is wide variability in the structure at pinch-off and the size and shape of the spindles fluctuates greatly from drop to drop. The other is the presence of the particles and the addition of a new length scale to the problem. Despite these limitations the technique may be useful for determining the thinning rate of the liquid thread after a particle-free region has developed since it is possible that the behavior at some scale will retain the similarity characteristics. Regardless, the scales involved are below the level of detection in this work and rates of thinning were not measured in this regime.

The addition of the particle size as a new length scale in the problem is directly responsible for the decrease in the pinch-off length of the suspensions relative to the pure liquid. This effect is obviously not attributable to the modification of the bulk viscosity of the mixture, as is the slowed thinning rate away from pinch-off, since the higher viscosity pure liquids have the opposite effect. The higher viscosity pure liquids attain much longer thread lengths than the lower viscosity suspending liquid. The effect can also not be viewed as the particles increasing the viscosity of the mixture up until a certain point, when the discreteness of the particles become important,

and then reverting to the viscosity of the pure liquid since this would also lead to longer thread lengths. Again recalling the picture of the thread at times where its width approaches that of individual particles, the most reasonable explanation why the threads for the suspensions are shorter than the corresponding pure liquid is that individual particles within the thread make up a certain volume of the total of the thread. This portion of the total volume, which would consist of entirely liquid in the $\phi = 0$ case, cannot deform and the ability of the thread to stretch is diminished. This simple explanation is clear for the cases where particles are captured within the liquid thread (*i.e.* resulting in particle-laden satellite drops) but not so clear for the cases where all the particles are eventually swept out of the thread, leading to the formation of spindles. This may in fact be the reason that the decrease in thread length is much less pronounced for the smaller orifice since particles are rarely captured in the thread in this case. However, the movement of the particles in the thread which lead to the formation of the spindle structures will also reduce the volume of liquid in the thread in that some liquid will be carried along with the particles.

The particles also increase the variability in the process, as presented in section 4.5, where the variability in the thread length (ΔL) is used as the measure of the particle-induced fluctuations. One striking feature of these measurements is the time at which the fluctuations start to increase. From the analysis of the thinning data in section 4.4 we found that times fairly close to pinch-off ($t_0 - t \approx 0.03$ s) were able to be fit to the model equation which indicated that up until these times the fluctuations should be somewhat minimal. However, for each of the orifice diameters and particle sizes examined the fluctuations actually start to increase at $t_0 - t \approx 0.07 - 0.08$ s, much sooner than expected based on the fitting of the model equation. This indicates that the influence of the particles can be felt in the lengthening of the forming drop at times well-removed from the pinch-off.

Another interesting result from the particle fluctuation analysis is the presence

of an intermediate particle concentration for which the fluctuations are maximized. For each orifice this concentration corresponds to the next to highest ϕ investigated ($\phi = 0.20$ for $d = 0.16$ cm and $\phi = 0.30$ for $d = 0.32$ cm). This result supports the idea that increasing ϕ can actually produce a stabilizing effect on the process (as discussed in Chapter 3 concerning the reduction in the number of satellite drops observed at elevated ϕ).

4.6.2 Validity of two-stage necking model

The two-stage necking model we have proposed for concentrated suspensions derives from observations of the pendant drop formation process for the experiments presented in this, and the preceding, chapter. This model captures the basic physics of the problem and is useful in understanding the changing role of the particles in the different stages.

The two stages of the necking model, initial and final necking, essentially involve the transition from a regime where the thread dynamics are governed by bulk properties to one where individual particle effects dominate. According to this description, the particle effects in the first stage can be attributed solely to an increase of the effective viscosity of the mixture and the discrete nature of the particles ignored. In the second stage, the width of the thread has thinned sufficiently that a continuum description of the material is no longer possible. At this point the discreteness of the particles and the individual particle motions within the collapsing thread are responsible for the very different pinch-off structures observed for the suspensions. Although the individual particle motions are important in this stage for changing the ultimate structure of the forming drop (*e.g.* size of spindles, satellite drops), the thinning just prior to rupture occurs over a region of pure liquid and, hence, presumably in the same manner as that for pure liquids of similar thread thicknesses although this has not been investigated here.

The initial necking stage of the 2-step process has been investigated using the model equation presented in section 4.4 for the exponential decay of the thread radius. The resulting fits of the data using this equation are quite good, which indicates that the early necking stage of the drop formation is well described by this expression. Using this technique we found that the thinning rate scales linearly with the orifice diameter (as did Clanet & Lasheras (1999) [10]) and with viscosity to the $-1/3$ power. This scaling with viscosity is valid for the various suspensions examined and seems to fit equally well for both low- and high-ϕ, small and large d_p, and both diameter orifices. This indicates that during initial necking our assumption that the primary particulate effect is to add viscosity to the mixture is valid and that the particle size is not relevant. The insignificance of particle size on the process during initial necking is presumably valid until d/d_p becomes small enough that a continuum description of the material in the forming drop is no longer feasible. In this work this minimum value of d/d_p investigated was 12.8 so as long as $d/d_p \geq 12.8$ the influence of particle size on the initial necking stage appears to be negligible.

Implicit in the proposition that the necking process of suspensions is described using a two-stage model is the need to identify the transition between the two stages. Towards this end we attempted to determine the key parameter governing when this transition occurs. Based on the argument that the transition accompanied the change in the dominant length scale in the problem from the orifice diameter to the particle diameter, the transition should be a function of R/a, the minimum thread radius scaled by the particle radius. This would yield the thread thickness when the length scale of the particles becomes important. Using the minimum time away from pinch-off above which the fits were possible we were able to determine the thickness of the thread at this time for the various suspensions. These values are presented in Table 7.

From the average values for a given orifice and particle size combination it seems possible that the transition between the two stages using this technique is dependent

Table 7: Thread thickness at the minimum time used in fitting the R/a data.

ϕ	d (cm)	d_p (μm)	$t_0 - t$ (s)	R/a
0.05	0.16	106-125	0.01	2.6
0.10	0.16	106-125	0.01	2.9
0.20	0.16	106-125	0.01	3.2
0.30	0.16	106-125	0.01	3.4
average				3.0
0.05	0.32	212-250	0.03	4.0
0.10	0.32	212-250	0.03	3.8
0.20	0.32	212-250	0.03	4.3
0.30	0.32	212-250	0.03	4.7
0.40	0.32	212-250	0.03	4.4
average				4.2
0.10	0.32	106-125	0.03	7.9
0.20	0.32	106-125	0.03	8.9
0.30	0.32	106-125	0.03	7.5
0.40	0.32	106-125	0.03	8.0
average				8.1

on the ratio of the capillary to particle diameter, d/d_p. The similar values for the two different orifices with the same d/d_p ratio ($R/a \sim 3-4$) seem to indicate this although the values for the different size particles through the larger orifice have the same absolute half-width (R) at transition which seems to indicate that particle size is irrelevant. In this case we would expect the thickness of the thread at the transition between the stages to be smaller for the smaller particles.

To assess the overall validity of the two-stage model we must consider how well it allows us to understand the observed behavior in a more generalized context without losing important physical characteristics of the problem. In viewing the drop formation in two stages we are introducing a significant simplification of the actual process. In effect we are removing all the added complexity in the problem due to the particles during the first stage of necking by treating the mixture as a continuum. This treatment seems justified based on the results presented in section 4.4 where the thinning rate was shown to depend on the effective viscosity of the suspension.

Based on this work there are two main limitations of the two-stage model. The first is the inability of the model to account for the observed decrease in the thread length due to the particles. This effect is presumed to be the result of particle motions within the thread during the second stage of the model once particle size has become important relative to the width of the thread. This necking stage is quite complex since the particle motions within the thread must be considered and the interactions between the particles and with the free surface are extremely complicated. The other main limitation of this model is the ambiguity of determining the point where the transition between the two stages occurs. In this work the technique utilized to determine the transition was to essentially back out the location from the fits to the thinning data which yielded values of $R/a \approx 4$ for $d/d_p = 12.8$ and $R/a \approx 8$ for $d/d_p = 25.6$ and it is not clear that these values are at all general.

Despite these limitations the two-stage process is still very useful. The ability to

use an effective viscosity treatment of the material during the first stage of necking is justified based on the experimental results and leads to a significant simplification of the problem which could be taken advantage of in future work to numerically model flows of this nature. Additionally, it is the behavior of the drop formation process during this first stage which determines many of the characteristics of the process which are important in industrial applications (drop size) and this simplification is likely to be useful in these environments.

4.7 Concluding remarks

In this chapter we have investigated the dynamics of the thread during necking in detail and provided validation for the two-stage necking model we introduced in Chapter 3. We have measured the thinning and stretching of various suspensions and fit the thinning data to a model equation allowing quantification of the thinning rate, as well as investigated the fluctuations introduced by the particles during the process.

The presence of the particulate phase leads to added resistance to the thinning and the stretching of the thread during necking. This added resistance to the thinning occurs in the first stage of the two-stage necking model and occurs in a similar manner to that observed for increasingly viscous pure liquids. The thinning rate of the various suspensions has been measured during this first necking stage using a technique where the thinning data is fit to an exponential decay equation and the thinning rate has been found to scale with $\mu_{\text{eff}}^{-1/3}$. This result validates the assumption that the suspension can be treated as a continuum during the first stage of necking, a considerable simplification in this problem.

The particle resistance to the thread stretching occurs predominantly in the second stage of the two-stage model and leads to shorter thread lengths at pinch-off for the suspensions. This resistance occurs when the thread has thinned to such an extent that individual particle sizes become significant and must be rearranged within the

thread to yield a location free from particles where final necking and pinch-off can ultimately occur.

The deviations in the thread length during necking have also been measured and used to quantify the particle-induced fluctuations during the process. This technique reveals that the particles influence the thread length much earlier than thought previously. The stabilizing effect described in Chapter 3 is also evident in these measurements where the largest fluctuations are observed for particle concentrations below the highest examined.

CHAPTER 5

JET TRANSITION AND NEAR-ORIFICE JET SHAPE

In this chapter we depart from the focus of the previous two chapters (pendant drop formation) and move on to a consideration of drop formation at more elevated flow rates. We examine both the transition from dripping to jetting and the resulting jet shapes for particle-laden mixtures and present qualitative and quantitative analysis of the particulate effects in each case.

5.1 Transition from dripping to jetting

To study particulate effects on the transition from dripping to jetting, the pinching event was studied for suspensions of varying ϕ and orifices of different diameter, d, over a range of increasing flow rates. In each experiment the initial flow rate was such that dripping was observed. This rate was increased slowly over the course of additional experiments until jetting was observed. The thread length was measured as a function of time in each experiment and used in identifying the transition. All results presented in this section are for drops forming into ambient air.

Typical time series illustrating L/d are presented in Figure 59. The first graph (Figure 59(a)) shows the results for the pure liquid. At early times, $t < 3$ s, drops are formed in the dripping mode with a constant period. At $t \approx 3$ s the flow rate is increased a small amount (from 12.7 cm^3/min to 12.8 cm^3/min) and the system undergoes an abrupt transition and forms a column of liquid stable to $\sim 50d$; in Figure 59(a) $L/d = 15$ represents the field of view of the camera and breakup of the pure liquid jet occurs much further downstream (the position was determined in

independent experiments) by the familiar capillary instability. Although other researchers have reported an intermediate oscillatory regime between periodic dripping and jetting [2, 10] this was not observed in our experiments, apparently due to our larger liquid viscosity.

Also shown in Figure 59 are results illustrating L/d near the transition for suspensions of $\phi = 0.05$ and 0.20. In the case of $\phi = 0.05$, shown in Figure 59(b), the behavior is quite similar to that of the pure liquid in the sense that an abrupt lengthening of the thread is observed due to a small increase in flow rate, with a similar flow rate at transition. What is different, however, is that the accompanying lengthening of the thread is much less for the suspension: $L/d \approx 10$ for $\phi = 0.05$ compared with $L/d \approx 50$ for the pure liquid. The behavior of the more concentrated suspension ($\phi = 0.20$) is shown in Figure 59(c). In this case a transition is evident when Q is increased from 11 to 12 cm^3/min, although the behavior prior to transition is different from that of either the pure liquid or the low-ϕ suspension. It appears that prior to the onset of jetting the suspension goes through an intermediate mode where the minimum value of L/d fluctuates. Lengthening of the liquid column attached to the tip of the orifice occurs when the liquid thread following rupture is unable to retract fully before a new drop begins to form. Following the transition the corresponding lengthening of the thread is lower still than the $\phi = 0.05$ suspension.

Quantitative results for the transition experiments are presented in Figures 60 and 61 in which the dimensionless thread length, $(L/d)_{\min}$, is plotted as a function of Q for all ϕ studied. The quantity $(L/d)_{\min}$ represents the coherent length of the liquid or mixture attached to the orifice, as it is an average of the minimum values of L/d observed over all drop formation events in an experiment (the minima in the L/d of the time series). For example in Figure 59(a), $(L/d)_{\min} = 1.8$ for $\phi = 0$ before the transition. For $\phi = 0.05$, $(L/d)_{\min}$ at transition decreases greatly relative to the pure liquid, from $\sim$ 90 to $\sim$ 11 for the smaller orifice ($d = 0.16$ cm) and from $\sim$ 50

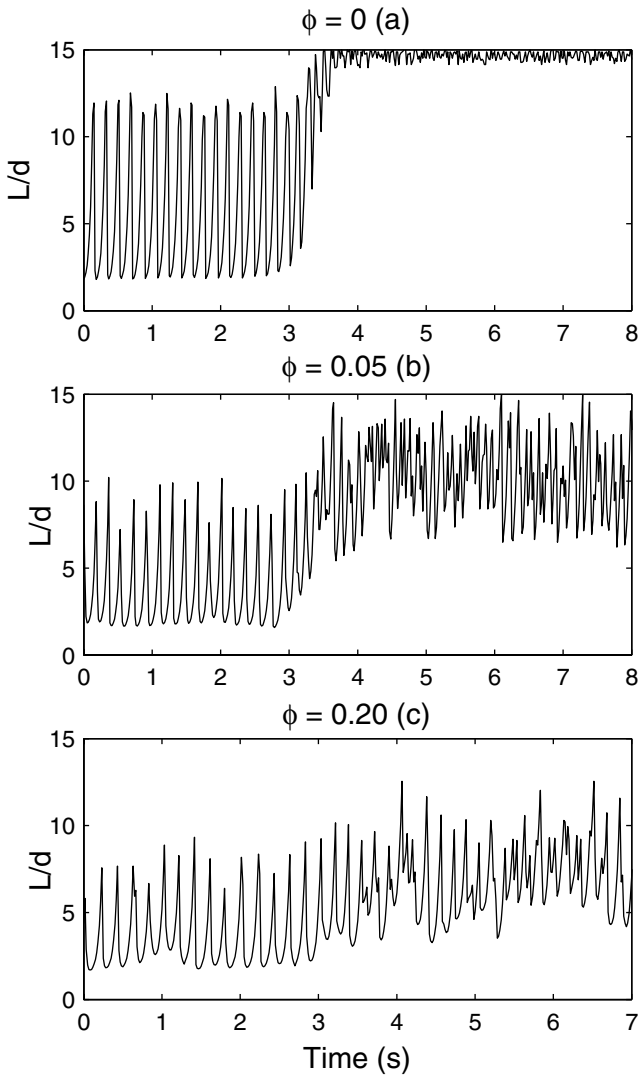

Figure 59: Results of typical experiments for the transition from dripping to jetting for (a) $\phi = 0$, (b) 0.05, and (c) 0.20 with $d = 0.32$ cm, $d_p = 212 - 250$ μm in which dimensionless thread length (L/d) is plotted as a function of time. The transition in each case follows changes in Q: (a) 12.7 to 12.8 cm^3/min, (b) 12.9 to 13.0 cm^3/min, and (c) 11.0 to 12.0 cm^3/min. In (a) $L/d = 15$ corresponds to the camera field of view with the actual $L/d \approx 50$ after the transition.

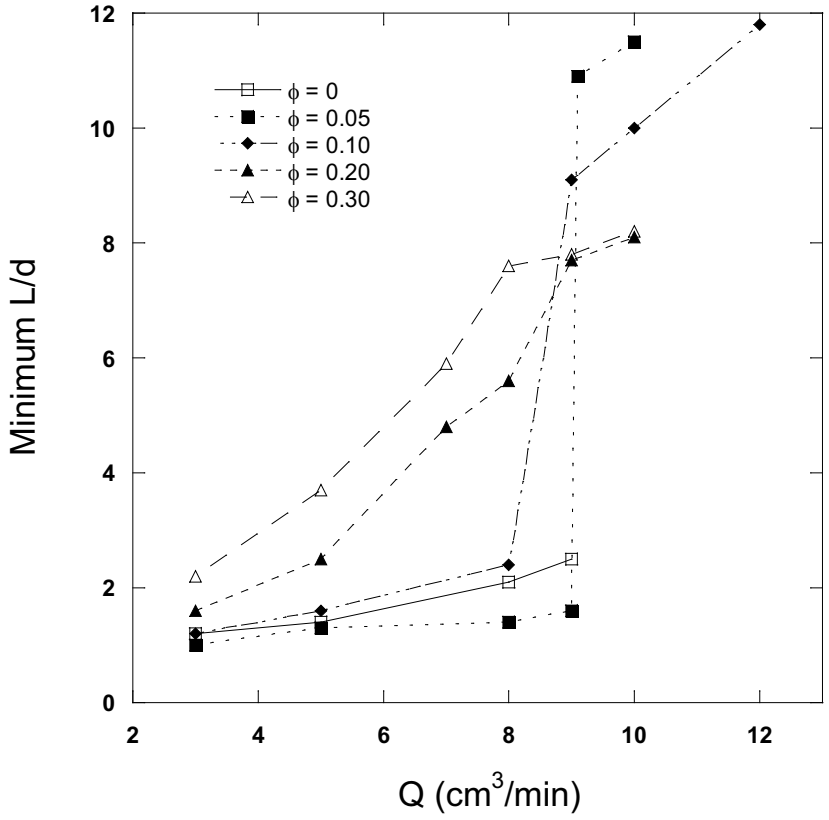

Figure 60: Dimensionless minimum thread length, $(L/d)_{\min}$, as a function of Q for $d = 0.16$ cm, $d_p = 212 - 250$ μm. The data point after transition for the pure fluid, $\phi = 0$, is omitted.

to $\sim$ 9 for the larger ($d = 0.32$ cm). The data points corresponding to $(L/d)_{\min}$ at rates above transition for $\phi = 0$ in both Figures 60 and 61 are omitted so that the effects of increasing ϕ can be presented more clearly.

Although the coherent jet lengths following transition are substantially shorter, Figures 60 and 61 show that low-ϕ suspensions otherwise behave similarly to the pure liquid. Prior to transition, suspensions at both $\phi = 0.05$ and 0.10 have $(L/d)_{\min}$ very similar to the pure liquid. These mixtures also display sharp transitions at flow rates very nearly the same as that observed for the pure liquid. As ϕ is further increased two trends are apparent: first, the lengthening of the liquid column leading to transition occurs more gradually and, second, it begins at progressively lower Q.

Smoothing of the transition at higher ϕ is evident for both orifices examined, and

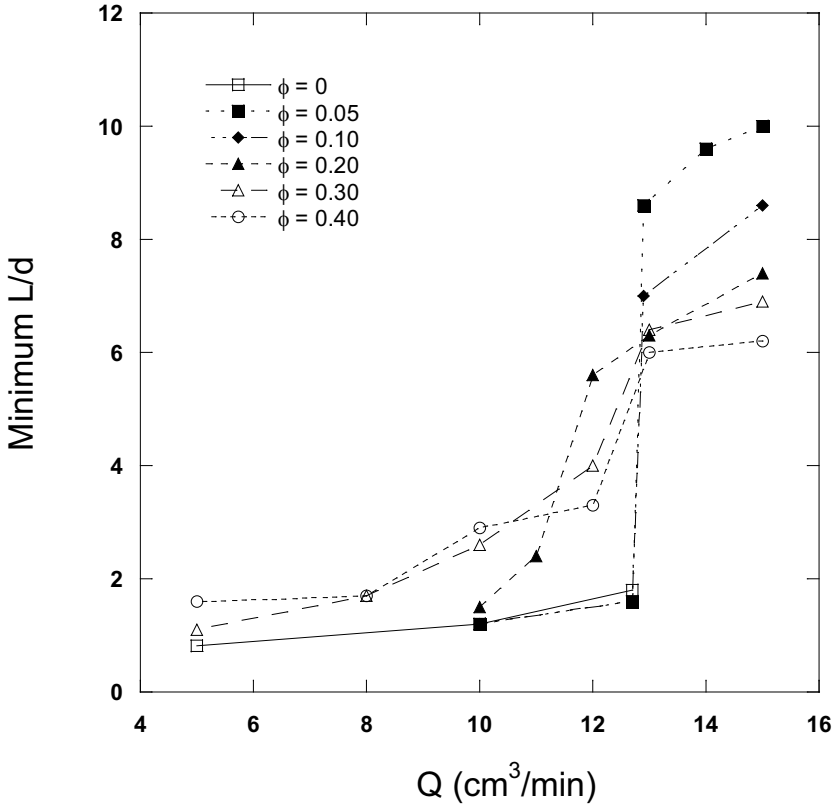

Figure 61: Dimensionless minimum thread length, $(L/d)_{\min}$, as a function of Q for $d = 0.32$ cm, $d_p = 212 - 250$ μm. The data point after transition for the pure fluid, $\phi = 0$, is omitted.

is most pronounced for the smaller orifice (Figure 60). Here $(L/d)_{\min}$ for $\phi = 0.20$ and 0.30 gradually increases from 2 to nearly 8 with no obvious abrupt transition, although the column of liquid stable to $\sim\ 8d$ at the largest volume fraction is indicative of jet-like behavior. Hence, the most we can safely say about these two concentrated suspensions is that between $Q = 3$ cm^3/min and 9 cm^3/min the behavior changes gradually from dripping to jetting. The two highest ϕ for the larger orifice also display smoothing of the transition.

The onset of earlier jetting is clearly evident for $\phi = 0.20$ in the $d = 0.32$ cm orifice, as shown in Figure 61. In this case an abrupt lengthening is seen when the flow rate is increased from 11 to 12 cm^3/min. Although the difference between the transition Q for $\phi = 0$ and 0.20 is small (12.7 and 12.0 cm^3/min, respectively), jetting is induced by the addition of particles at a flow rate for which periodic dripping is observed for pure liquid.

Experiments on the jet transition were also performed using smaller particles ($d_p < 106$ μm) and the results are presented in Figure 62. Only $\phi = 0.05$ and 0.10 were examined in these experiments, whose purpose was to compare the transition behavior — both the transition flow rate and the jet length attained just above the transition flow rate — of small- and large-particle suspensions. In Figure 62 it is illustrated that the coherent jet length in the form $(L/d)_{\min}$ for the smaller particles was nearly twice that of the larger particles, but only about one-half the length of the pure liquid jet. The flow rate at transition for the smaller particles is the same as that for the pure liquid and the larger particle suspensions for $\phi = 0.05$; for $\phi = 0.10$ with sub-106 μm particles, the transition occurs at a slightly lower flow rate than in the pure liquid.

In addition to the transition to jetting from dripping, the reverse case of slowing flow rate to transition from jetting to dripping was also examined in a limited set of experiments. Since the abrupt nature of the transition disappears at elevated ϕ, only

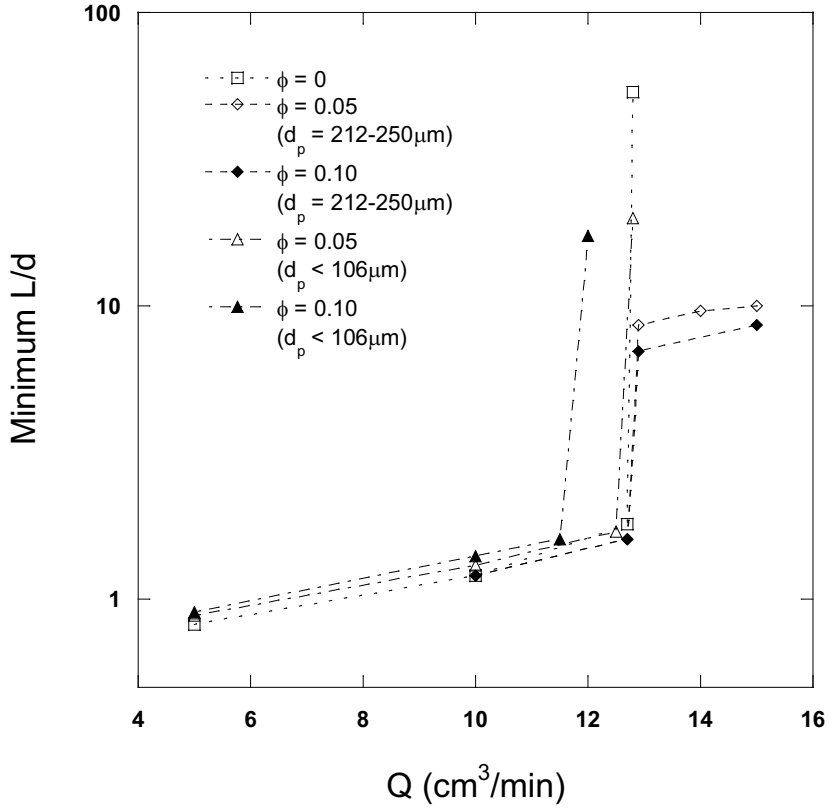

Figure 62: Dimensionless minimum thread length, $(L/d)_{\min}$, as a function of Q for $d = 0.32$ cm, $d_p = 212 - 250$ μm and $d_p < 106$ μm. Note that $(L/d)_{\min}$ is plotted on a logarithmic scale.

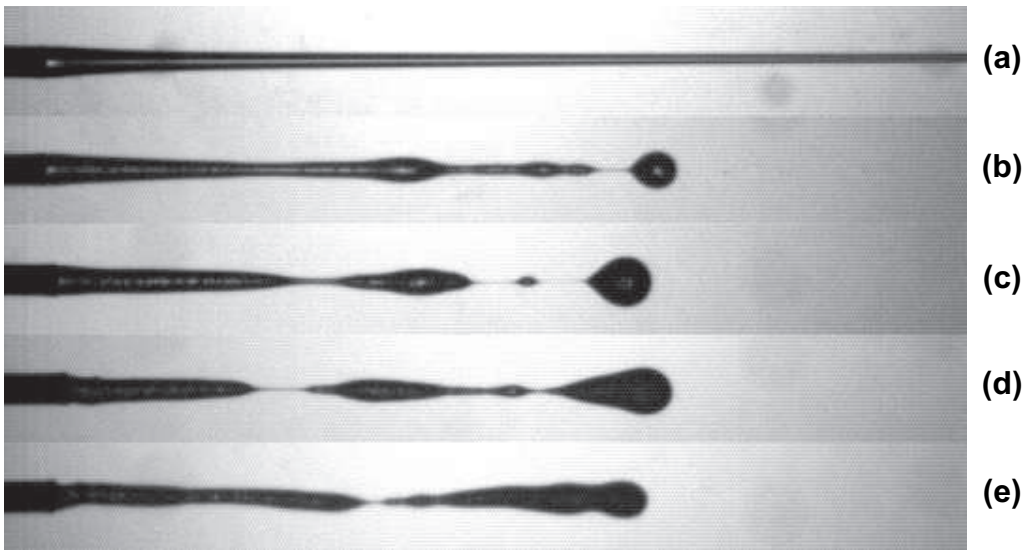

Figure 63: Representative jet structures for $d = 0.16$ cm, $d_p = 212 - 250$ μm, (a) $\phi = 0$, (b) 0.05, (c) 0.10, (d) 0.20, and (e) 0.30. $Re \approx 0.4$ (varies slightly with ϕ).

suspensions of $\phi = 0.05$ for $d_p = 212 - 250$ μm and $d_p < 106$ μm were examined in flow through the $d = 0.32$ cm orifice. All of the cases examined displayed hysteresis, as the flow rate Q_+ for transition to jetting from dripping differed from the flow rate Q_- for transition to dripping from jetting. For pure liquid and the small particle suspension, $Q_+ = 13$ cm^3/min and $Q_- = 10$ cm^3/min, while for the larger particles, $Q_+ = 13$ cm^3/min and $Q_- = 11$ cm^3/min. The larger particles appear to reduce hysteretic effects, perhaps due to the large fluctuations induced.

Two other, more qualitative, results were obtained in examining the process once the transition from dripping to jetting was complete: at large ϕ the jet developed a "swinging" side-to-side motion and the wetting of the orifice changed with increasing ϕ. Figures 63 and 64 show the jet structures for various ϕ for both $d = 0.16$ and 0.32 cm.

The swinging motion is most pronounced for the smaller orifice and is evident in Figure 63(e), which illustrates the jet structure for $\phi = 0.30$. Swinging is observed for the highest concentrations and flow rates, and seems to develop due to unbalanced forces in the retraction after breakup. This behavior results from asymmetric particle

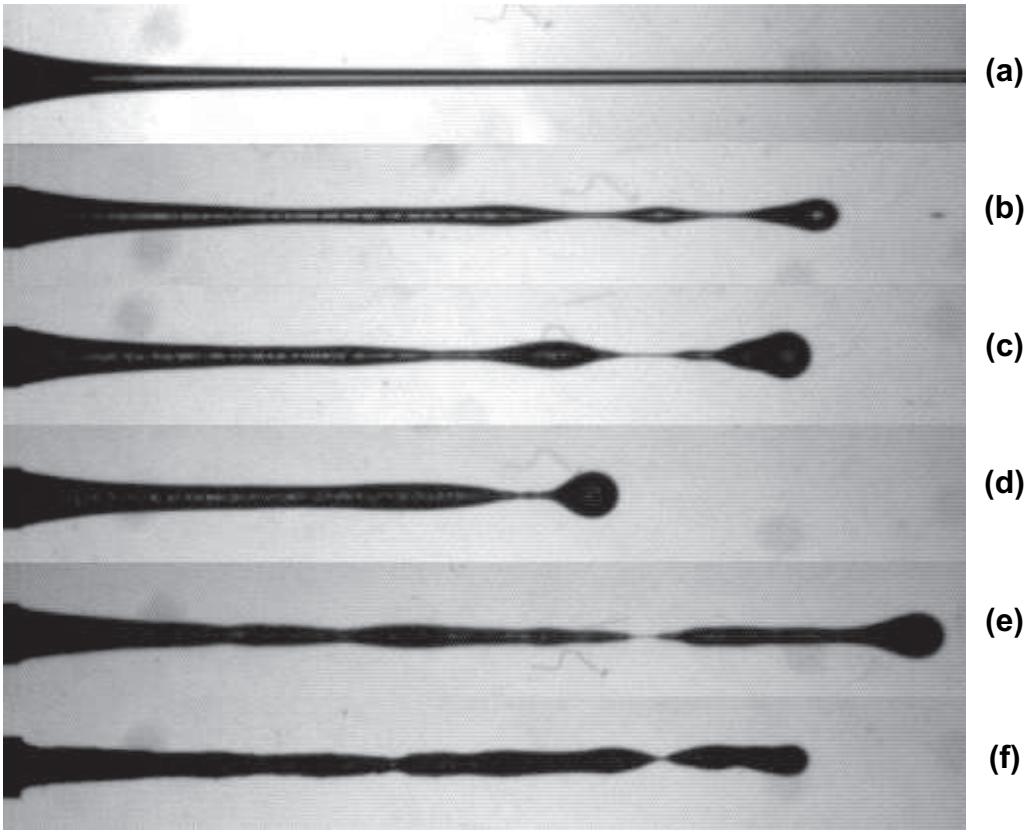

Figure 64: Representative jet structures for $d = 0.32$ cm, $d_p = 212 - 250$ μm, (a) $\phi = 0$, (b) 0.05, (c) 0.10, (d) 0.20, (e) 0.30, and (f) 0.40. $Re \approx 0.3$ (varies with ϕ).

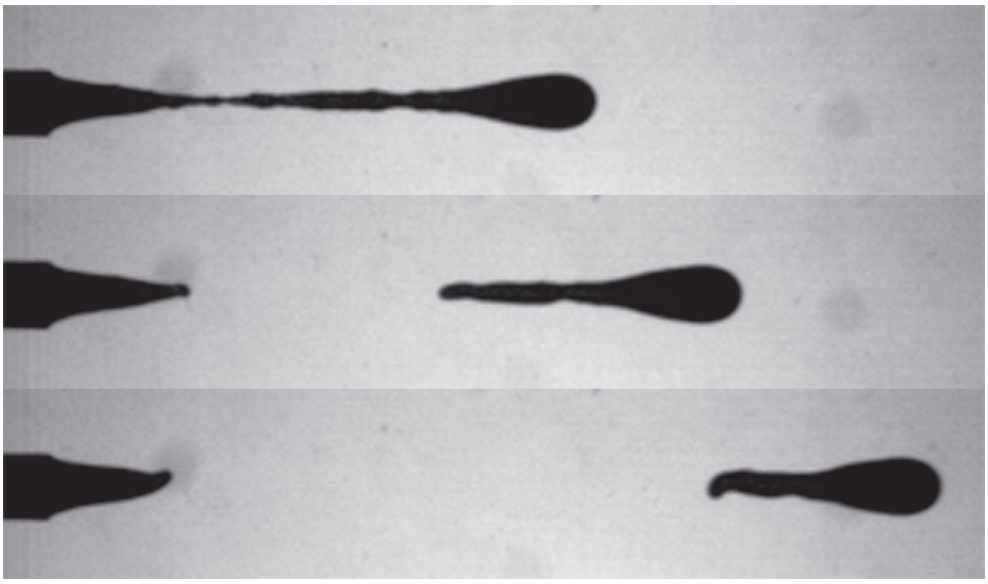

Figure 65: Asymmetric pinch-off for $\phi = 0.40$, $d = 0.32$ cm, $d_p = 212 - 250$ μm, $Q = 3$ cm^3/min ($Re = 0.06$).

configurations in the suspension above and below the pinch location, which then interact in a nonaxisymmetric fashion with the unbalanced surface tension. Although the swinging motion develops at high Q, the asymmetric retraction following pinch-off is observed at low Q while pendant drops are still forming (Figure 65).

However, the time between drops is sufficiently large that all lateral motion induced following pinch-off of a drop subsides prior to the development of the subsequent drop. The second observation is that the shape of the mixture near the orifice changes with increasing ϕ. Specifically, the film wetting the cut face of the capillary tube becomes thinner under high flow rate and elevated ϕ, appearing to almost dewet, as illustrated in Figures 63 and 64. This observed effect motivated the investigation presented in the following section in which the particulate effect on the shape of the jet near the exit of the capillary is probed.

5.2 Jet shape near the orifice

In this section the results of a separate set of experiments are presented in which the shape of the jet is investigated. In this investigation the scope is limited to looking

at the particle effects on the jet very near the region of the orifice ($z \leq 1.5d$). The preceding section presented the observation which instigated this work: the particles appear to cause a significant contraction of the jet near the orifice at elevated particle concentrations. This effect is clearly evident for the $d = 0.32$ cm capillary at $\phi = 0.40$ shown in Figure 64(f). In these new experiments we will magnify this region and seek to develop an understanding of the particle effects on the shape of the jet.

These experiments involve the use of the same apparatus and general procedure as described previously. The mixture is forced through the capillary at a constant flow rate sufficiently large to ensure that jetting is fully developed (well beyond the transition region described in 5.1). In all of the experiments the Reynolds number (based on the average velocity in the capillary and the orifice inner diameter) is small ($Re < 1$). The evolution of the jet is captured with increased resolution, relative to that presented previously in this chapter, and the resulting images analyzed. Snapshots of the developed jets near the orifice for the mixtures investigated in this study are presented in Figures 66-68.

Figure 66 presents the results for various suspensions through the $d = 0.32$ cm capillary with $d_p = 212 - 250$ μm and $Q = 15$ cm^3/min (the same conditions as those in Figure 64). From these photographs we can clearly see the increasing influence of the particles on the jet. At $\phi = 0.05$ and 0.10 (Figure 66(b)-(c)) the shape of the jet is very similar to that of the pure liquid (Figure 66(a)) although particle-induced deformations to the jet surface can be seen in each. These images were chosen from a large number in order to highlight the particle effects and in many of the images for the lower-ϕ suspensions the surface of the jet does not display these particle-induced disturbances. However, we note that these effects are only visible in the current images for a very small percentage of the jet circumference and they are surely more numerous when considering the jet as a whole. As ϕ is increased to 0.20 and 0.30 (Figure 66(d)-(e)), these surface deformations become more numerous

and the jet starts to contract slightly near the exit of the capillary. Once the particle concentration is increased to $\phi = 0.40$ the behavior of the jet is quite dramatically altered ((Figure 66(f)). The surface of the jet has now contracted very noticeably near the outlet and no longer retains the gradual sloping appearance of the pure liquid and the lower concentration suspensions. The particles within the mixture are also creating many more surface deformations to the jet at $\phi = 0.40$. These deformations are observed to occur very near the orifice exit as well as further downstream. One additional note for clarification is in order with regard to these images. In certain images (most notably in Figure 66(c) and (e)) white discolorations are evident within the jet. These white spots are actually reflections of light off the particles within the jet from illumination from the light source which is transmitted through the jet.

The photographs of the jet shapes near the orifice for $d = 0.32$ cm with the smaller particle size distribution, $d_p = 106 - 125$ μm, are shown in Figure 67. These images indicate that the behavior of the smaller particle suspensions is similar to that of the larger particle suspensions. Again, we observe that the jet shapes for the lower-ϕ suspensions ($\phi = 0.10$ and 0.20) are very similar to that of the pure liquid and at elevated ϕ the shape of the jet near the orifice becomes contracted. For these smaller particle suspensions this contraction seems to be more pronounced at $\phi = 0.30$ (Figure 67(c)) than it was in the case for the larger particles. Another difference between the two particle sizes is that the smaller particles are causing smaller deformations to the surface of the jet; this is a reasonable expectation for smaller particle suspension jets and will be quantified later in this section. These observations will be further explored as well as quantified later in this section where we will examine the behavior of the jet shape over a range of times.

Figure 68 shows two images of the jet shape for the smaller orifice, $d = 0.16$ cm. The first image (Figure 68(a)) is for the pure liquid and the second (Figure 68(b)) is for the most concentrated suspension, $\phi = 0.30$, examined for this orifice. The

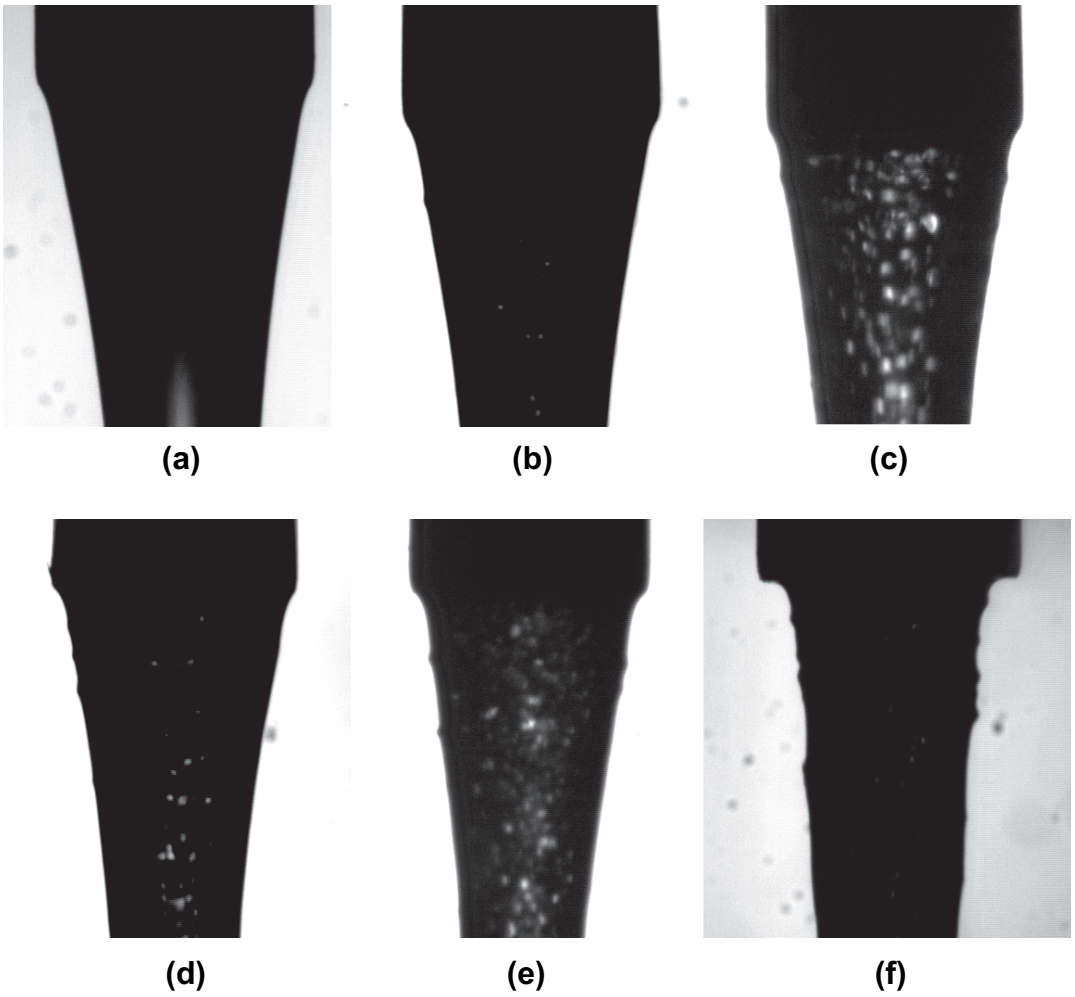

Figure 66: Jet shapes near the orifice for $d = 0.32$ cm, $d_p = 212 - 250$ μm, and $Q = 15$ cm^3/min ($Re = 0.6$) for the pure liquid and various suspensions with (a) $\phi = 0$, (b) 0.05, (c) 0.10, (d) 0.20, (e) 0.30, and (f) 0.40.

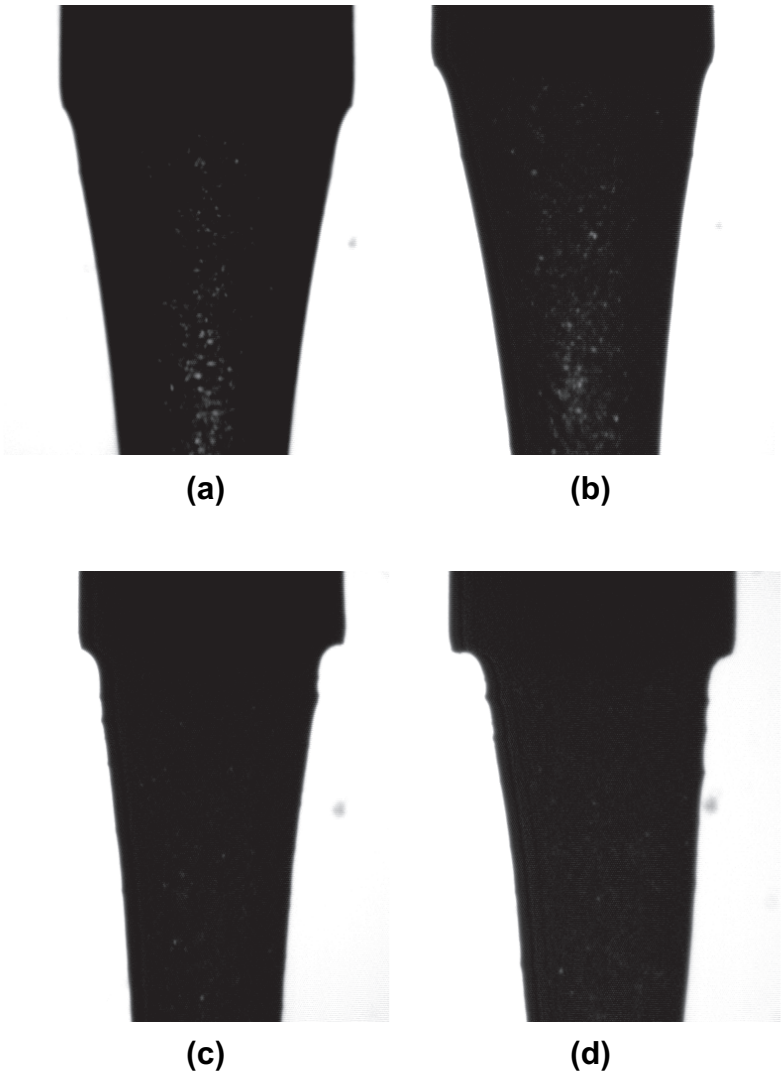

Figure 67: Jet shapes near the orifice for $d = 0.32$ cm, $d_p = 106 - 125$ μm, and $Q = 15$ cm^3/min ($Re = 0.6$) for various suspensions with (a) $\phi = 0.10$, (b) 0.20, (c) 0.30, and (d) 0.40.

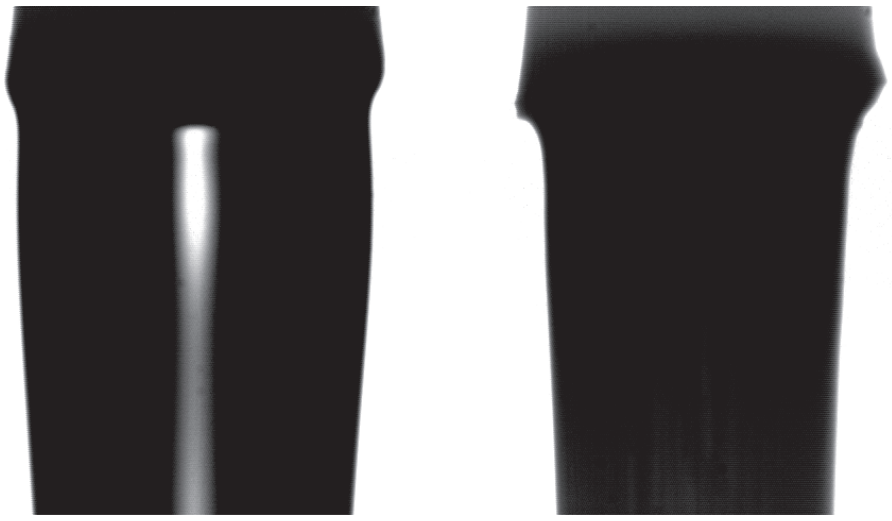

Figure 68: Jet shapes near the orifice for $d = 0.16$ cm, $d_p = 106 - 125$ μm, and $Q = 11$ cm^3/min ($Re = 0.9$) with (a) $\phi = 0$ and (b) 0.30.

results from this orifice are not as clear as those for the larger one and will only be discussed briefly and not further quantified. The problem with the results for this orifice is that the wetting characteristics of the orifice change during the course of the experiments. This can be seen in image (b) for the $\phi = 0.30$ suspension where the tip of the capillary appears quite asymmetric. This is actually caused by suspension which has "climbed" the outside of the capillary during the build-up to jetting and remained attached to the outer capillary wall. Despite this problem, which precludes further quantitative analysis, we can still make certain qualitative observations based on these images. A similar contraction of the jet shape to that observed for the larger capillary is also seen here although the sharp deformations to the surface of the jet are not. This latter effect is different from the larger capillary even though the d/d_p ratio is the same as that for the larger orifice with the larger particles, and is presumably due to the greater effect of surface tension at the smaller scale.

The images of the various jets shown in Figures 66-68 are just single snapshots of the process as it occurs in time and are presented in order to illustrate certain

qualitative features of the particulate influence on the jet shapes. In the experiments, photographs of the process were taken at 60 fps in order to analyze the jetting behavior as a function of time. At a camera frame rate of 60 fps for the resolution utilized (512 x 480) a total of 546 pictures can be save to the camera hard drive, yielding an observation time of 9.1 s. Each image is analyzed in a similar manner to that described in Chapter 2 and the edge of the jet is detected in order to examine the jet shape as it changes with time. Sample results of this procedure are presented in Figure 69.

In Figure 69 the shape of the jet for each of the 546 images obtained for the pure liquid and a suspension of $\phi = 0.40$ are presented graphically. In the graphs the ordinate, x/d, is the dimensionless horizontal position from the edge of the orifice and the abscissa, z/d, represents the axial (parallel to gravity) direction measured from the tip of the capillary. In this configuration the graphs have the effect of showing the jet as if it were rotated 90° counterclockwise with the outer edge of the capillary tip at the origin. In these graphs the location of the inner wall of the capillary is at $x/d = 0.15$ and is important in understanding the physical situation. For the pure liquid the shape of the jet is essentially constant with very little variation observed over the time ranges examined (recall that 546 curves from sequential images are plotted on this graph). This result is expected and serves as additional validation that our experimental set-up introduces very minimal fluctuations in the process. The bottom graph in Figure 69 shows the shapes for a suspension of $\phi = 0.40$. In this case the shape of the jet is varying greatly from image to image with the variability beginning very near the orifice outlet and increasing with distance in the z-direction. These fluctuations are not surprising recalling the image of the jet for this concentration (shown in Figure 66(f)) in which many particle-induced perturbations to the jet surface are evident. However, the contrast between the pure liquid and $\phi = 0.40$ is quite striking in Figure 69; both in the general shape of the jet (especially

very near the orifice outlet where the large contraction is evident for $\phi = 0.40$) and in the increased variability introduced by the particulate phase. In the remainder of this section we will investigate both of these effects by looking at the mean shape of the jet for the various suspensions as well as the fluctuations about the mean introduced by the particles.

To understand the overall impact of the particles on the shape of the jet near the orifice, the average shapes were determined for the various particle concentrations from raw data similar to that presented for in Figure 69. Although fluctuations introduced by the particles to the surface of the jet increase with increasing ϕ, the mean shapes for different ϕ are significantly different from one another—beyond the deviations introduced by the particles—that comparison of the average shapes are meaningful. The average jet shapes are presented in Figures 70 and 71 for $d_p = 212 - 250$ μm and $d_p = 106 - 125$ μm, respectively, and in Figure 72 for pure liquids of varying viscosity.

Figure 70 shows the average jet shapes near the outlet of the capillary for $d = 0.32$ cm and the larger particles, $d_p = 212 - 250$ μm. In the top graph the mean jet shapes for the pure liquid and the two lowest-ϕ suspensions ($\phi = 0.05$ and 0.10) are presented. From these curves it is apparent that the jet shapes are very similar in general and almost exactly the same very near the orifice. Further away from the orifice the shapes become somewhat different, with the jet widening with increasing ϕ. The bottom graph in Figure 70 shows the jet shapes for the more concentrated suspensions ($\phi = 0.20$, 0.30, and 0.40) as well as the pure liquid shape for comparison. Starting with $\phi = 0.20$ the jet starts to contract noticeably near the orifice ($z/d \approx 0.1$). For this concentration the observed effect of jet-thickening away from the orifice changes and the shape is actually more similar to that of the pure liquid than either the $\phi = 0.05$ or $\phi = 0.10$ suspensions. Increasing ϕ to 0.30 causes a contraction of the jet near the orifice similar to that of $\phi = 0.20$ although the jet becomes

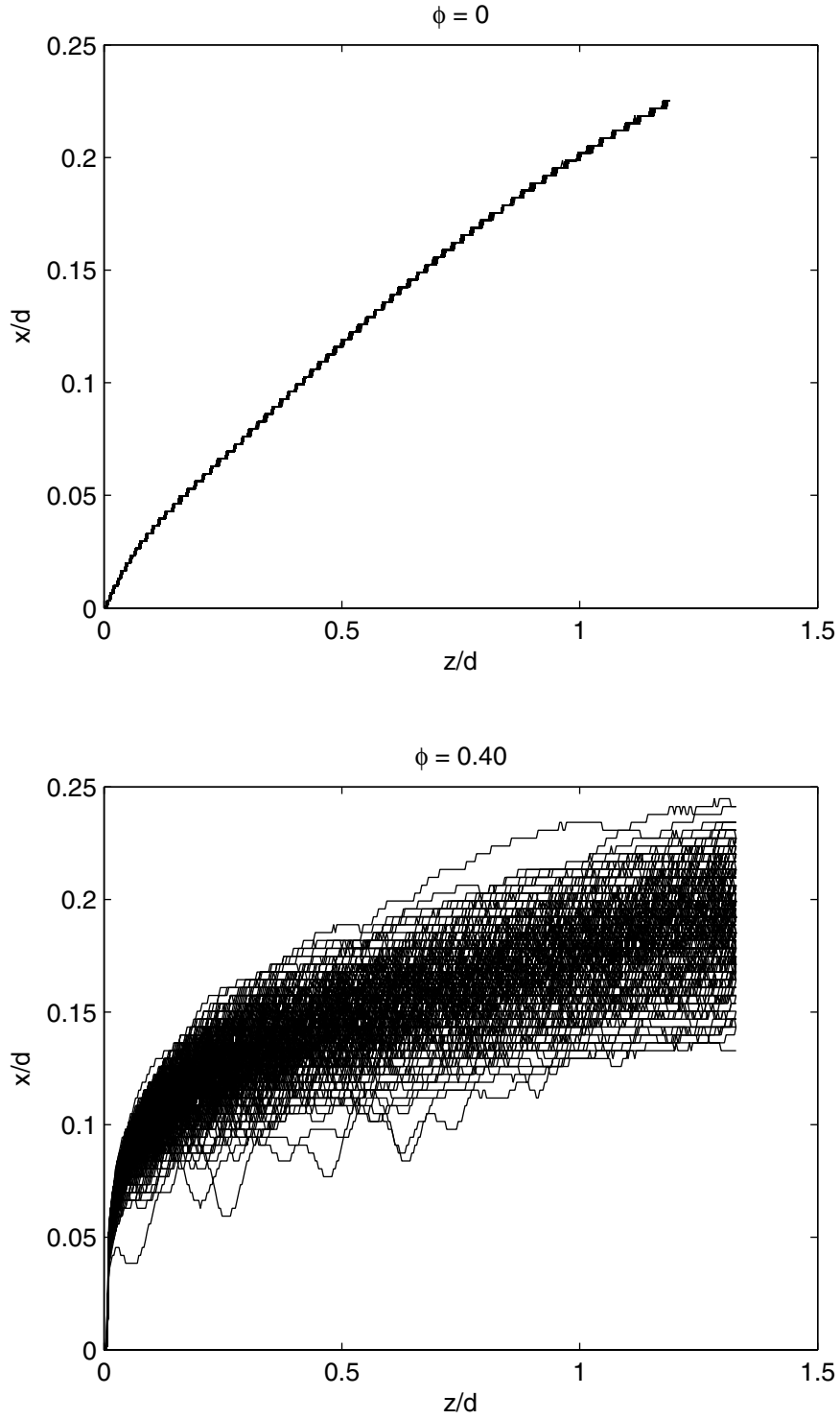

Figure 69: Jet shapes near the orifice for $\phi = 0$ and 0.40 for $d = 0.32$ cm and $d_p = 212 - 250$ μm. Each line represents the jet shape at a given instant in time and a total of 546 different lines are plotted in each graph (representing an observation time of the jet of 9.1 s.

much wider further downstream. At $\phi = 0.40$ the contraction near the orifice is much more pronounced and the shape away from the orifice much flatter than the other concentrations. In these graphs it is insightful to recall that the inner wall of the capillary is located at $x/d = 0.15$ and that a particle of diameter 250 μm has $x/d = z/d = 0.08$. This suggests that the region of the jet just beyond the tip of the capillary in the space between the inner and outer diameters ($x/d \leq 0.15$) where the jet is contracting with increasing ϕ is composed of pure liquid.

The average jet profiles for $d = 0.32$ cm and $d_p = 106 - 125$ μm are shown in Figure 71 and show very similar trends to that observed for the larger particle suspensions. The $\phi = 0.10$ suspension shows the same widening of the jet away from the orifice and this trend is again reversed at $\phi = 0.20$ although with a much less pronounced contraction near the orifice, if any at all. At higher concentrations, $\phi = 0.30$ and 0.40, the contraction of the jets near the orifice is evident with the $\phi = 0.30$ suspension contraction more pronounced than in the case for the larger particles. This greater contraction for the $\phi = 0.30$ (as well as for $\phi = 0.40$ although not to as great a degree) suspension indicates that the smaller particles are having a greater effect on the shape of the jet near the orifice. This effect is counterintuitive in that decreasing the particle size is typically associated with more liquid-like behavior.

The jetting behavior of two, more viscous, pure liquid mixtures was also investigated. These two additional mixtures are the same as those described in Chapter 4 and are composed of 35% UCON ($\rho = 520$ cP) and 40% UCON ($\rho = 870$ cP) while the suspending liquid used in the suspensions was a 30% UCON mixture ($\rho = 310$ cP). A comparison of the jet shapes for these different mixtures is presented in Figure 72. From this figure it is clear that the main effect of increasing viscosity is to cause a thickening of the jet away from the orifice with little or no change in the shape immediately beyond the exit. This trend of increasing the jet thickness due to increasing viscosity is a well-known result in the literature [20, 49] although the situation here

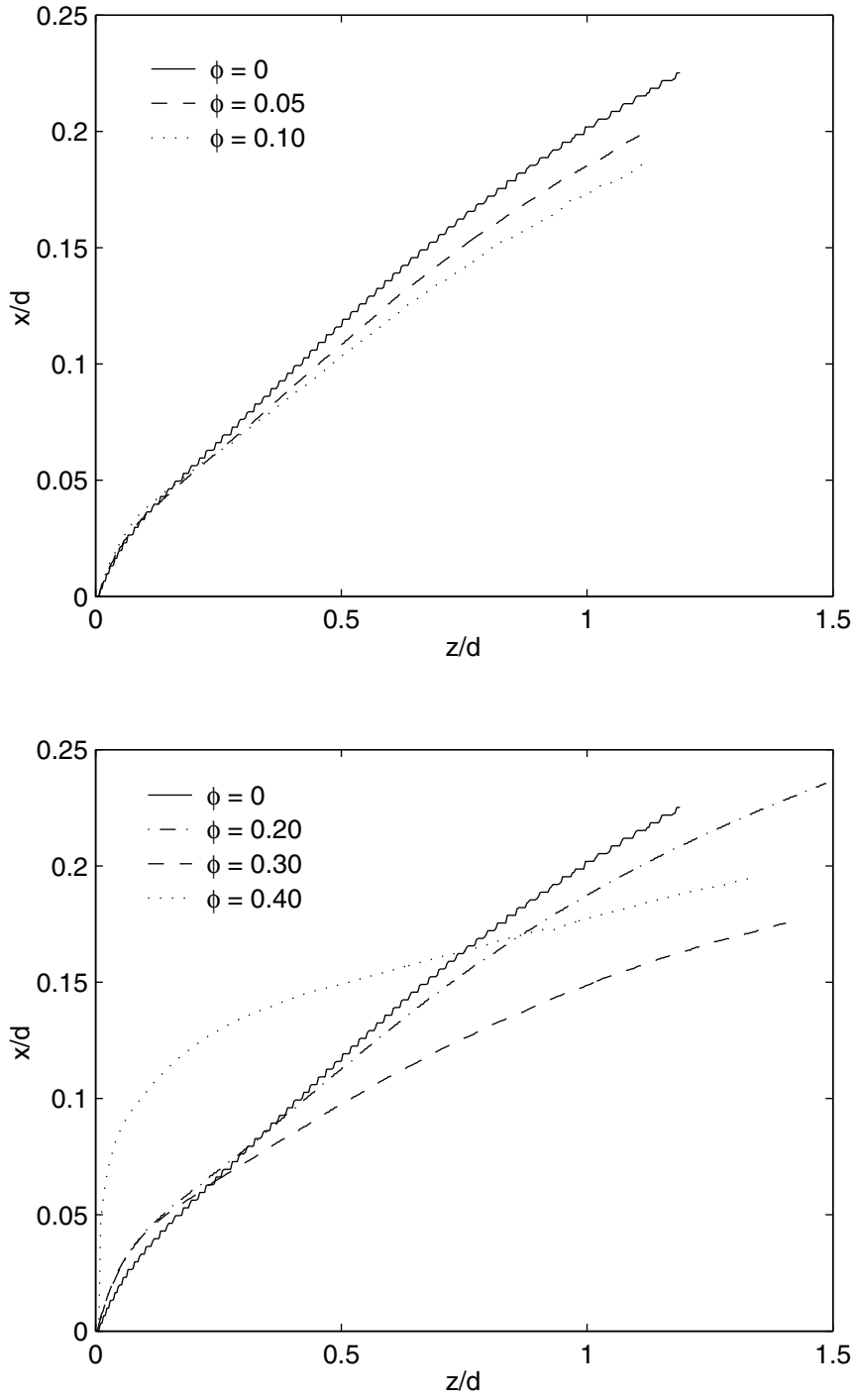

Figure 70: Average jet shapes near the orifice for $d = 0.32$ cm, $d_p = 212 - 250$ μm.

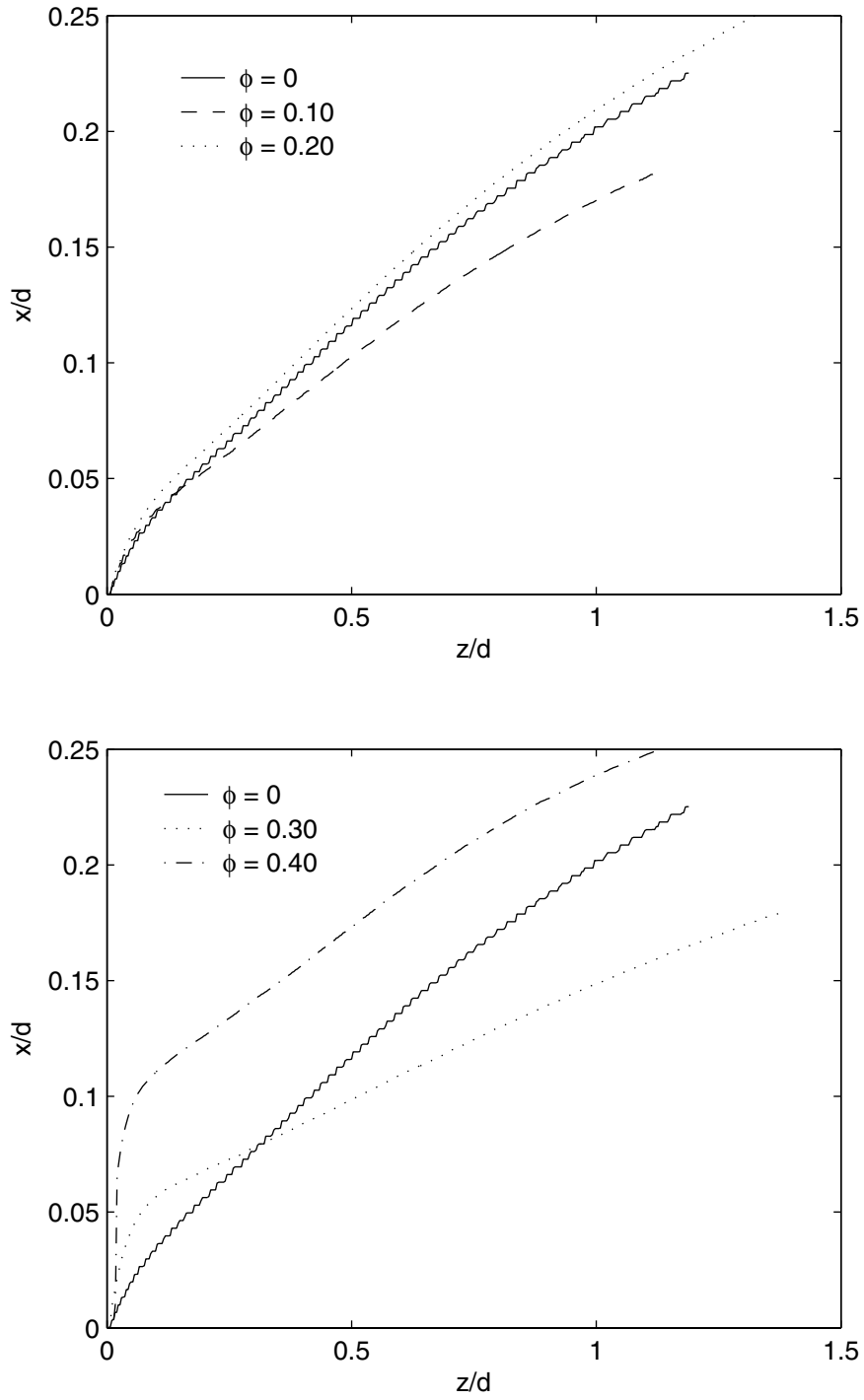

Figure 71: Average jet shapes near the orifice for $d = 0.32$ cm, $d_p = 106 - 125$ μm.

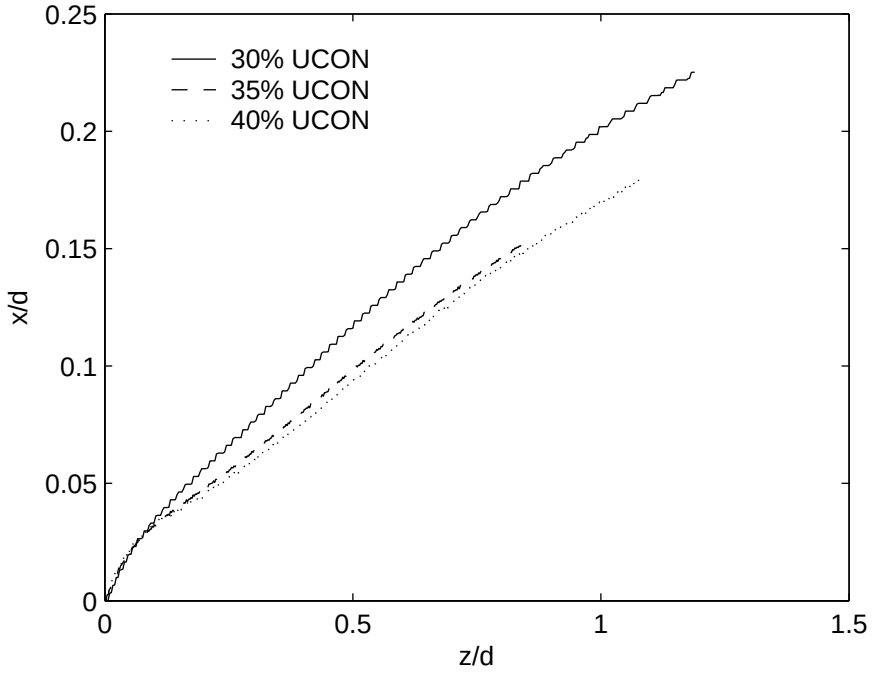

Figure 72: Average jet shapes near the orifice for pure liquids of various viscosity for $d = 0.32$ cm.

is different in that the end surface of the capillary (the region of the tip between the inner and outer diameter) is fully wetted. The trends observed for the higher viscosity pure liquids in Figure 72 are similar to those observed for the low particle concentration suspensions ($\phi \leq 0.10$) for both particle sizes investigated. The magnitude of the thickening for the pure liquids is most similar to the $\phi = 0.10$ suspension for both particle size distributions although it is unlikely that any correlation between the suspension effective viscosity and the jet shape behavior is possible.

In the preceding results the effect of the particulate phase on the jet shape near the orifice was described in terms of the mean shape and comparisons made between the various concentrations. This description is only half of the story in that the particles also introduce large fluctuations to the jet surface, as shown in the photographs of the jets (Figures 66 and 67) and in the graph depicting the different shapes of the jet as the process occurs in time (Figure 69). To quantify these particle fluctuations

we take a similar approach to that described in Chapter 4 and look at the deviation of the shapes from the mean as a function of axial position from the orifice outlet. These results are presented in Figure 73 which plots the percent standard deviation of the jet shape ($\%\Delta x/d$) versus axial position (z/d).

The top graph in Figure 73 shows the results for $d_p = 212 - 250$ μm for all of the suspensions examined as well as the higher viscosity pure liquids. The 30% and 35% UCON mixtures (labelled $\phi = 0$ in the graph) have negligible deviation from the mean and represent the noise in the experimental set-up and detection algorithms, while the 40% UCON mixture shows a slight increase in deviation away from the orifice. The deviations for the suspensions increase with ϕ as well as with position away from the orifice. This increase in deviation is quite rapid at small z/d after which it levels off somewhat and continues to increase slowly as z/d increases further. The sharp peak in the deviation curve for $\phi = 0.10$ near $z/d = 1$ is a result of a lighting abberation in the experimental set-up (only observed for this concentration) which caused the edge of the jet at this position to be incorrectly identified and does not indicate a localized increase in the particle fluctuations.

The bottom graph shown in Figure 73 is the jet shape fluctuations for the smaller particles. In this case, the particle fluctuations to the jet shape also increase with increasing ϕ although there are some clear differences from the case of the larger particles. The fluctuations of the smaller particles is roughly one-half of those for the larger particles. This indicates that the magnitude of the particle-induced fluctuations scales with the particle size. The other distinction between the two graphs is the rapidity with which the particle fluctuations to the jet shape increase for the two highest concentrations ($\phi = 0.30$ and 0.40) near the orifice. In the case of the smaller particles this increase occurs much closer to the orifice than for the larger particles, as indicated by the steepness of the slope of the curves. This effect seems to be solely due to particle size and indicates that the smaller particles are able to "turn the

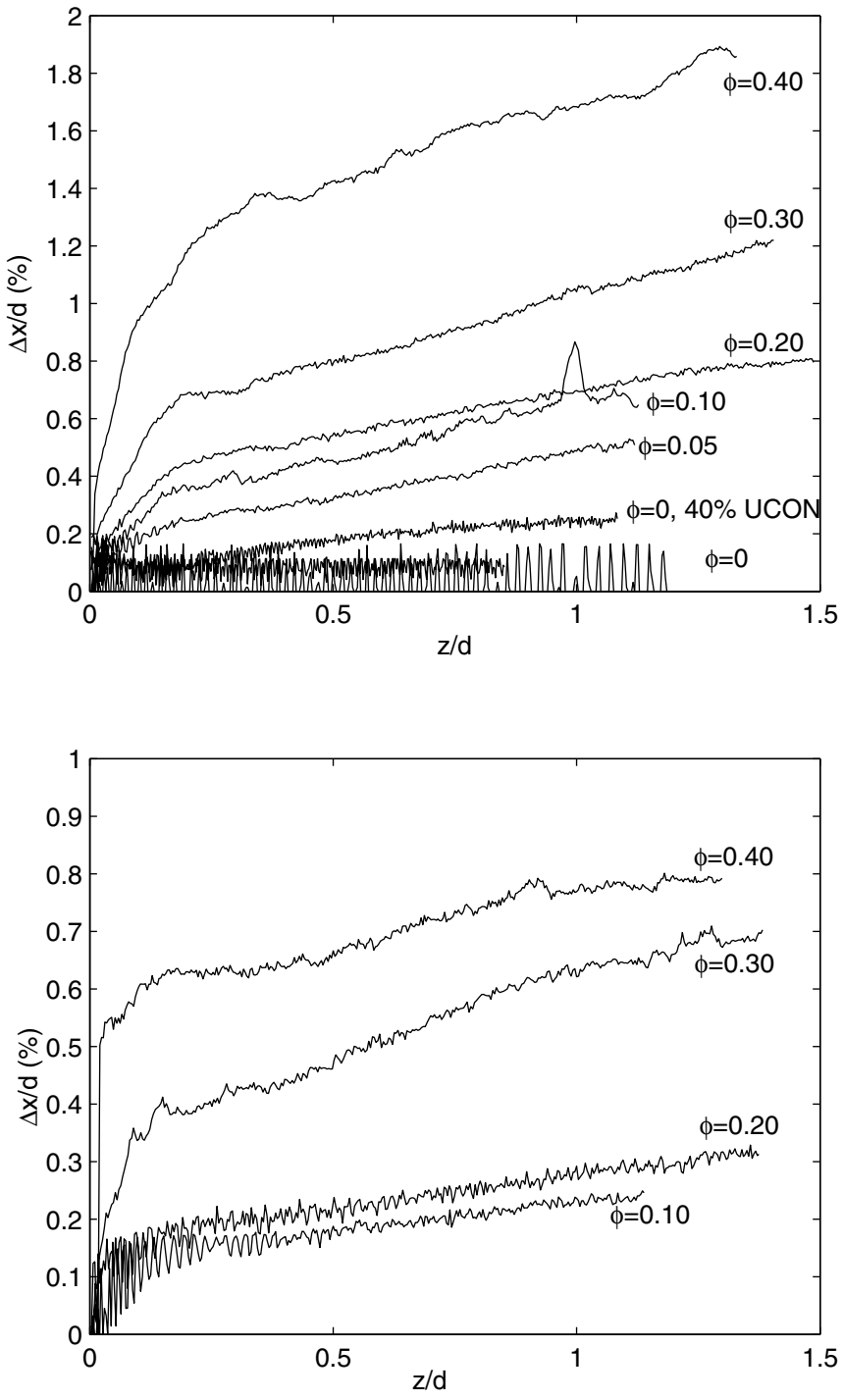

Figure 73: Fluctuations in the jet shape near the orifice for $d = 0.32$ cm with $d_p = 212 - 250$ μm (top) and $d_p = 106 - 125$ μm (bottom).

corner" after exiting the capillary more easily than the larger ones.

5.3 Discussion

In this section we consider the experimental results presented in the previous two sections of this chapter. In this discussion we will consider the particulate effects on both the jetting transition and the jet shape near the orifice beyond this transition.

5.3.1 Particle effects on jetting transition

The presence of particles affects the transition from dripping to jetting, leading to drastically shorter jets and, at higher ϕ, smoothing the abrupt nature of the transition with respect to flow rate. In liquids, the onset of jetting is characterized by an abrupt and large increase in length of the coherent column of fluid connected to the orifice and is easily identified visually. Once particles are introduced, identifying this transition becomes more complicated. Eventually, at sufficiently elevated ϕ, the process does not exhibit an identifiable transition but gradually changes from dripping to jetting over a range of flow rates. The introduction of particles thus appears to eliminate the critical nature of the parameter (flow rate for a given system) associated with the transition in a pure liquid.

The particles within the forming jet appear to have two conflicting effects. The first of these is that the particles within the jet create disturbances to the free surface, inducing earlier breakup. The second effect is that large numbers of particles in the jet resist thinning of the liquid column. Based on the results presented in Figures 60 and 61, it appears that the first effect is dominant and is responsible for the much shorter jet lengths observed for the suspensions. The second, stabilizing, effect would seem to induce earlier jetting of highly concentrated suspensions because the large numbers of particles present are unable to rearrange themselves to allow pinch-off before the next forming drop over-runs the first. This may explain, for low flow rates, the observed increase in $(L/d)_{\min}$ relative to the pure liquid for the highest

ϕ studied. A consequence of increased $(L/d)_{\min}$ at low flow rates is the decrease in drop size for large ϕ in Figures 21 and 22. From Figures 60 and 61 it is evident that the concentrations exhibiting this decrease in drop size (0.20 and 0.30 for the smaller orifice and 0.40 for the larger one) correspond to those with longer $(L/d)_{\min}$.

Consideration of particle rearrangement within the liquid column seems to be critical to understanding the process. The ease with which the particles can accomplish this rearrangement determines how the jet transition occurs. Particle rearrangement should be easiest for particles small relative to the orifice (large d/d_p) and low ϕ. In fact as the particles become progressively smaller, the behavior of the pure liquid is expected to be asymptotically recovered, an assertion supported by the experiments performed using smaller particles where the jet length was observed to increase relative to the larger particle suspensions. At the other extreme (small d/d_p) individual particles take up a greater percentage of the liquid cross-section and rearrangement is more difficult. In all of this discussion, it should be noted that rearrangement is within a liquid column where the motions encounter resistance by a flexible surface and not a rigid boundary. Clear evidence of surface deformation by the particles is seen in the work we have presented. It is to be expected that particle and drop scale will play a strong role in this aspect of the problem, as capillary forces become stronger as the scale is reduced.

5.3.2 Particle effects on the jet shape near the orifice

The two primary effects of the particles on the shape of the jet are: causing a contraction of the jet near the outlet of the capillary, and introducing increased fluctuations to the jet surface. In this section we discuss these two effects and seek to provide insight into both.

In considering the jet contraction the geometry of the system is critical. The region of the jet where the contraction occurs is outside the inner diameter of the capillary

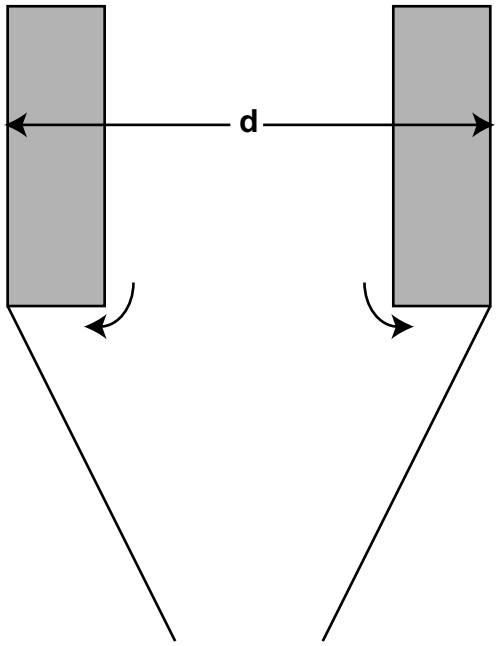

Figure 74: Drawing of the geometry capillary tip illustrating the corner flow.

and below the solid annular ring of the capillary tip (see Figure 74). This portion of the jet is composed of material following outward radial streamlines after exiting the orifice, presumably from the region within the capillary tube nearest the walls. It is interesting to note that in most studies of jets the case we are examining is typically avoided by ensuring that the outer region of the capillary is not wetted, typically by machining the orifice so that it has sharp edges. However, it is just this wetting which makes the contraction possible and likely only occurs for a narrow range of conditions. Indeed it is quite serendipitous that we observed this behavior during our investigation of the dripping-to-jetting transition, which involves initial conditions in the dripping regime where the outer diameter of the orifice is fully wetted.

The flow of material around the corner of the orifice is similar to a case studied by Moffat (1964) [30] who developed similarity solutions for the flow of viscous fluid around a sharp corner. In this work, Moffat showed that the streamlines around such a corner spread due to retarding effects associated with the corner. This spreading of

the streamlines could play a role here.

The contraction of the jet seems to be a direct result of the reduced availability of material to fill this region as the particle concentration is increased. Based on the size of the region and the size of the particles, we expect this region to be largely, if not entirely, composed of liquid. As ϕ increases, the liquid phase of the suspension becomes essentially "trapped" between the large numbers of particles present. In order to maintain the same shape near the orifice as in the $\phi = 0$ case, a certain portion of the liquid in the vicinity of the capillary walls must be able to separate itself from the particles and, in doing so, increase the particle concentration in the central region of the jet. It is easy to envision that this separation will become increasingly more difficult and unfavorable as ϕ increases. Certainly the region near the walls will always maintain a particle-free zone, but this region becomes ever smaller as ϕ becomes larger.

As the concentration increases, the interparticle spacing decreases which leads to stronger lubrication forces between the particles. This is likely the cause of the large change observed in the behavior of the jet as ϕ is increased from 0.30 to 0.40 for $d_p = 212 - 250$ μm and from 0.20 to 0.30 for $d_p = 106 - 125$ μm. The surface separation between particles, h, can be determined [17] from:

$$\frac{h}{d_p} = \left\{ \frac{(\phi/\phi_{max})^{1/3}}{1 - (\phi/\phi_{max})^{1/3}} \right\}^{-1} \tag{12}$$

assuming that the particles are arranged in a cubic structure. The values of the distances between particles, as determined using (12), are shown in Table 8 where h_{250} and h_{125} are the distances between particles for the $d_p = 212 - 250$ μm and $d_p = 106 - 125$ μm particles, respectively.

In examining the different interparticle distances for the different ϕ and d_p, the goal was to look for similarities between the distances in order to explain the observed onset of the jet contraction phenomenon for the different conditions. Specifically, to answer the question: why is the contraction more pronounced at a lower ϕ for the

Table 8: Surface separation of particles as determined by (12).

ϕ	h/d_p	h_{250} (μm)	h_{125} (μm)
0.05	1.34	335	168
0.10	0.86	214	107
0.20	0.48	119	60
0.30	0.29	71	36
0.40	0.17	43	22

smaller particles? Comparing the values of h in Table 8 allows us to partially answer this question.

The values of h are twice as large for the larger particles as they are for the smaller ones at a given ϕ, which indicates that the smaller particle suspensions should exhibit stronger lubrication forces in the region between particles and essentially lead to greater overall adhesion of the liquid to the particles. This effect can explain the general trend that the smaller particle suspensions exhibit greater jet contraction although we are not prepared to use the results to predict the magnitude of the contraction. Based on values of h alone we would expect the $\phi = 0.30$ suspension jet for the smaller particles to contract to a similar, if not greater, extent as the $\phi = 0.40$ jet for the larger particles since their values are similar, although this is not observed. This leads us to conclude that, although interparticle spacings are important in understanding the jet contraction of suspension jets, other factors are also important; at least one of these must act opposite to the particle spacing effect due to the observed behavior.

One effect of reducing the particle size which could be responsible for decreasing the observed contraction, relative to that seemingly predicted by particle spacings, is the improved ability of smaller particles to navigate around the corner of the orifice. As the particles become smaller, it is possible for them to follow streamlines nearer the walls of the capillary. This effect should compete with that of the particle spacing

effect as particle size decreases. Even though the particles are getting closer to one another, and holding the liquid between them ever more tightly, their improved ability to flow around the corner and fill the region where the contraction occurs should offset this effect. Indeed if the particle size were to approach zero the pure liquid behavior should be recovered (*i.e.* no contraction of the jet) and this effect would be dominant.

The contraction of the jet is also a function of the flow rate although that has not been investigated in detail here. However, a few experiments have been conducted which indicate the qualitative influence of flow rate on the process. At sufficiently elevated flow rates, the time required to wet the outer surface of the capillary will exceed that characteristic of the flowing material and at this point the mixture will jet directly from the inner diameter. In the limited experiments performed where this was investigated, the contraction of the jet for high-ϕ suspensions was observed to increase with flow rate and, in certain cases, dewetting of the orifice was observed. The dewetting was not uniform around the entire capillary but instead occurred at localized points around the capillary circumference, presumably at locations dictated by small irregularities along the capillary surface.

The other primary effect of the particles on the jet is the increased fluctuations to the jet surface. Far downstream, away from the orifice, the particles cause deformations to the jet surface as the jet constricts and eventually breaks up. These disturbances have been reported in the literature by Ogg & Schetz (1985) [35] and also observed in section 5.1 during our investigation of the jetting transition. The sharp disturbances to the jet surface very near the orifice (see Figure 66), especially for $\phi = 0.05$, the lowest particle concentration examined in these experiments, indicate that the particles also have an influence on the jet shape shortly after it emerges from the capillary.

These disturbances to the surface are quite sharp which indicates that they are caused by either individual or small groups of particles deforming the surface of the

jet. That these disturbances are observed along the entire surface of the jet within the field of view in these experiments indicates that the particle motions within the jet are quite complex and that they are not just following the plug flow behavior characteristic of pure liquid jets.

This observation that the sharp particle fluctuations to the surface can occur along the entire jet, within the field of view, leads to the question of whether or not there is a location along the jet where the fluctuations are greatest, or where the particles deform the jet most frequently. Based on the geometry of the system such a point on the surface could occur in the vicinity where the jet surface intersects an imaginary cylinder extending from the inner diameter of the capillary. This idea is basically that particles within the capillary tube near the inner wall would emerge from the capillary on trajectories that would carry them toward the jet surface and that they would preferentially deform the surface at a certain location just outside the orifice.

From Figure 73, which presents the fluctuations to the jet shapes, it appears that there is no such preferred location where the particle fluctuations are most pronounced. The fluctuations measured are not just the sharp deformations to the surface but any deviation of the jet from the mean shape which result from both individual and large group particle motions as well as from deformations to the jet in unobserved locations. However, there does appear to be a slight maximum evident in the particle fluctuation curves fairly close to the orifice outlet for the two highest concentrations examined for both particle sizes. After these maxima, the fluctuations increase more or less linearly with distance from the orifice. Whether or not these slight maximum values indicate preferred locations on the jet where particle fluctuations are most pronounced is uncertain from this data although in our opinion it is likely such locations exist.

5.4 Concluding remarks

In this chapter we have examined drop formation of suspensions as the flow rate is increased and the process undergoes a transition from dripping to jetting. We have also examined the shape of the jet once jetting is complete in order to investigate the influence of the particles on the jet shape near the orifice.

The presence of the particulate phase leads to two opposing effects in the transition from dripping to jetting. The first effect is that the suspension jets formed after transition are much shorter (nearly a factor of ten) than those for the suspending liquid. This effect can be viewed as a destabilizing effect on the process and is due to the increased fluctuations introduced within the jet by the presence of the particles.

The second effect of the particles on the transition process, which occurs only at elevated particle concentrations, is the development of an intermediate regime where the process is neither clearly dripping or jetting. This intermediate region is a departure from the very sharp transition observed for pure liquids and dilute suspensions and is related to the cause of the decreased drop sizes measured in Chapter 3 at elevated flow rates. It also can lead to jetting at earlier lower flow rates, or so-called particle-induced jetting.

In examining the shape of the jet we have found that the particles lead to a significant contraction of the jet near the orifice at elevated particle concentrations. This effect is due to the unique geometry of our experimental apparatus where the region between the inner and outer diameter of the capillary is fully wetted. The contraction occurs in this region and is the result of the decreased availability of pure liquid to fill this volume once the particle concentration becomes so large that the liquid is essentially trapped between the particles; this is a consequence of the decreased spacings between particles. We have also measured the fluctuations to the surface of the jet as a function of particle concentration and distance from the orifice and found that the fluctuations increase with both.

CHAPTER 6

CONCLUSIONS AND RECOMMENDATIONS

In this work we have experimentally examined the formation of drops of suspension composed of a viscous liquid and spherical, neutrally buoyant, noncolloidal particles. Various drop formation regimes have been studied including pendant drop formation and low Reynolds number jetting, as well as the transition between the two. In this chapter we will summarize our conclusions and present recommendations concerning this work's potential impact on future research directions and applications.

6.1 Conclusions

In the dripping mode the pinch-off structures for the particle-laden systems are qualitatively different from the pure liquid case. For low concentration suspensions the macroscopic behavior is similar to that of the pure liquid in that the structure is that of the well-known needle-sphere configuration familiar in the study of pure liquid drops [37, 44] although either individual or groups of particles can become trapped in the forming neck and produce satellite drops which would otherwise not be present. As ϕ is increased the pinch-off structures change: the particles form thick cone-like structures (termed "spindles" here) both near the orifice and the trailing edge of the forming drop. This change in structure is not explained simply as the result of an increase in the effective viscosity of the mixture.

During necking, particles in the thread resist its further thinning and, depending on the number of particles present, this resistance can have either a destabilizing or a stabilizing effect on the thread relative to the case of the pure liquid. The presence of a small number of particles in the thread introduces regions within the

thread which cannot thin beyond the size of an individual particle and leads to earlier rupture. A large number of particles in the thread tends to have a stabilizing effect both before and after pinch-off. In this case there are sufficient particles present in the thread that their individual motions are restricted and the necking of the thread is slowed. These two conflicting particulate effects provide an explanation for the observed changes in satellite drop generation and jetting transition with increasing ϕ. The stabilizing effect of high ϕ suppresses satellite drops and induces earlier jetting while the destabilizing effect is responsible for reducing the coherent jet lengths.

The ability of a two-stage model to describe the necking of suspensions for pendant drop formation has also been proposed. The first stage, termed initial necking, applies for times relatively far away from pinch-off and occurs in a manner similar to that of pure liquids, but with added resistance to thinning due to the particulate phase. During initial necking, the effect of the particles on the thread thinning can be accounted for by increasing the effective viscosity of the mixture. In this stage the size effects of the particles are negligible as long as the orifice to particle diameter ratio is large enough (≥ 12.8 in this study).

The second stage is the final necking stage and occurs at times close to pinch-off and when the thread has thinned to only a small number of particle diameters. During this stage the particles resist the stretching of the thread and lead to shorter pinch-off lengths than those for the pure suspending liquid. In this stage the motions of individual particles and the complex interactions between the particles and the free surface of the thread lead to the formation of the new spindle structures observed at pinch-off. The individual particles also resist the thinning of the thread during this stage and must be rearranged within the thread so that a region devoid of particles forms where the thread ultimately ruptures. At times near pinch-off, the transition from thinning over a region with particles to one free of particles causes a sharp increase in the thinning rate as particle concentration is increased.

The ability to describe the thinning of concentrated suspensions using the effective viscosity of the mixture represents a considerable simplification of the process. From the experiments, we found that the rate of thinning of the mixture scales as the effective viscosity to the $-1/3$ power for all of the suspensions examined, which indicates a similar scaling with the capillary number. This result will likely be of value to future researchers interested in modelling such flows and, while the scaling result may be unique to the specific experiments conducted here, the general conclusion that effective bulk properties can adequately describe the drop formation of concentrated suspensions during the early stages of necking should be widely applicable.

6.2 Recommendations

This work is a first attempt at probing the effects of a particulate phase on drop formation, a largely unexplored area, and many directions are open for further research in this area. In this section we will comment upon a number of these directions which seem particularly relevant (and interesting) based on what we have learned from this present research.

The relevance of this research to ink-jet printing technology, one of the motivations for this work, is not immediately evident due to the smaller scales and very different drop formation mechanisms involved in typical printing applications. However, the stabilizing effect of the particles at elevated concentrations that we have identified in this research is a very promising result for this technology. Typically, the concentration of particles in inks is kept below around 5%. In our work this is the concentration at which we see the onset of the destabilizing effect of the particles on the thread. However, it is not until higher particle loadings are reached that the thread starts to become stabilized due to the presence of the particles. This may indicate that higher particle loadings in inks may actually help to eliminate satellite drops, especially in printers using drop-on-demand technology. In these types of printers a slug of liquid

is ejected from an orifice which, under ideal conditions, coalesces into a single drop without undergoing secondary breakup and generating satellite drops. This is exactly the case where we observe the large stabilizing effects of the particles: after initial rupture has occurred and the spindle structures resist further breakup. The similarity of the slug of liquid ejected from this type of printer to that of the long spindles after initial rupture of the thread indicates that additional stabilization would result from higher particle concentrations. Of course this idea ignores the added difficulty of ejecting highly concentrated inks through the orifice (an area not investigated here) but the idea appears promising and, we think, worth pursuing.

It is of interest to consider the extent to which the results obtained apply to drop formation in this motivating application by comparing the effects of the particles at the smaller scales characteristic of ink-jet printing. As the size of the particles decrease, the effects of Brownian motion become important and may alter the behavior. The smaller particles will also affect the surface deformation during necking. To address these two issues we can compare the relevant dimensionless quantities, the Péclet number and a particle based capillary number, between the experiments performed in this thesis and those characteristic of drop-on-demand ink-jet printers. The Péclet number is

$$Pe = \frac{6\pi\mu\dot{\epsilon}a^3}{kT}, \tag{13}$$

and the particle based capillary number is given as

$$Ca_p = \frac{\mu\dot{\epsilon}a}{\sigma}, \tag{14}$$

where $\dot{\epsilon}$ is the characteristic stretch rate of the material, k is the Boltzmann constant, and T the temperature. In the larger scale experiments conducted in this work $Pe = O(10^9)$ and $Ca_p = O(10^{-2})$ indicating that the influence of the Brownian motion of the particles is negligible. Chen *et al.* [8] investigated the thermal drop-on-demand ink-jet and from this work we estimate that the corresponding values are

$Pe = O(10^2)$ and $Ca_p = O(10^{-5})$ assuming a particle radius of 100 nm. This indicates that at the smaller scales the influence of Brownian motion is still small compared with the hydrodynamic motion of the process while the influence of the particles on the surface deformation should be significantly smaller.

Another area open for further investigation is the use of a liquid bridge apparatus to probe the final necking stage in more detail. A liquid bridge apparatus consists of two endplates with liquid between them. The endplates are pulled apart in a controlled manner and the deformation of the liquid as it undergoes elongational stretching can be studied (see McKinley & Sridhar (2002) [27] for a review of liquid bridge rheometry). This technique has been used extensively to study the stretching of polymeric fluids although little attention has been focused on using it to study suspensions. Using this technique, the motions of the particles within a stretching liquid column could be studied, as could the particle interactions with the free surface. It would also be very interesting to use this technique to measure the extensional viscosity of the mixture and to investigate how this quantity changes as the thread thins and goes from a relatively uniform particle concentration to one where the thread is no longer homogeneous and pure liquid regions exist at various points along the thread.

Further pendant drop experiments could also be useful for probing the effect of particle size and the effect of varying the liquid properties more widely. The main limitation to doing this with the current experimental apparatus is the need for neutral buoyancy of the particles. The requirement of neutrally buoyant particles is not needed during the actual necking process since the time scale of the necking event is quite small. As long as the time for significant settling to occur is much greater than the time between drops, neutral buoyancy should not be required. In our apparatus the main need for neutrally buoyant particles was the need to keep the particles suspended in the reservoir over the times needed for the experiments (typically 3-5

hours). Adding a stirring mechanism to our apparatus or devising a new apparatus in which the particles and the liquid are mixed just prior to entering the capillary would allow for the investigation of a wider range of particle/liquid combinations.

The contraction of the jet near the capillary outlet is another area where further experimentation may be fruitful. Although we observed this behavior for jetting suspensions, this geometry may not be the most suitable for careful investigation of this phenomena. Since the issue seems to be that of the flow around the corner of the orifice, and also into the corner between the edge of the orifice and the free surface of the jet, a study of the flow of suspension over a slot may yield insights into the physics of the problem for a much simpler geometry.

Lastly, our work represents a large resource for researchers interested in numerically modelling drop formation of suspensions. We have developed detailed descriptions of the behavior of forming suspension drops for a wide variety of conditions in both the pendant drop and jetting modes. Our two-stage model of drop formation of suspensions in the pendant case presents a basis for modelling which highlights the dominant particulate effects during the different stages. In the first stage our results indicate that a technique involving modified bulk properties should be adequate while in the second a more detailed accounting of the individual particle motions is needed.

APPENDIX A

A CATALOGUE OF PINCH-OFF PICTURES

This appendix includes the photographs of the last image captured before thread rupture for the experiments presented in Chapter 4. In each figure a number of drops are presented for the same condition in order to highlight the different structures which develop once particles are introduced. Figures 75-79 show the pinch-off structures for the smaller orifice ($d = 0.16$ cm) and the smaller particles ($d_p = 106 - 125$ μm), Figures 80-85 the structures for the larger orifice ($d = 0.32$ cm)and the larger particles ($d_p = 212 - 250$ μm), and Figures 86-89 the structures for the larger orifice ($d = 0.32$ cm) and the smaller particles ($d_p = 106 - 125$ μm). The flow rate in each case is such that $Re = 0.01$; $Q = 0.25$ cm^3/min for the smaller orifice and $Q = 0.50$ cm^3/min for the larger one.

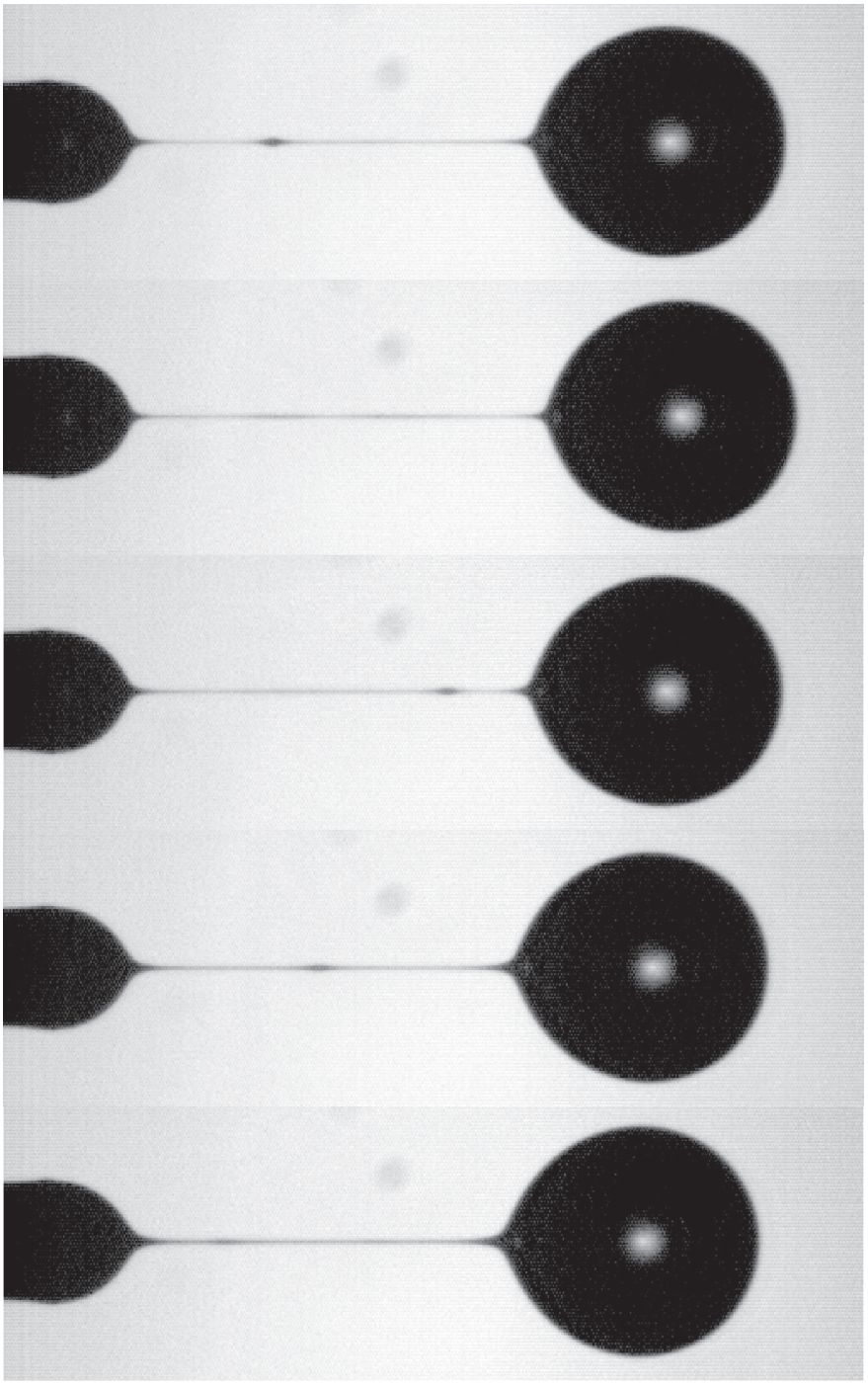

Figure 75: Pinch-off pictures for $\phi = 0$, $d = 0.16$ cm.

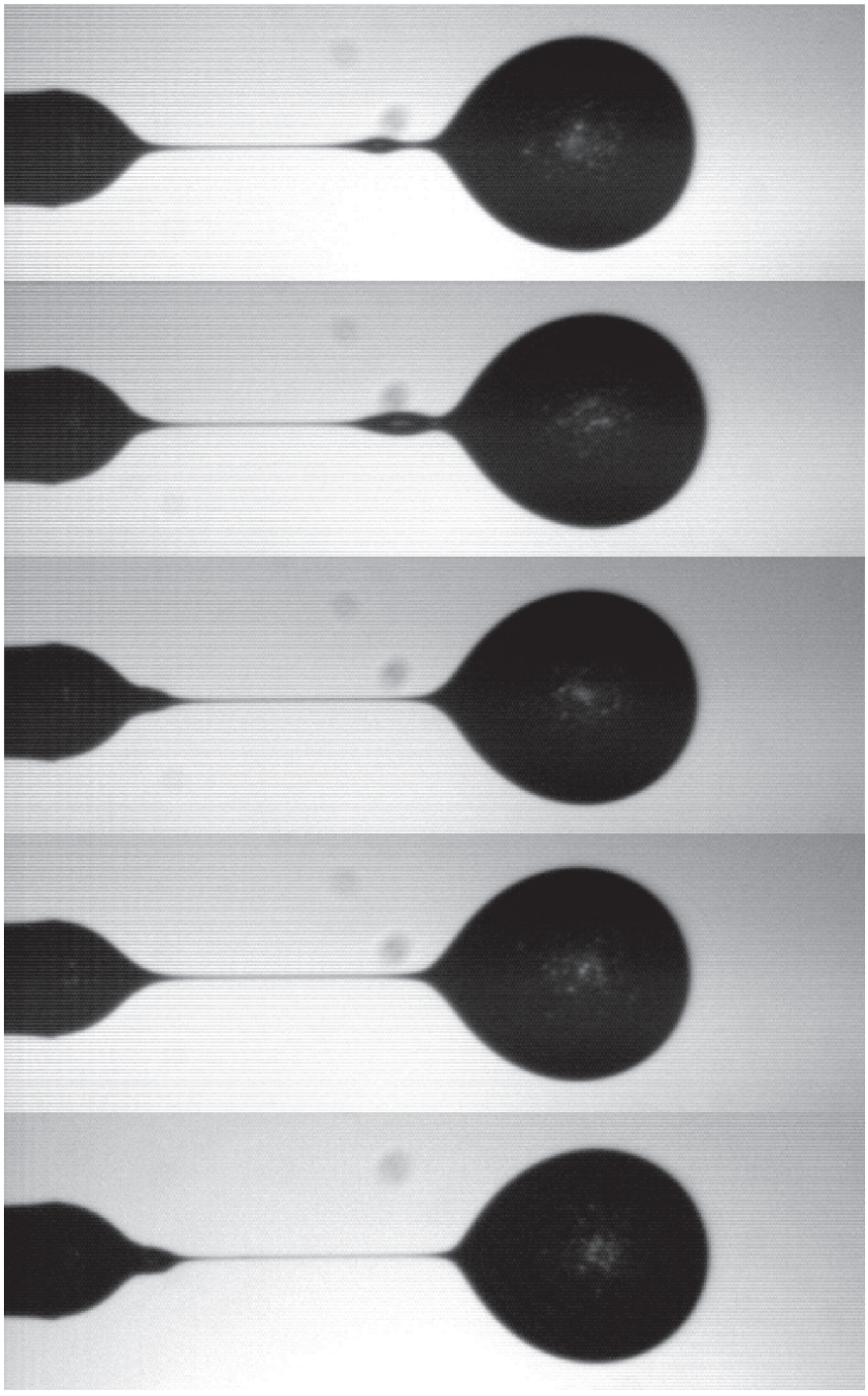

Figure 76: Pinch-off pictures for $\phi = 0.05$, $d = 0.16$ cm, $d_p = 106 - 125$ μm.

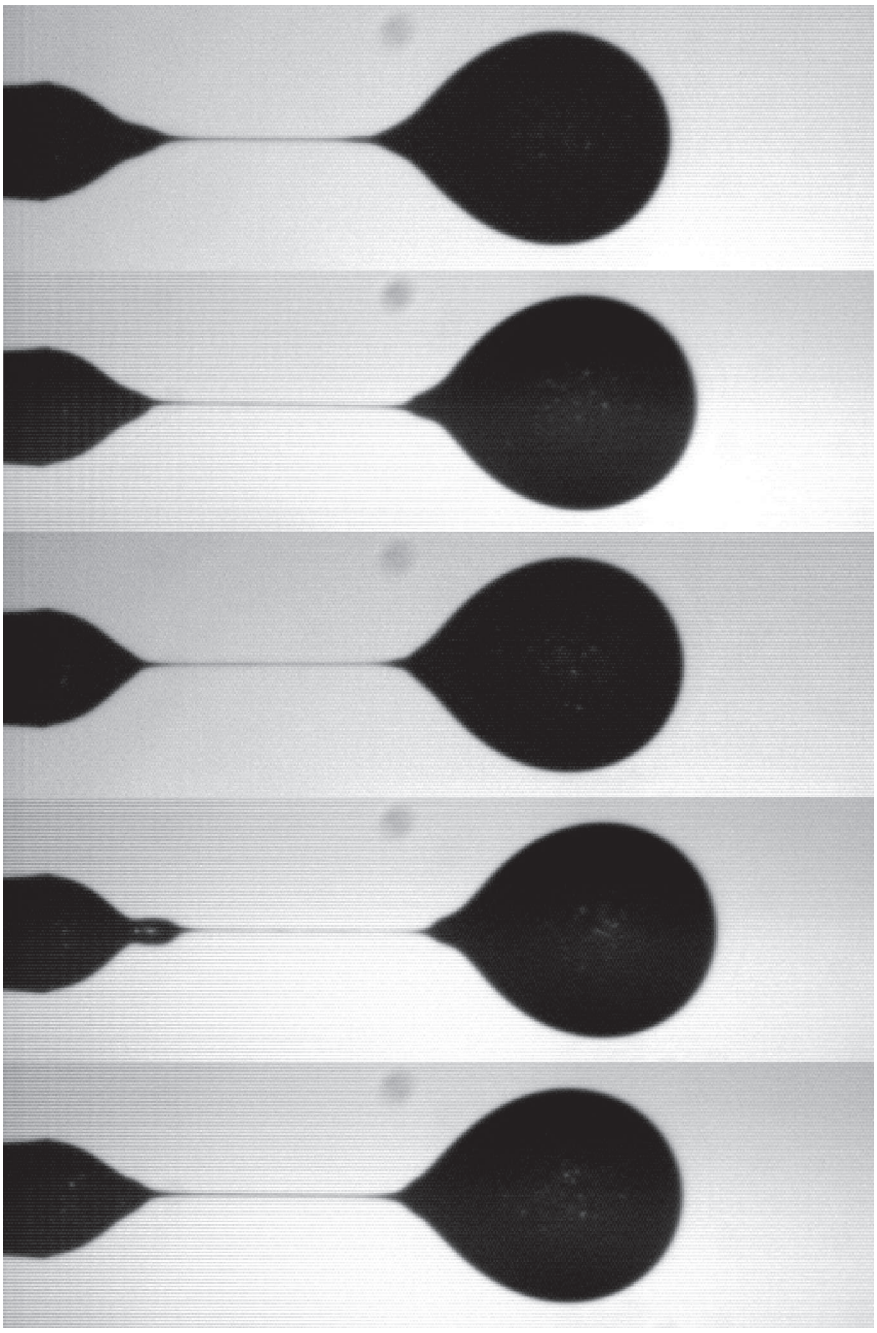

Figure 77: Pinch-off pictures for $\phi = 0.10$, $d = 0.16$ cm, $d_p = 106 - 125$ μm.

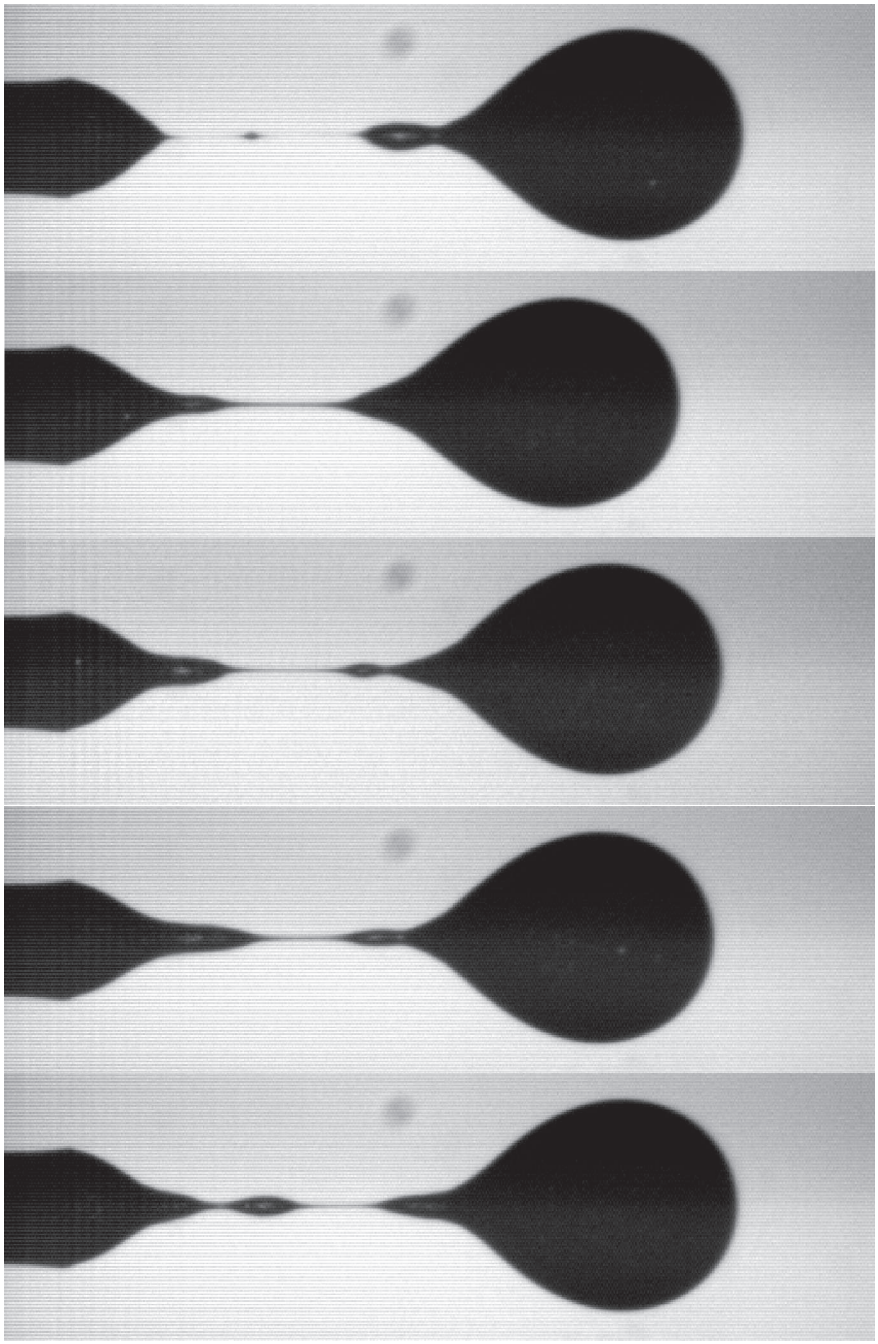

Figure 78: Pinch-off pictures for $\phi = 0.20$, $d = 0.16$ cm, $d_p = 106 - 125$ μm.

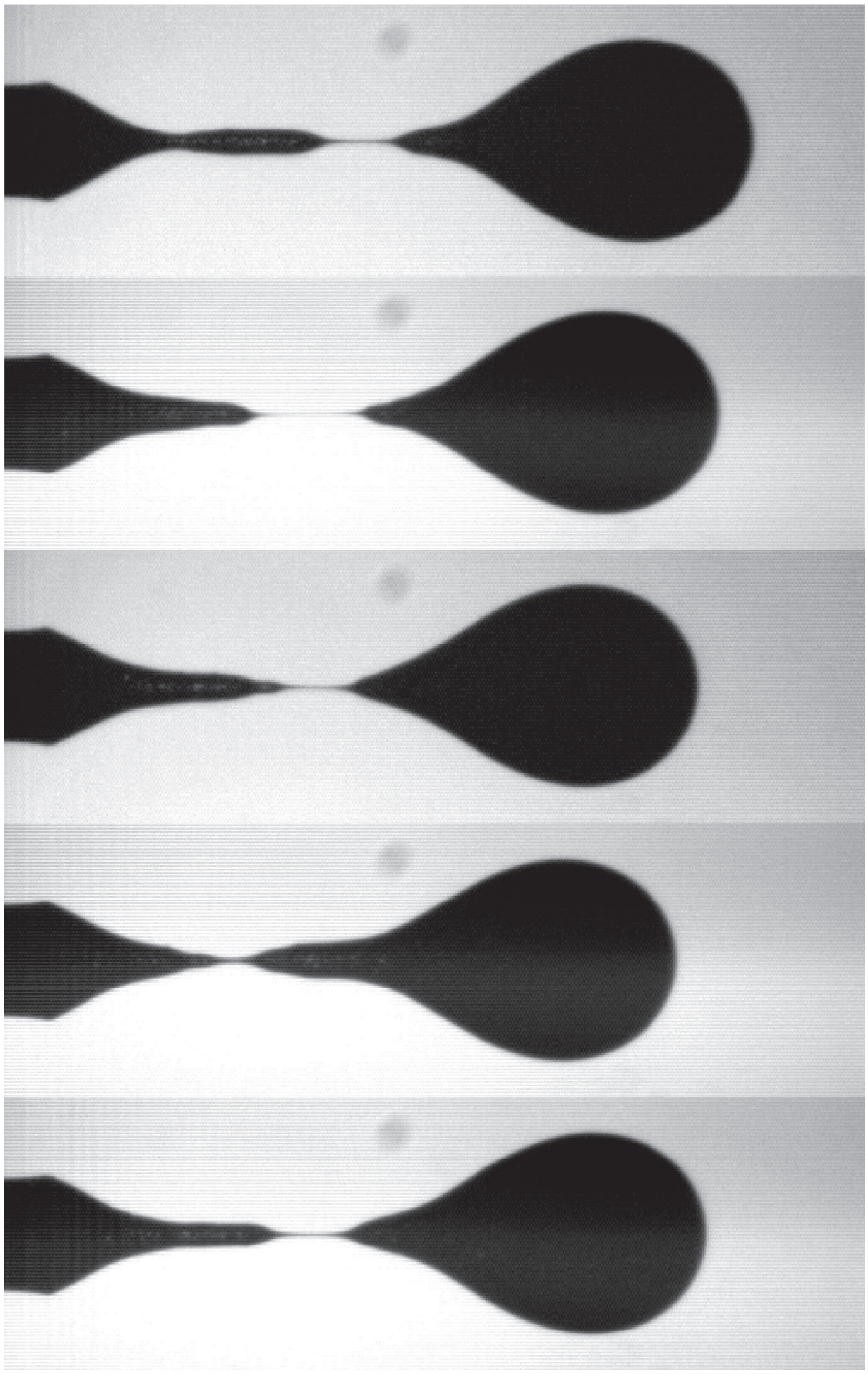

Figure 79: Pinch-off pictures for $\phi = 0.30$, $d = 0.16$ cm, $d_p = 106 - 125$ μm.

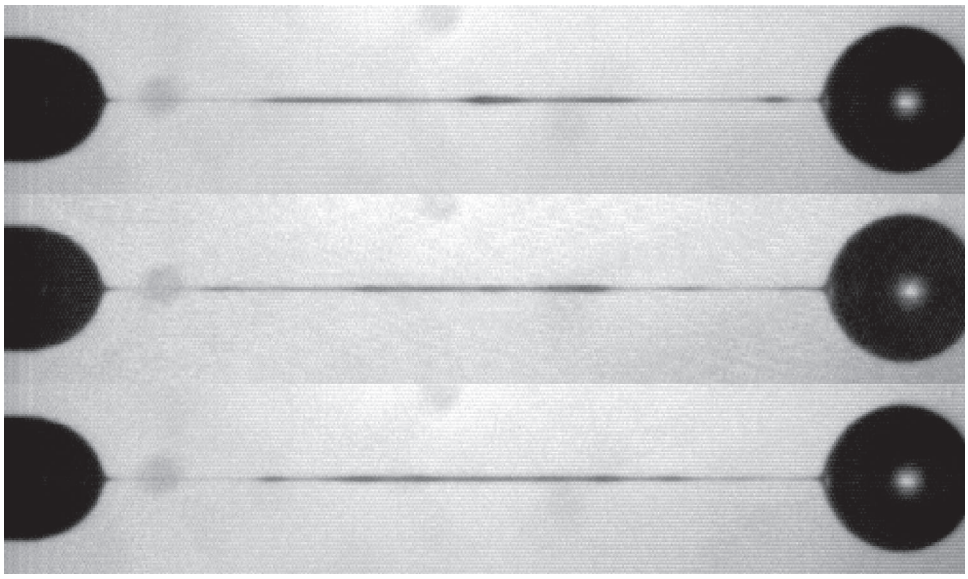

Figure 80: Pinch-off pictures for $\phi = 0$, $d = 0.32$ cm.

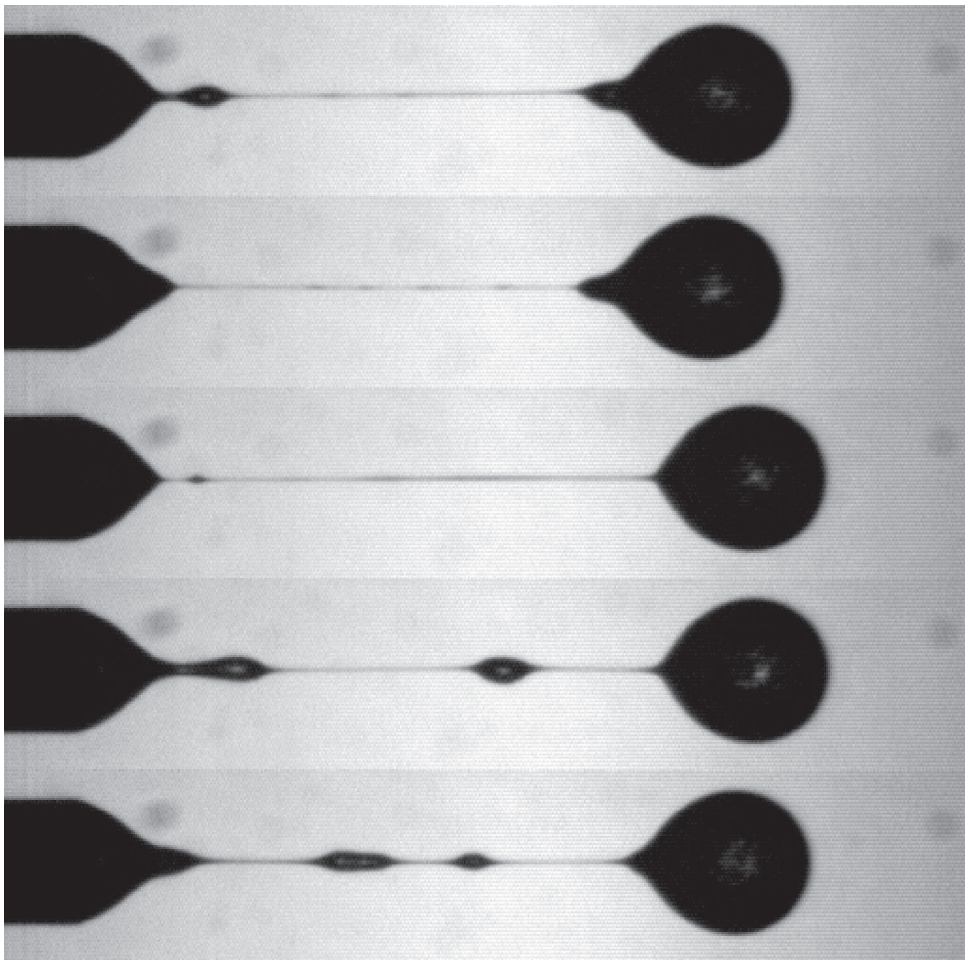

Figure 81: Pinch-off pictures for $\phi = 0.05$, $d = 0.32$ cm, $d_p = 212 - 250$ μm.

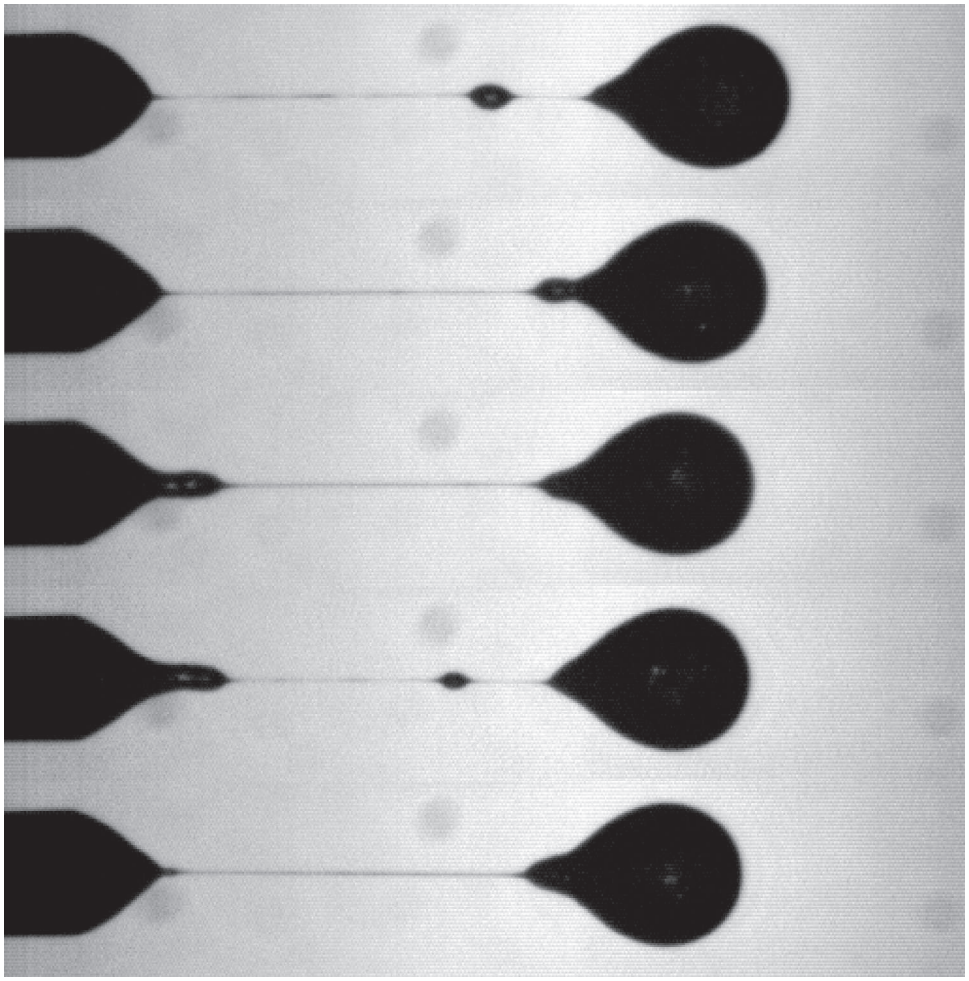

Figure 82: Pinch-off pictures for $\phi = 0.10$, $d = 0.32$ cm, $d_p = 212 - 250$ μm.

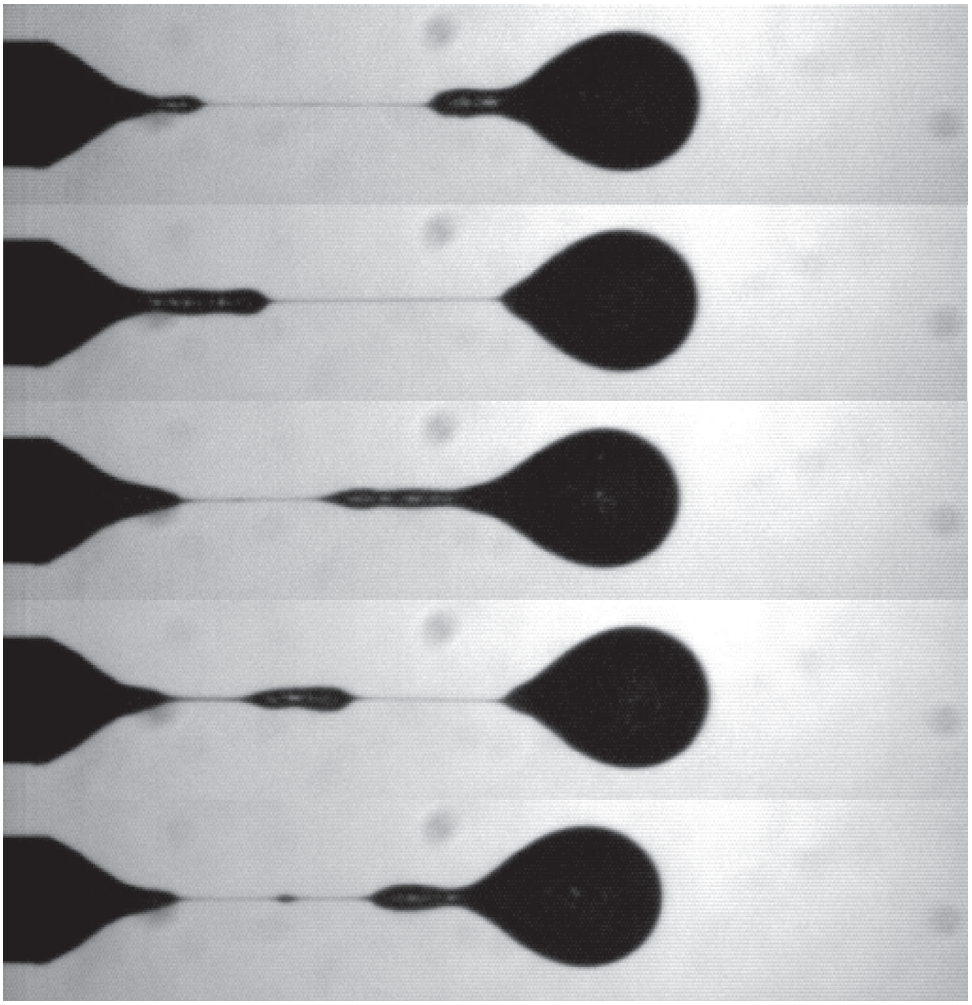

Figure 83: Pinch-off pictures for $\phi = 0.20$, $d = 0.32$ cm, $d_p = 212 - 250$ μm.

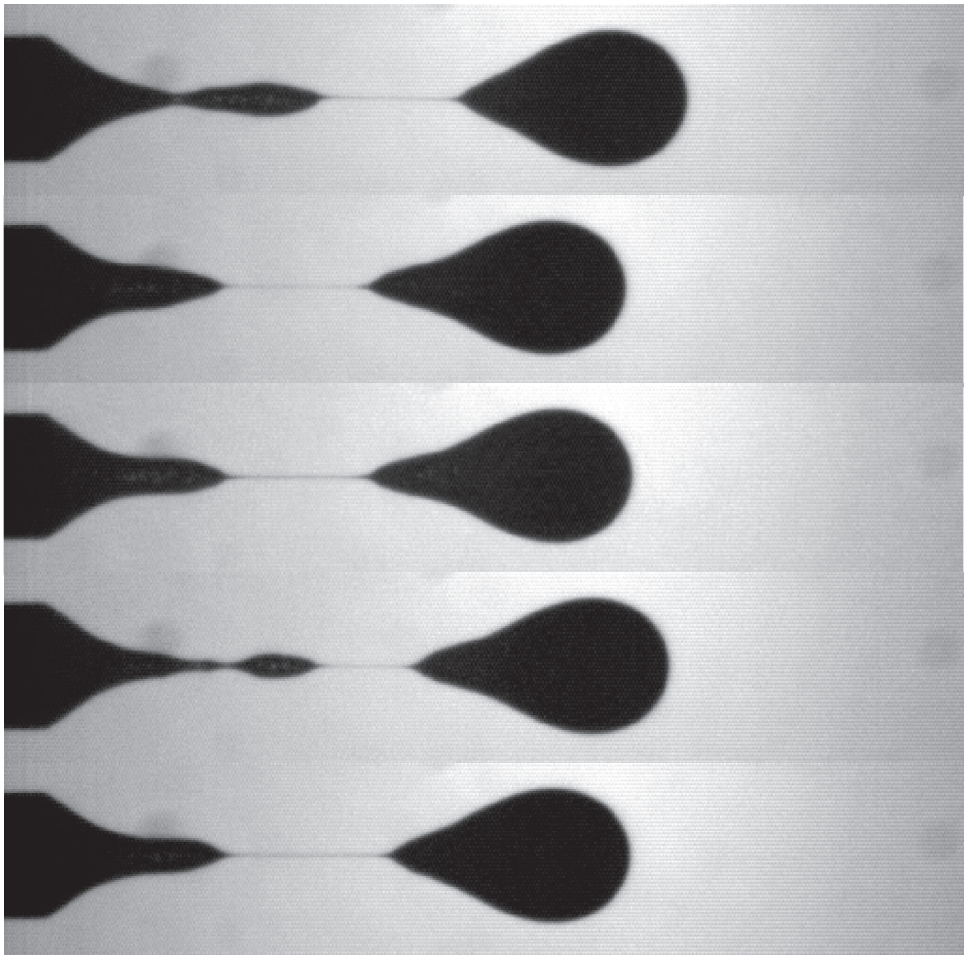

Figure 84: Pinch-off pictures for $\phi = 0.30$, $d = 0.32$ cm, $d_p = 212 - 250$ μm.

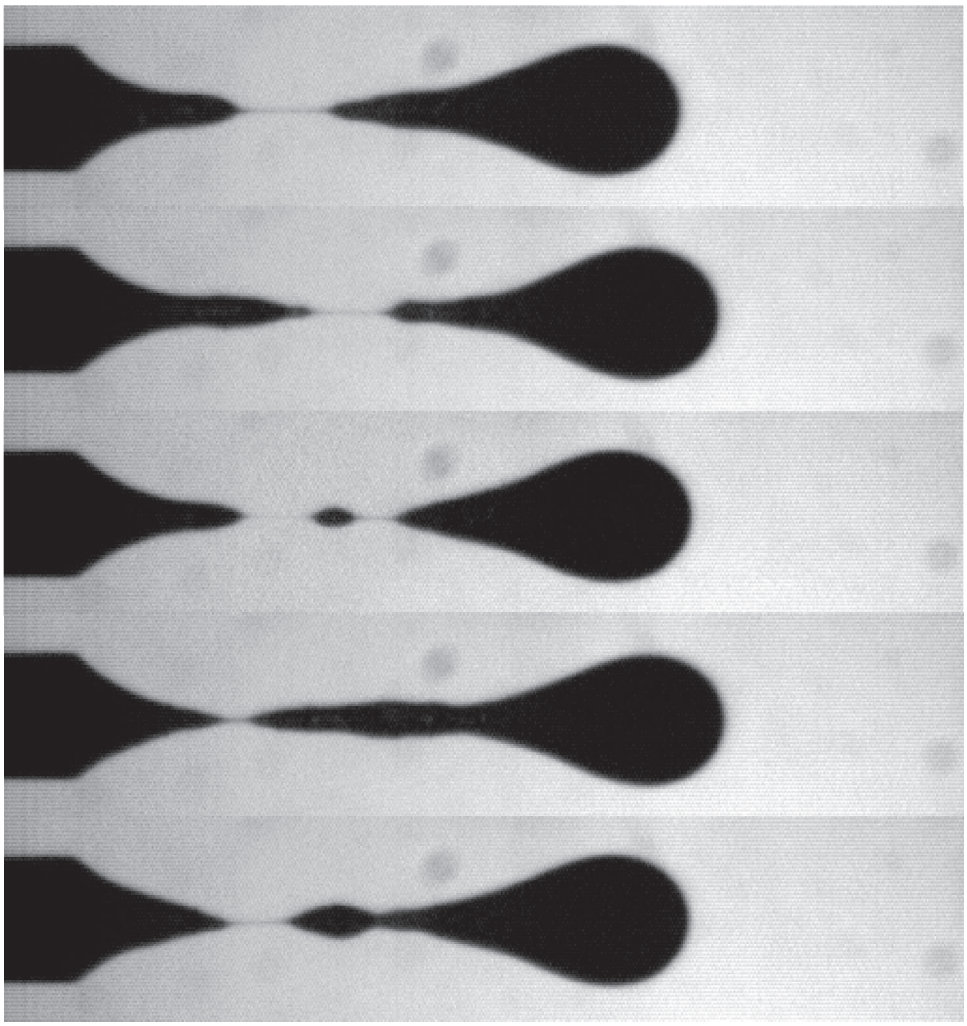

Figure 85: Pinch-off pictures for $\phi = 0.40$, $d = 0.32$ cm, $d_p = 212 - 250$ μm.

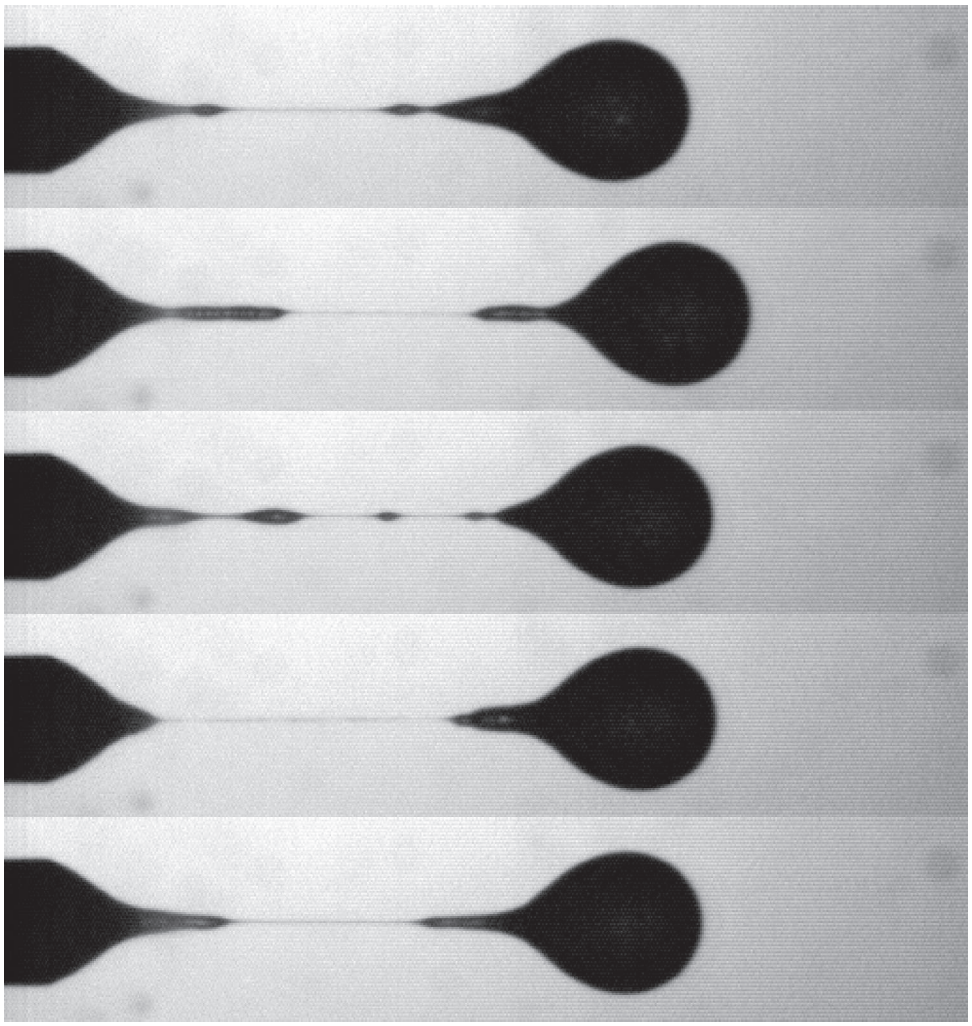

Figure 86: Pinch-off pictures for $\phi = 0.10$, $d = 0.32$ cm, $d_p = 106 - 125$ μm.

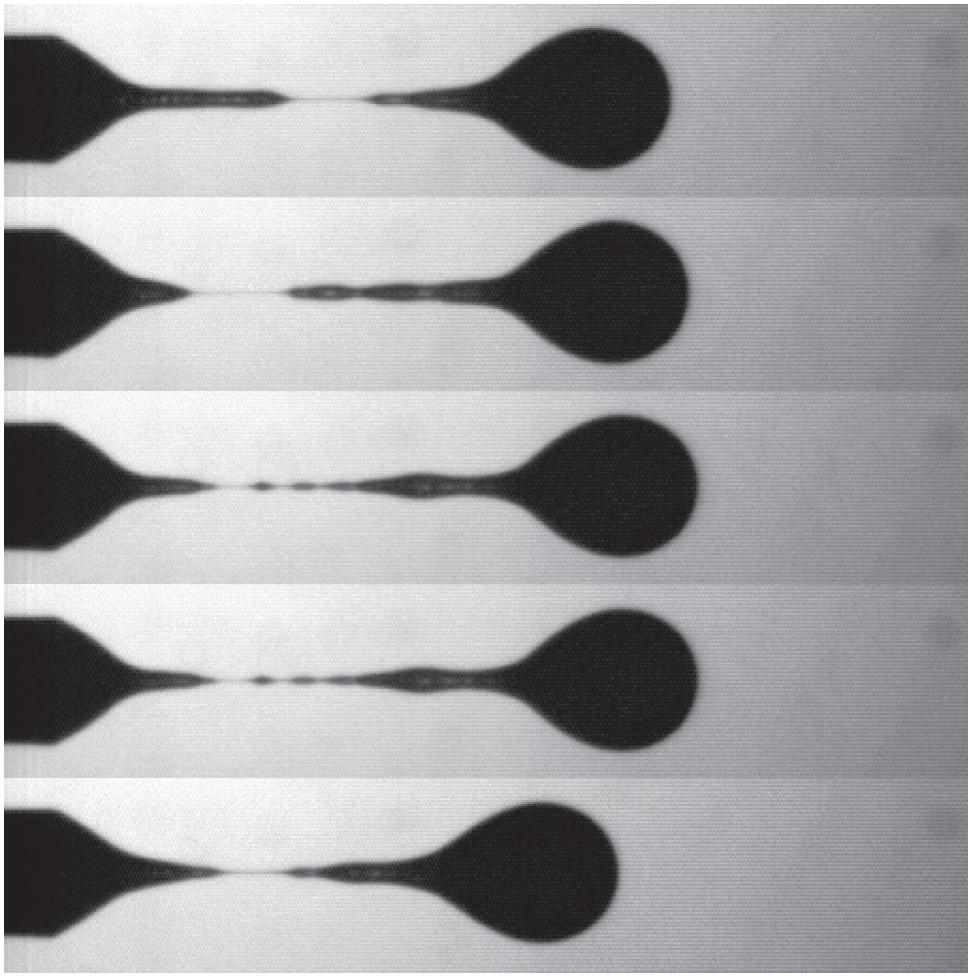

Figure 87: Pinch-off pictures for $\phi = 0.20$, $d = 0.32$ cm, $d_p = 106 - 125$ μm.

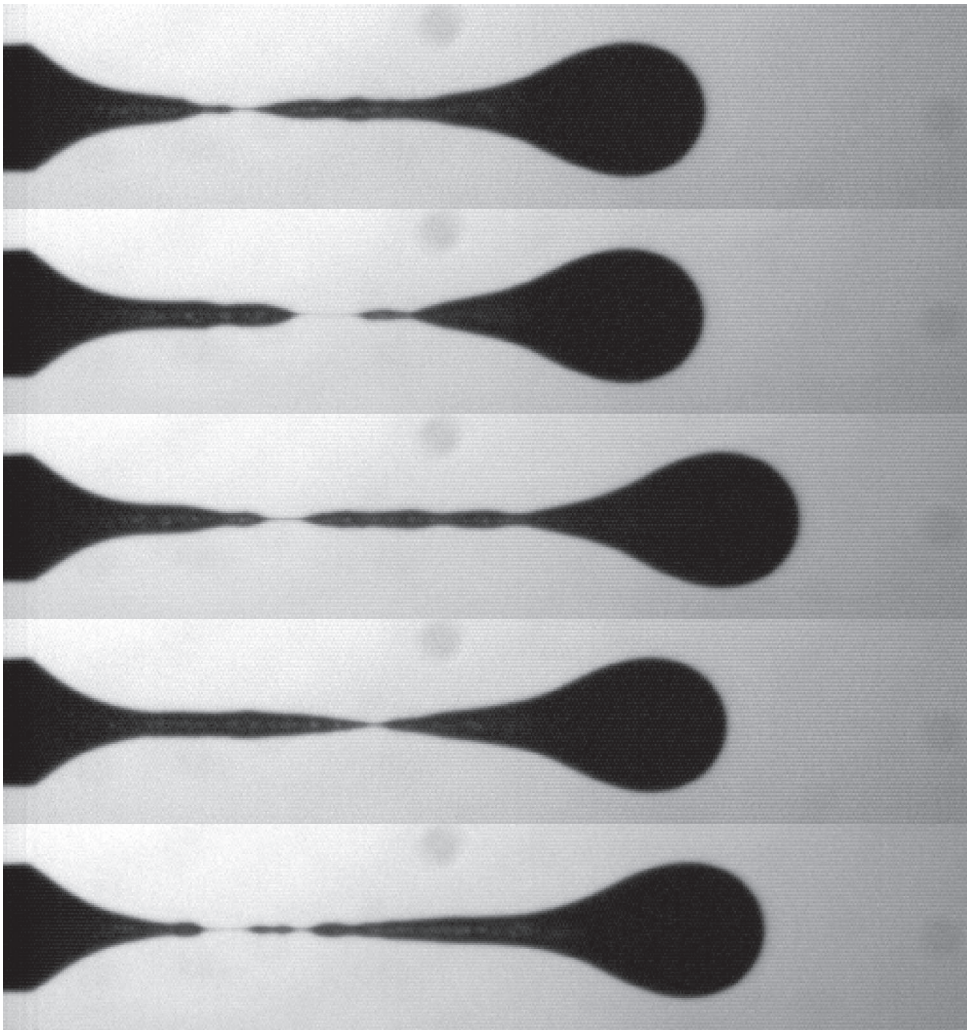

Figure 88: Pinch-off pictures for $\phi = 0.30$, $d = 0.32$ cm, $d_p = 106 - 125$ μm.

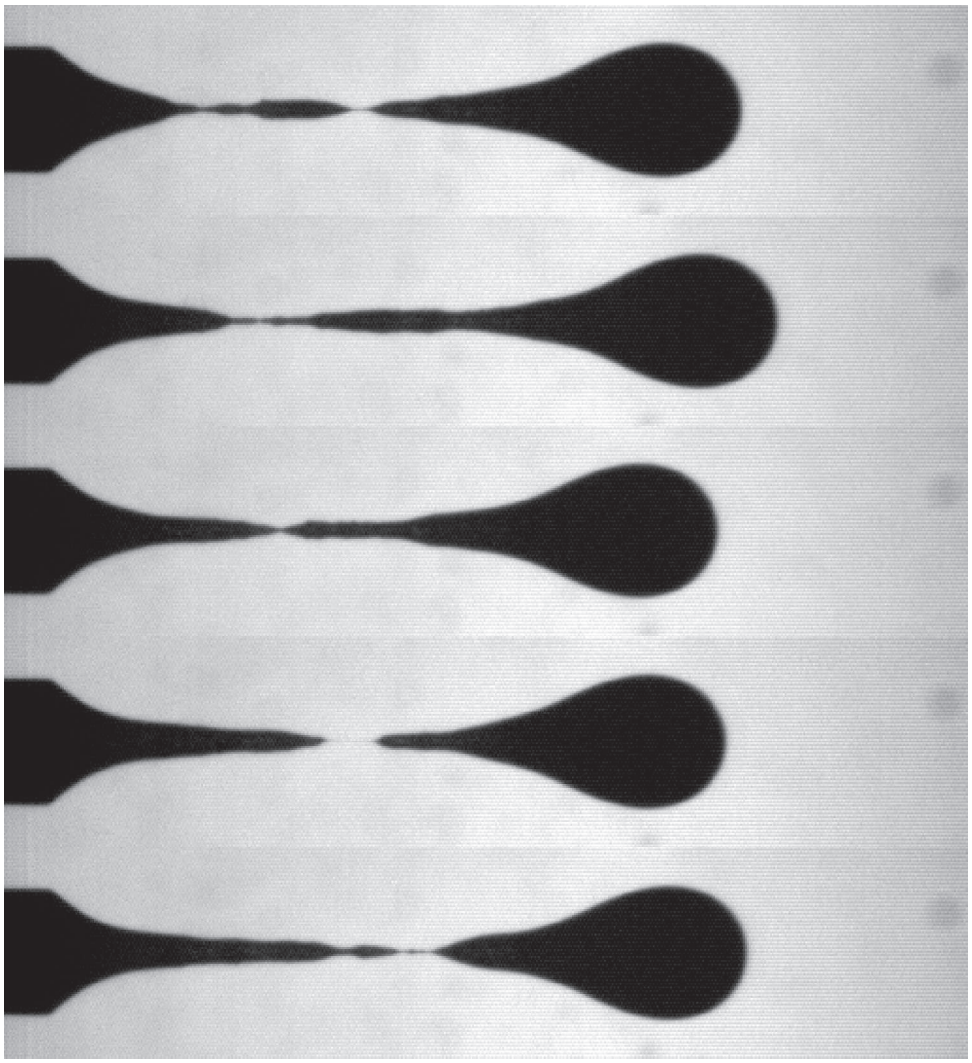

Figure 89: Pinch-off pictures for $\phi = 0.40$, $d = 0.32$ cm, $d_p = 106 - 125$ μm.

REFERENCES

[1] Alaoui, O., *Contribution a l'etude des instabilités de jets injection de liquides et de suspensions dans un autre fluide non-miscible.* PhD thesis, L'Universite de Provence (Aix-Marseille I), 1991.

[2] Ambravaneswaran, B., Phillips, S. D., and Basaran, O. A., "Theoretical analysis of a dripping faucet," *Phys. Rev. Lett.*, vol. 85, no. 25, pp. 5332–5335, 2000.

[3] Ambravaneswaran, B., Wilkes, E. D., and Basaran, O. A., "Drop formation from a capillary tube: Comparison of one-dimensional and two-dimensional analyses and occurrence of satellite drops," *Phys. Fluids*, vol. 14, no. 8, pp. 2606–2621, 2002.

[4] Blazdell, P. F., Evans, J. R., Edirisinghe, M. J., Shaw, P., and Binstead, M. J., "The computer aided manufacture of ceramics using multilayer jet printing," *J. Mater. Sci. Lett.*, vol. 14, pp. 1562–1565, 1995.

[5] Bogy, D. B., "Drop formation in a circular liquid jet," *Ann. Rev. Fluid Mech.*, vol. 11, pp. 207–228, 1979.

[6] Brenner, M. P., Eggers, J., Joseph, K., Nagel, S. R., and Shi, X. D., "Breakdown of scaling in droplet fission at high reynolds number," *Phys. Fluids*, vol. 9, no. 6, pp. 1573–1590, 1997.

[7] Chen, A. U., Notz, P. K., and Basaran, O. A., "Computational and experimental analysis of pinch-off and scaling," *Phys. Rev. Lett.*, vol. 88, no. 17, pp. 174501–1–174501–4, 2002.

[8] Chen, P., Chen, W., and Chang, S., "Bubble growth and ink ejection process of a thermal ink jet printhead," *Int. J. Mech. Sci.*, vol. 39, no. 6, pp. 683–695, 1997.

[9] Christanti, Y. and Walker, L. M., "Surface tension driven jet break up of strain-hardening polymer solutions," *J. Non-Newtonian Fluid Mech.*, vol. 100, pp. 9–26, 2001.

[10] Clanet, C. and Lasheras, J. C., "Transition from dripping to jetting," *J. Fluid Mech.*, vol. 383, pp. 307–326, 1999.

[11] Clift, R., Grace, J. R., and Weber, M. E., *Bubbles, drops, and particles.* Academic, 1978.

[12] Drazin, P. G. and Reid, W. H., *Hydrodynamic stability.* Cambridge University Press, 1981.

[13] Eggers, J., "Theory of drop formation," *Phys. Fluids*, vol. 7, no. 5, pp. 941–953, 1995.

[14] Eggers, J., "Nonlinear dynamics and breakup of free-surface flows," *Rev. Mod. Phys.*, vol. 69, no. 3, pp. 865–929, 1997.

[15] Eggers, J. and Dupont, T. F., "Drop formation in a one-dimensional approximation of the navier-stokes equation," *J. Fluid Mech.*, vol. 262, pp. 205–221, 1994.

[16] Entov, V. M., Barsoum, M., and Shmaryan, L. E., "On capillary instability of jets of magneto-rheological fluids," *J. Rheol.*, vol. 40, no. 5, pp. 727–739, 1996.

[17] Frankel, N. A. and Acrivos, A., "On the viscosity of a concentrated suspension of solid spheres," *Chem. Eng. Sci.*, vol. 22, pp. 847–853, 1967.

[18] Furbank, R. J. and Morris, J. F., "An experimental study of particle effects on drop formation," *Phys. Fluids*, vol. 16, no. 5, pp. 1777–1790, 2004.

[19] Goldin, M., Yerushalmi, J., Pfeffer, R., and Shinnar, R., "Breakup of a laminar capillary jet of a viscoelastic fluid," *J. Fluid Mech.*, vol. 38, pp. 689–711, 1969.

[20] Goren, S. L. and Wronski, S., "The shape of low-speed capillary jets of newtonian liquids," *J. Fluid Mech.*, vol. 25, pp. 185–198, 1966.

[21] Hampton, R. E., Mammoli, A. A., Graham, A. L., Tetlow, N., and Altobelli, S. A., "Migration of particles undergoing pressure-driven flow in a circular conduit," *J. Rheol.*, vol. 41, no. 3, pp. 621–640, 1997.

[22] Harkins, W. D. and Brown, F. E., "The determination of surface tension (free surface energy), and the weight of falling drops: the surface tension of water and benzene by the capillary height method," *J. Am. Chem. Soc.*, vol. 41, pp. 499–524, 1919.

[23] Henderson, D. M., Pritchard, W. G., and Smolka, L. B., "On the pinch-off of a pendant drop of viscous fluid," *Phys. Fluids*, vol. 9, no. 11, pp. 3188–3200, 1997.

[24] Henderson, D. M., Segur, H., Smolka, L. B., and Wadati, M., "The motion of a falling liquid filament," *Phys. Fluids*, vol. 12, no. 3, pp. 550–565, 2000.

[25] Jaworek, A. and Krupa, A., "Classification of the modes of ehd spraying," *J. Aerosol Sci.*, vol. 30, no. 7, pp. 873–893, 1999.

[26] Krieger, I. M., "Rheology of monodisperse lattices," *Adv. Colloid Interface Sci.*, vol. 3, no. 2, pp. 111–136, 1972.

[27] McKinley, G. H. and Sridhar, T., "Filament-stretching rheometry of complex fluids," *Annu. Rev. Fluid Mech.*, vol. 34, pp. 375–415, 2002.

[28] Meister, B. J. and Scheele, G. F., "Drop formation from cylindrical jets in immiscible liquid systems," *AIChE J.*, vol. 15, no. 5, pp. 700–706, 1969.

[29] Meister, B. J. and Scheele, G. F., "Prediction of jet length in immiscible liquid systems," *AIChE J.*, vol. 15, no. 5, pp. 689–699, 1969.

[30] Moffat, H. K., "Viscous and resistive eddies near a sharp corner," *J. Fluid Mech.*, vol. 18, pp. 1–18, 1964.

[31] Morris, J. F. and Boulay, F., "Curvilinear flows of noncolloidal suspensions: The role of normal stresses," *J. Rheol.*, vol. 43, no. 5, pp. 1213–1237, 1999.

[32] Nicolas, M., "Experimental study of gravity-driven dense suspension jets," *Phys. Fluids*, vol. 14, no. 10, pp. 3570–3576, 2002.

[33] Nott, P. R. and Brady, J. F., "Pressure-driven flow of suspensions: simulation and theory," *J. Fluid Mech.*, vol. 275, pp. 157–199, 1994.

[34] Notz, P. K., Chen, A. U., and Basaran, O. A., "Satellite drops: Unexpected dynamics and change of scaling during pinch-off," *Phys. Fluids*, vol. 13, no. 3, pp. 549–552, 2001.

[35] Ogg, J. C. and Schetz, J. A., "Breakup and droplet formation of slurry jets," *AIAA J.*, vol. 23, pp. 432–439, 1985.

[36] Perçin, G. and Khuri-Yakub, B. T., "Piezoelectric droplet ejector for ink-jet printing of fluids and solid particles," *Rev. Sci. Instrum.*, vol. 74, no. 2, pp. 1120–1127, 2003.

[37] Peregrine, D. H., Shoker, G., and Symon, A., "The bifurcation of liquid bridges," *J. Fluid Mech.*, vol. 212, pp. 25–39, 1990.

[38] Rayleigh, L. J. W. S., "On the instability of jets," *Proc. London Math. Soc.*, vol. 10, pp. 4–13, 1879.

[39] Richards, J. R., Beris, A. N., and Lenhoff, A. M., "Drop formation in liquid-liquid systems before and after jetting," *Phys. Fluids*, vol. 7, no. 11, pp. 2617–2630, 1995.

[40] Schaflinger, U. and Machu, G., "Interfacial phenomena in suspensions," *Chem. Eng. Technol.*, vol. 22, pp. 617–619, 1999.

[41] Scheele, G. F. and Meister, B. J., "Drop formation at low velocities in liquid-liquid systems: Part i. prediction of drop volume," *AIChE J.*, vol. 14, no. 1, pp. 9–15, 1968.

[42] Scheele, G. F. and Meister, B. J., "Drop formation at low velocities in liquid-liquid systems: Part ii. prediction of jetting velocity," *AIChE J.*, vol. 14, no. 1, pp. 15–19, 1968.

[43] Schulkes, R. M. S. M., "The evolution and bifurcation of a pendant drop," *J. Fluid Mech.*, vol. 278, pp. 83–100, 1994.

[44] Shi, X. D., Brenner, M. P., and Nagel, S. R., "A cascade of structure in a drop falling from a faucet," *Science*, vol. 265, pp. 219–222, 1994.

[45] Subia, S. R., Ingber, M. S., Mondy, L. A., Altobelli, S. A., and Graham, A. L., "Modelling of concentrated suspensions using a continuum constitutive equation," *J. Fluid Mech.*, vol. 373, pp. 193–219, 1998.

[46] Tate, T., "On the magnitude of a drop of liquid formed under different circumstances," *Phil. Mag.*, vol. 27, pp. 176–180, 1864.

[47] Tay, B. Y. and Edirisinghe, M. J., "Investigation of some phenomena occurring during continuous ink-jet printing of ceramics," *J. Mater. Res.*, vol. 16, no. 2, pp. 373–384, 2001.

[48] Tincher, W. C., Hu, Q., and Li, X., "Ink jet systems for printing fabric," *Text. Chem. Color.*, vol. 30, no. 5, pp. 24–27, 1998.

[49] Trang, C. T. and Yeow, Y. L., "Extrudate swell of newtonian and non-newtonian fluids–the effect of gravitational body force," *J. Non-Newtonian Fluid Mech.*, vol. 20, pp. 103–116, 1986.

[50] Wilkes, E. D., Phillips, S. D., and Basaran, O. A., "Computational and experimental analysis of dynamics of drop formation," *Phys. Fluids*, vol. 11, no. 12, pp. 3577–3598, 1999.

[51] Wilson, S. D. R., "The slow dripping of a viscous fluid," *J. Fluid Mech.*, vol. 190, pp. 561–570, 1988.

[52] Windle, J. and Derby, B., "Ink jet printing of pzt aqueous ceramic suspensions," *J. Mater. Sci. Lett.*, vol. 18, pp. 87–90, 1999.

[53] Zhang, X., "Dynamics of drop formation in viscous flows," *Chem. Eng. Sci.*, vol. 54, pp. 1759–1774, 1999.

[54] Zhang, X., "Dynamics of growth and breakup of viscous pendant drops into air," *J. Colloid Interface Sci.*, vol. 212, pp. 107–122, 1999.

[55] Zhang, X. and Basaran, O. A., "An experimental study of dynamics of drop formation," *Phys. Fluids*, vol. 7, no. 6, pp. 1184–1203, 1995.

VITA

Roy Jeffrey Furbank was born in Landstuhl, Germany on August 22, 1972 to Christine and Jeffrey Furbank. After graduating from Austin High School in El Paso, Texas in 1990 Roy attended the University of Texas at Austin and earned a B.S. in Chemical Engineering (with Honors) in 1995. Upon graduation Roy received a commission as a 2nd Lieutenant in the United States Army and spent the next four years as a combat engineer officer in the 2nd Armored Cavalry Regiment and the 46th Engineer Battalion, both at Fort Polk, Louisiana. During this time Roy participated in the NATO peacekeeping mission in Bosnia-Herzegovina as well as in relief efforts following Hurricane Mitch in Nicaragua.

Following his active duty military service Roy began graduate studies in Chemical Engineering at the Georgia Institute of Technology in 1999 under the advisement of Dr. Jeffrey Morris in the field of complex fluids and multiphase flow. During his graduate career Roy co-authored one peer-reviewed journal article and made a number of presentations of his research on the formation of drops from particulate suspensions; including two competitions in which he was awarded first place. Roy earned his Ph.D. in Chemical Engineering in May 2004 and will start work shortly with the Rohm and Haas Company in Spring House, Pennsylvania as a Senior Scientist in their research laboratories.